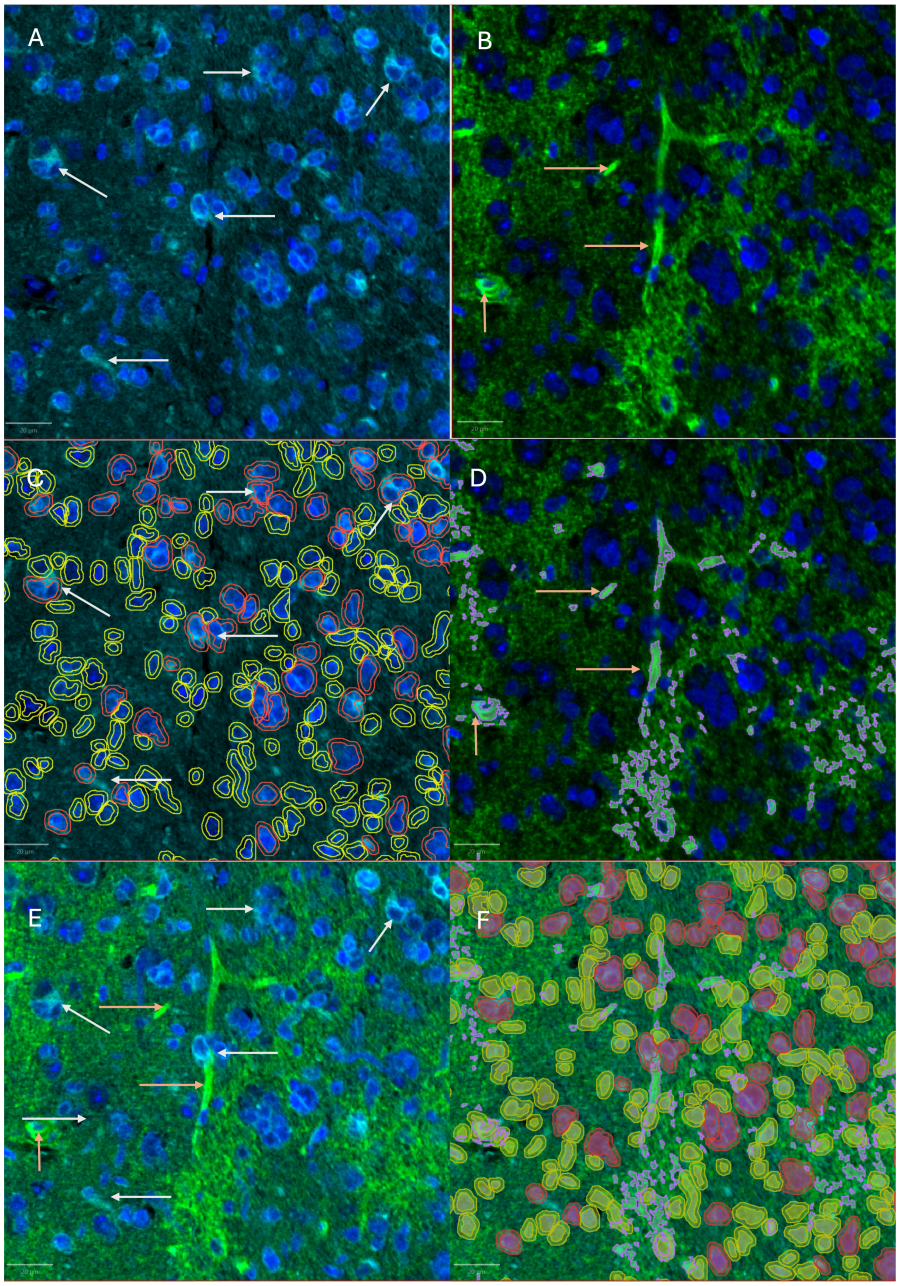

Figure 4.10: **Segmentation of HLA positive cells and GLUT-1 Positive Blood Vessels**
Human GBM xenograft in mouse tissue was stained using Multiplex IF for: **A)** HLA (cyan), used as a marker for human GBM cells (white arrows) in the mouse brain **B)** GLUT-1 (green), used as a marker for endothelial cells which line blood vessels (arrows) **C)** Identification of cells utilising DAPI staining (blue stain), followed by classification of cells as HLA positive (cyan stain) cells (red outline) or HLA negative (yellow outline). Arrows are the same as (A). **D)** Classification of positive GLUT-1 staining (green) using a threshold method to classify objects as blood vessels (purple outline). **E)** Combined image of Human GBM xenograft in mouse tissue was stained using IF for HLA (cyan stain) and GLUT-1 (green stain). Positive staining for HLA (white arrow) and positive staining for GLUT-1 positive blood vessels (orange arrows). **F)** Combined image of HLA positive cells (red), HLA negative cells (yellow) and GLUT-1 positive blood vessels (purple). All sections counter stained with the nuclear stain 4,6-diamidino-2-phenylindole (DAPI) (Blue). Scale bars = 20 μm

Those GBM cells that had a nearest GBM cell neighbour that was greater than 20μm away were classified as individuals, while the rest were classified as forming a cluster. 20μm was used as the threshold distance, as it has been suggested that cells respond to stiffness changes approximately 20μm away from the cell (Buxboim et al. [2010]).

Quantification of the percentage of cells located individually revealed the highest percentage in SJH1 cells (45%) followed by RN1 cells (39%), JK2 cells (10%) and WK1 cells (2%) (Figure 4.11).

4.2.6 Cell-Line Specific Associations with Blood Vessels

The distance between GBM cells and blood vessels was assessed to understand the distinct migration patterns of GBM cell lines relative to the more rigid blood vessels within the otherwise soft brain parenchyma (Figure 4.12). On average, WK1 cells were located further from blood vessels than SJH1 cells, which in turn were farther away than RN1 cells, and were more distant compared to JK2 cells (Table 4.4). Importantly, there was significant variability in all xenograft sections' measurements, potentially due to section orientation and the varied cell and blood vessel density in each section (Figure 4.1).

4.2.7 Cell-Line Specific Behaviours in Individually Migrating Cells and Cell Migration in Clusters

The difference in spatial association of cells located as individuals and those in clusters was then queried to determine whether an alteration in behaviours was observed between

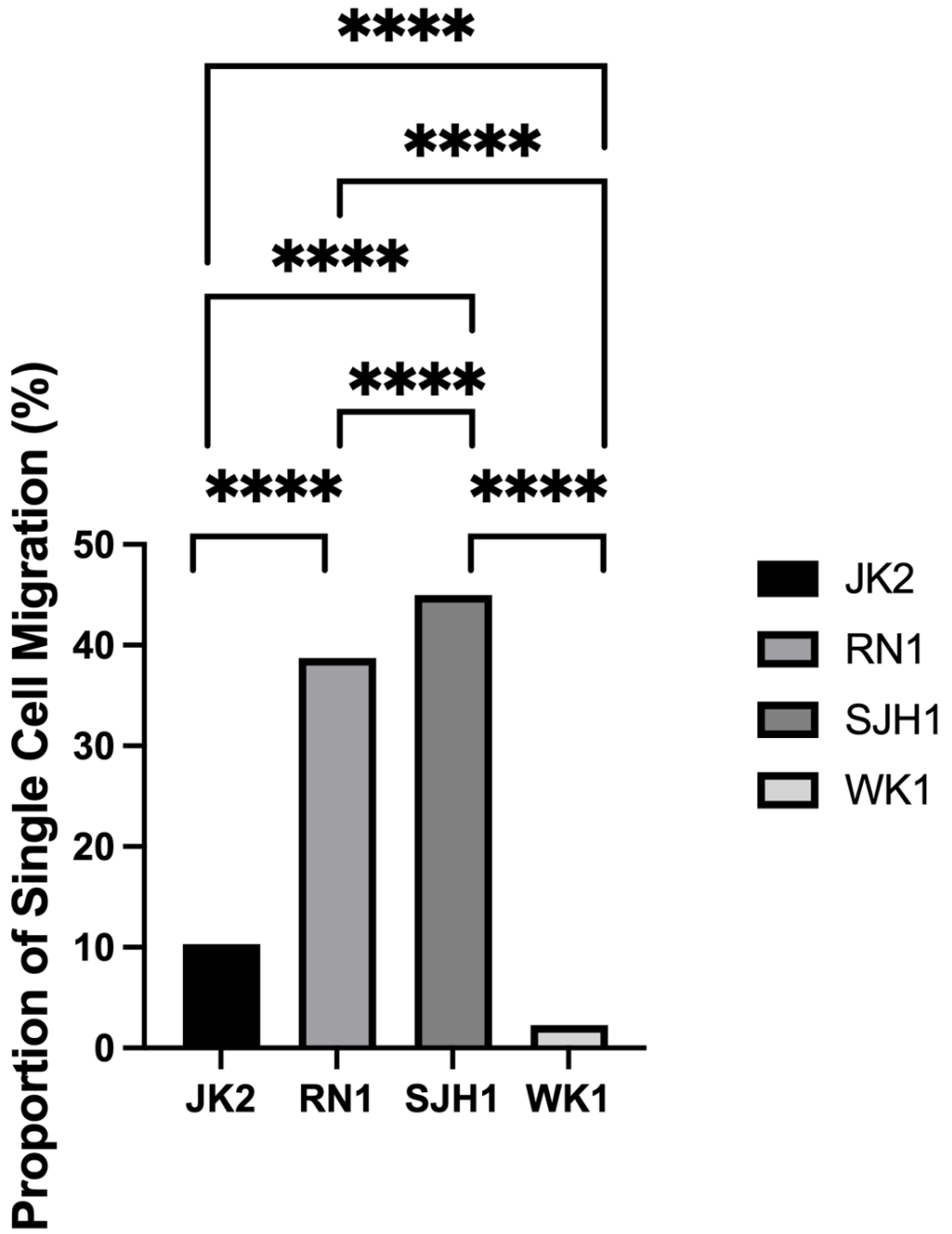

Figure 4.11: **Proportion of Xenograft GBM Cells Located as Individual Cells**

Following detection of cells from the brain parenchyma based on DAPI staining and segmentation of detected cells into human GBM cells based on positive HLA staining, cells were further segmented into individual cells and found as a cluster, based on nearest neighbour analysis, ****$p<0.0001$, two tail Z-Test for population proportions

Table 4.4: **Mean Distance away from blood vessels (μm) for JK2, RN1, SJH1 and WK1 human GBM xenograft in mouse brain**

Average distance from GLUT-1 positive blood vessels for cells segmented located as individual and those organised in clusters. Data obtained from entire brain sections with a thickness of 5μm. Results are shown as Mean +/- SD

	JK2	RN1	SJH1	WK1
Individual Cells	8.47 $\pm$ 6.90 (n= 8689)	25.71 $\pm$ 50.14 (n= 3365)	24.82 $\pm$ 40.16 (n= 8690)	142.0 $\pm$ 154.4 (n= 3507)
Clustered Cells	11.28 $\pm$ 10.26 (n= 75626)	24.27 $\pm$ 32.30 (n= 5325)	29.96 $\pm$ 23.82 (n= 8067)	85.50 $\pm$ 103.7 (n= 151934)
Total	10.99 $\pm$ 10.00 (n= 84316)	24.82 $\pm$ 40.16 (n= 8690)	29.50 $\pm$ 24.69 (n= 14665)	86.77 $\pm$ 105.5 (n= 155441)

these two groups (Figure 4.12). As outlined in Section 4.2.5, nearest-neighbour analysis was utilised to differentiate between cells located alone and those located in groups. The study indicated that SJH1 cells located individually are in closer proximity to GLUT-1 positive blood vessels than those found in clusters. In contrast, WK1 cells in clusters showed a closer proximity with GLUT-1 positive blood vessels compared to those cells found alone. JK2 and RN1 cells exhibited no significant difference in their proximity to GLUT-1 positive vessels, regardless of their grouping pattern. When examining individually located cells, WK1 cells were positioned further from GLUT-1 positive vessels than SJH1 and RN1 cells, both of which were further from these vessels than JK2 cells. Among cells found in clusters, WK1 cells were at a greater distance from GLUT-1 positive vessels than SJH1 cells, which were themselves further away compared to RN1 cells, and RN1 cells were more distant than JK2 cells.

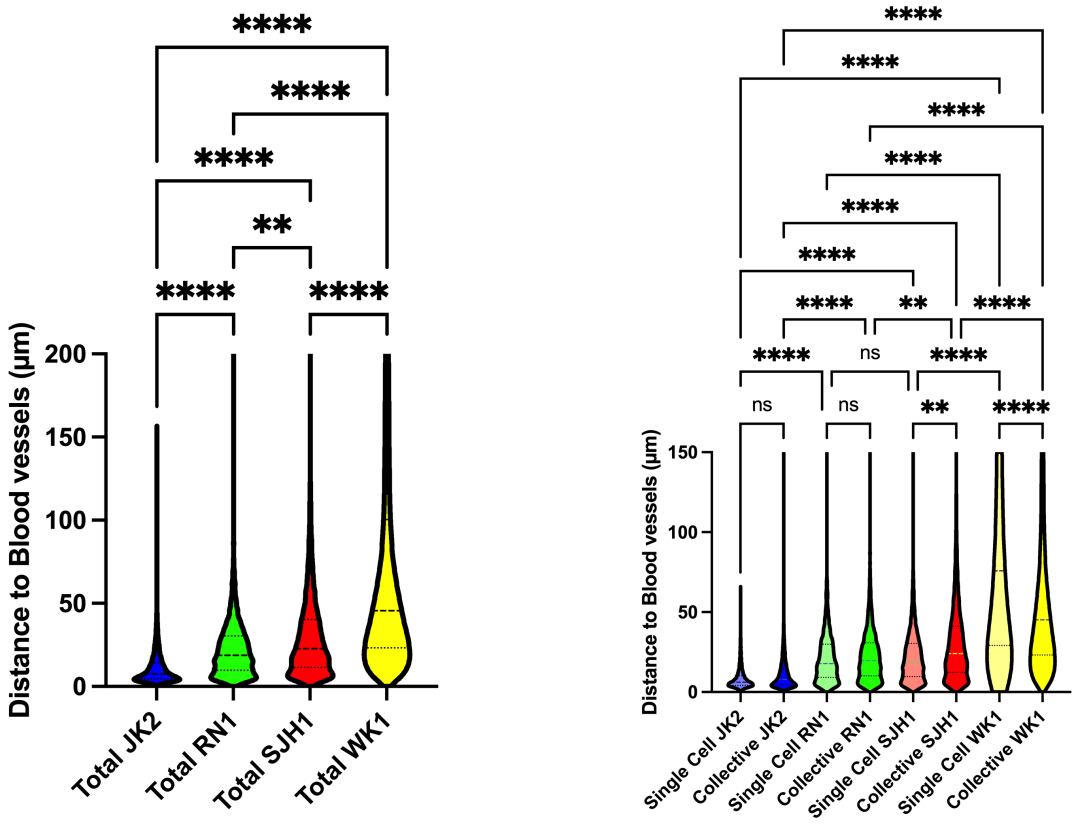

Figure 4.12: **Distance of Human Xenograft GBM Cells From the GLUT-1 Positive Blood Vessels**

Mean distance of human GBM cells in a xenograft mouse model from the blood vessels in the mouse brain (detected with GLUT-1 antibody staining) (left) and after segmentation into cells found individually and as clusters. Data collected in whole brain sections of 5μm thickness. *p<0.05, **p<0.01, ***p<0.001, ****p<0.0001, ns = not significant, One-way ANOVA and Tukey's multiple comparisons test.

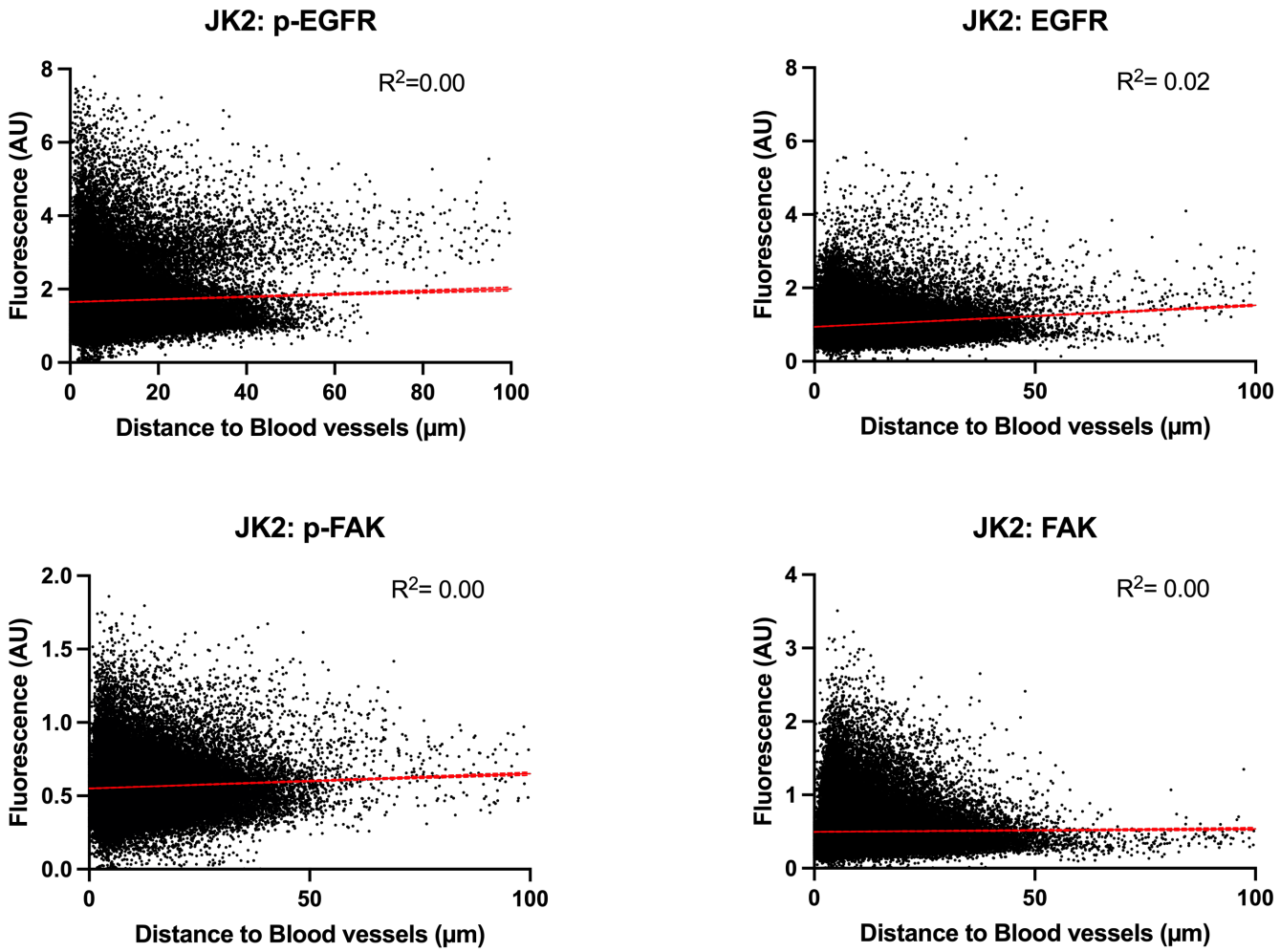

Figure 4.13: **Phosphorylation of EGFR and FAK in Human JK2 GBM Xenograft Relation to Distance from GLUT-1 Positive Blood Vessels in the Mouse Brain**

IF staining was performed for p-EGFR, EGFR, p-FAK and FAK in HLA positive cells in 5 μm thick, whole brain sections of human GBM JK2 cell lines. Fluorescence was measured as normalised counts (fluorescence intensity normalised to the exposure value for each section) . Individual values were plotted against the distance of the measured cell from the nearest GLUT-1 positive blood vessel. A linear regression analysis was performed to determine the line of best fit with the goodness of fit determined by the R^2 value.

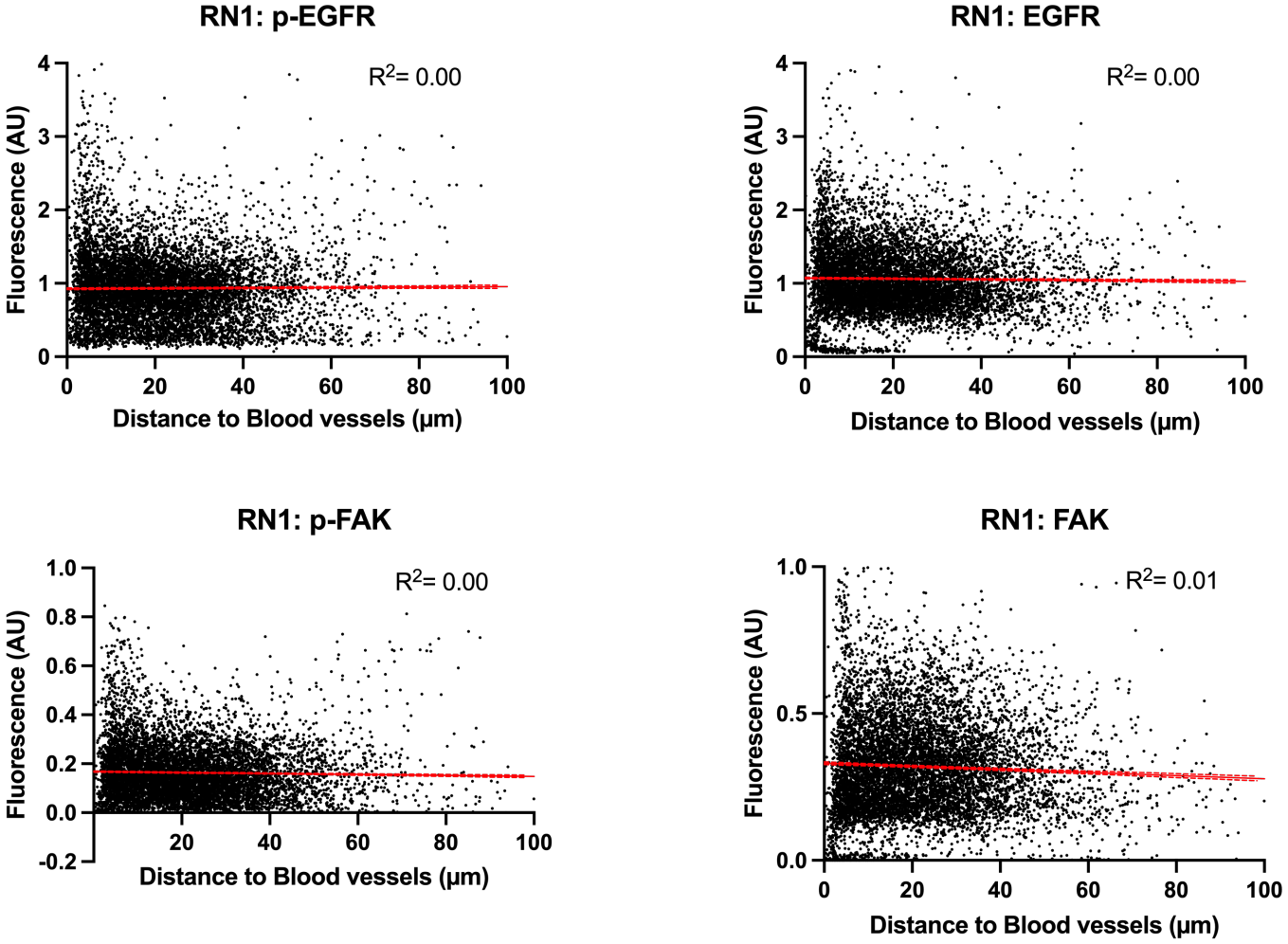

Figure 4.14: **Phosphorylation of EGFR and FAK in Human RN1 GBM Xenograft Relation to Distance from GLUT-1 Positive Blood Vessels in the Mouse Brain**

IF staining was performed for p-EGFR, EGFR, p-FAK and FAK in HLA positive cells in 5 μm thick, whole brain sections of human GBM RN1 cell lines. Fluorescence was measured as normalised counts (fluorescence intensity normalised to the exposure value for each section). Individual values were plotted against the distance of the measured cell from the nearest GLUT-1 positive blood vessel. A linear regression analysis was performed to determine the line of best fit with the goodness of fit determined by the R^2 value.

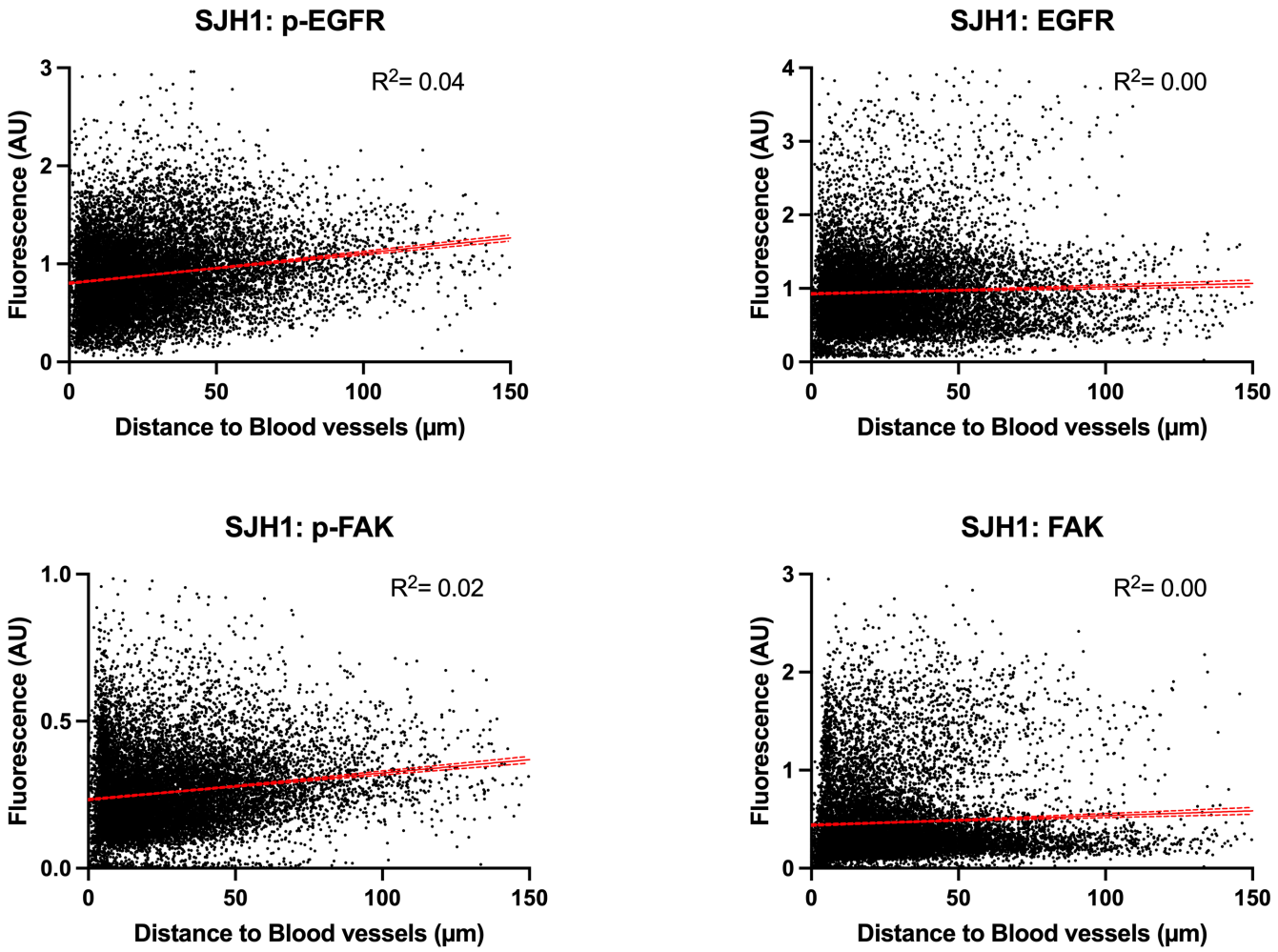

Figure 4.15: **Phosphorylation of EGFR and FAK in Human SJH1 GBM Xenograft Relation to Distance from GLUT-1 Positive Blood Vessels in the Mouse Brain**

IF staining was performed for p-EGFR, EGFR, p-FAK and FAK in HLA positive cells in 5 μm thick, whole brain sections of human GBM SJH1 cell lines. Fluorescence was measured as normalised counts (fluorescence intensity normalised to the exposure value for each section). Individual values were plotted against the distance of the measured cell from the nearest GLUT-1 positive blood vessel. A linear regression analysis was performed to determine the line of best fit with the goodness of fit determined by the R^2 value.

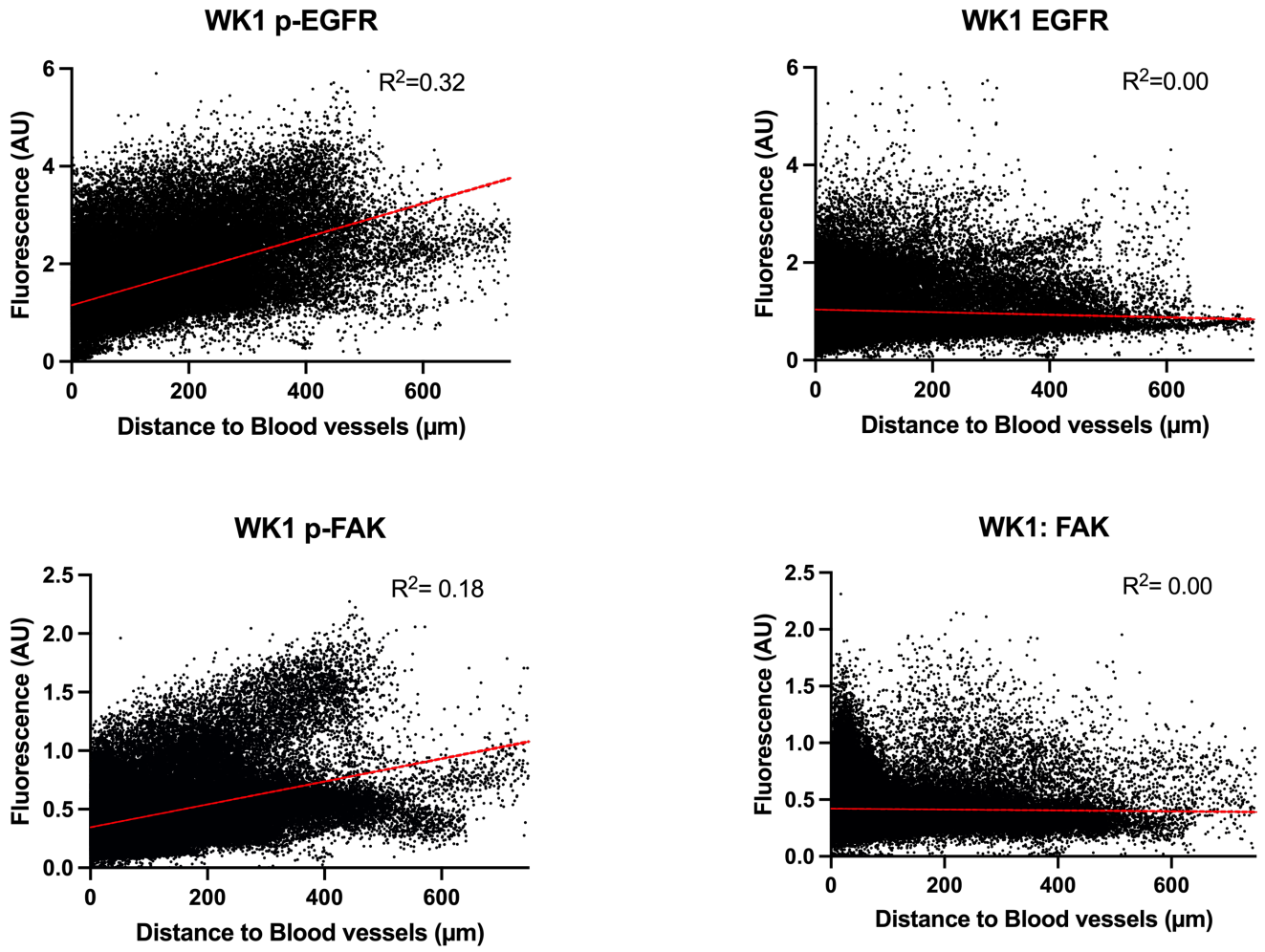

Figure 4.16: **Phosphorylation of EGFR and FAK in Human WK1 GBM Xenograft Relation to Distance from GLUT-1 Positive Blood Vessels in the Mouse Brain**

IF staining was performed for p-EGFR, EGFR, p-FAK and FAK in HLA positive cells in 5 μm thick, whole brain sections of human GBM WK1 cell lines. Fluorescence was measured as normalised counts (fluorescence intensity normalised to the exposure value for each section). Individual values were plotted against the distance of the measured cell from the nearest GLUT-1 positive blood vessel. A linear regression analysis was performed to determine the line of best fit with the goodness of fit determined by the R^2 value

4.2.8 Cell-Line-Dependent Phosphorylation of EGFR is Correlated to the Distance From Blood Vessel

EGFR phosphorylation positivity was quantified as a function of the distance from GLUT-1 positive blood vessels (Figures 4.13 - 4.15) to explore the role of mechanosensation in influencing the relationship of HGG cell location to GLUT-1 positive blood vessels. For JK2 (Figure 4.13), RN1 (Figure 4.14), and SJH1 (Figure 4.15) cell lines, there was no correlation between EGFR expression or EGFR phosphorylation as a function of distance from GLUT-1 positive blood vessels. Remarkably, in the WK1 cell line (Figure 4.16), while overall EGFR expression shows no correlation with proximity to GLUT-1 positive blood vessels (R^2=0.00), the phosphorylation of EGFR is positively correlated with the distance from these vessels (R^2=0.32). This suggests that the increase in EGFR phosphorylation is independently associated with an increased distance from GLUT-1 positive blood vessels and is not secondary to increased EGFR expression.

4.2.9 Cell-Line-Dependent FAK Phosphorylation is Correlated to the Distance From Blood Vessel

In the xenografts of JK2 (Figure 4.13), RN1 (Figure 4.14), and SJH1 (Figure 4.15) cell lines, there was no correlation between FAK expression or FAK phosphorylation as a function of distance from GLUT-1 positive blood vessels in the mouse brain. For WK1 (Figure 4.16), total FAK expression is not correlated with the distance from GLUT-1 positive blood vessels (R^2=0.00), however, cells show increased FAK phosphorylation with increasing distance from GLUT-1 positive blood vessels (R^2=0.18). This suggests that the

increase in FAK phosphorylation is independently associated with an increased distance from GLUT-1 positive blood vessels and not secondary to increased FAK expression in WK1 cells.

4.2.10 The Correlation of EGFR Phosphorylation to the Distance from Blood Vessels is Diminished in Single-Cell Migration in a Cell-Dependent Manner

Next, we segmented brain cancer cell populations into individual versus cell clusters and then compared EGFR phosphorylation positivity as a function of distance from GLUT-1 positive blood vessels in these two segmented populations for JK2, RN1, SJH1 and WK1 cell lines.

For JK2 (Figure 4.17), RN1 (Figure 4.18), and SJH1 cell lines (Figure 4.19), there is no correlation between EGFR expression or EGFR phosphorylation as a function of distance from GLUT-1 positive blood vessels in the mouse brain. In WK1 cells (Figure 4.20), following segmentation there continued to be no correlation between distance from blood vessels and EGFR expression (clusters: R^2=0.00, individual cells: R^2=0.07). However, there was a strong correlation between increased EGFR phosphorylation with distance from blood vessels in the cell clusters (R^2=0.34). By contrast, there was limited correlation seen in the individual cells (R^2=0.13). The differences in EGFR phosphorylation seen in individual cells compared to cell clusters might indicate that proximity to GLUT-1 positive blood vessels affects EGFR phosphorylation less in single cells than in cell clusters in WK1 cells.

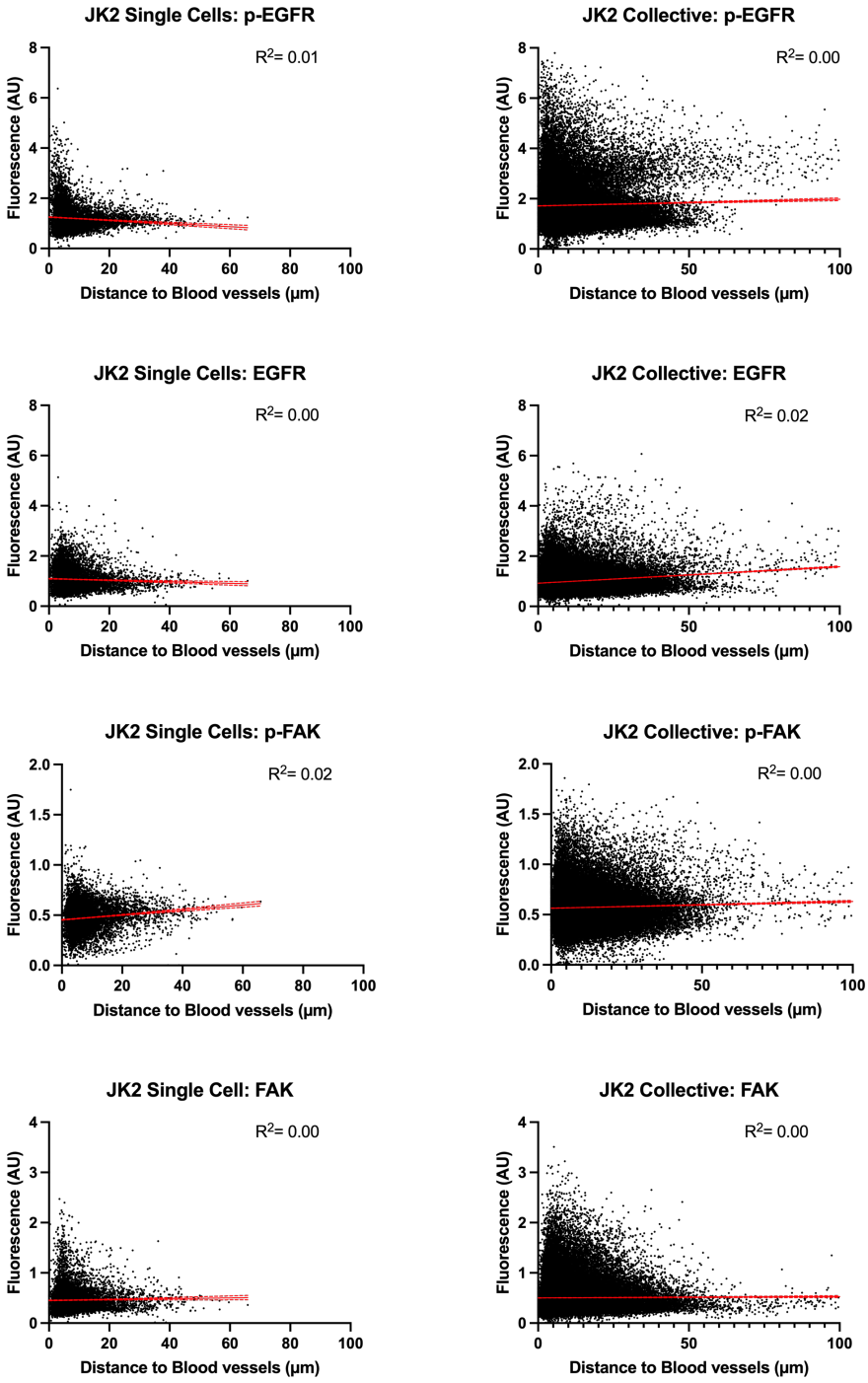

Figure 4.17: **Phosphorylation of EGFR and FAK in Human JK2 GBM Xenograft in Relation to Distance from the GLUT-1 Positive Blood Vessels in the Mouse Brain, Segmented by Cells Found Individually and as Clusters**

IF staining was performed for p-EGFR, EGFR, p-FAK and FAK in HLA positive cells in 5 μm thick, whole brain sections of human GBM JK2 cell lines. Cells were segmented into single-cells and clusters using nearest neighbour analysis. Fluorescence was measured as normalised counts (Fluorescent intensity normalised to the exposure value for each section). Individual values were plotted against the distance of the measured cell from the nearest GLUT-1 positive blood vessel. A linear regression analysis was performed to determine the line of best fit with the goodness of fit determined by the R^2 value.

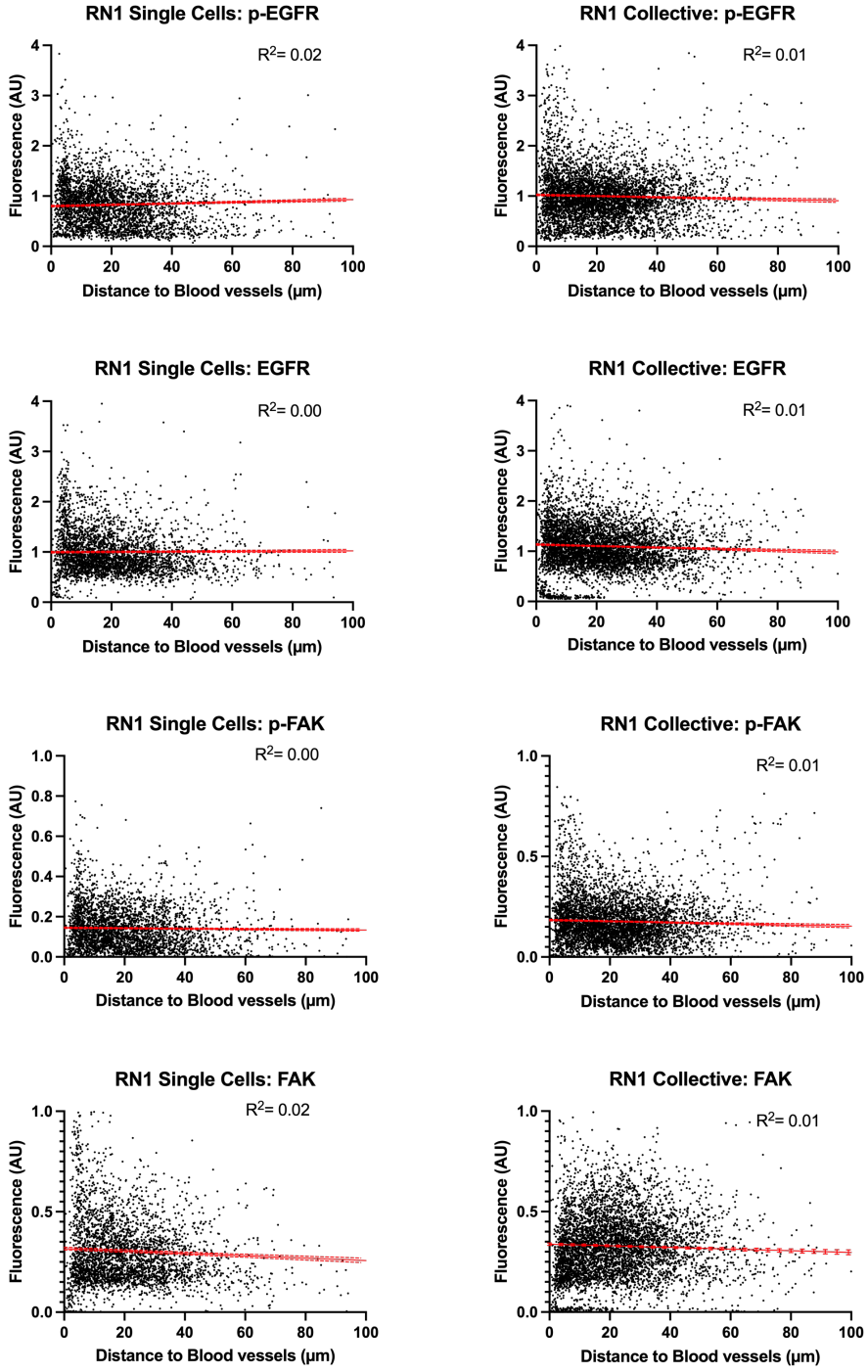

Figure 4.18: **Phosphorylation of EGFR and FAK in Human JK2 GBM Xenograft in Relation to Distance from the GLUT-1 Positive Blood Vessels in the Mouse Brain, Segmented by Cells Found Individually and as Clusters**

IF staining was performed for p-EGFR, EGFR, p-FAK and FAK in HLA positive cells in 5 μm thick, whole brain sections of human GBM JK2 cell lines. Cells were segmented into single-cells and clusters using nearest neighbour analysis. Fluorescence was measured as normalised counts (Fluorescent intensity normalised to the exposure value for each section). Individual values were plotted against the distance of the measured cell from the nearest GLUT-1 positive blood vessel. A linear regression analysis was performed to determine the line of best fit with the goodness of fit determined by the R^2 value.

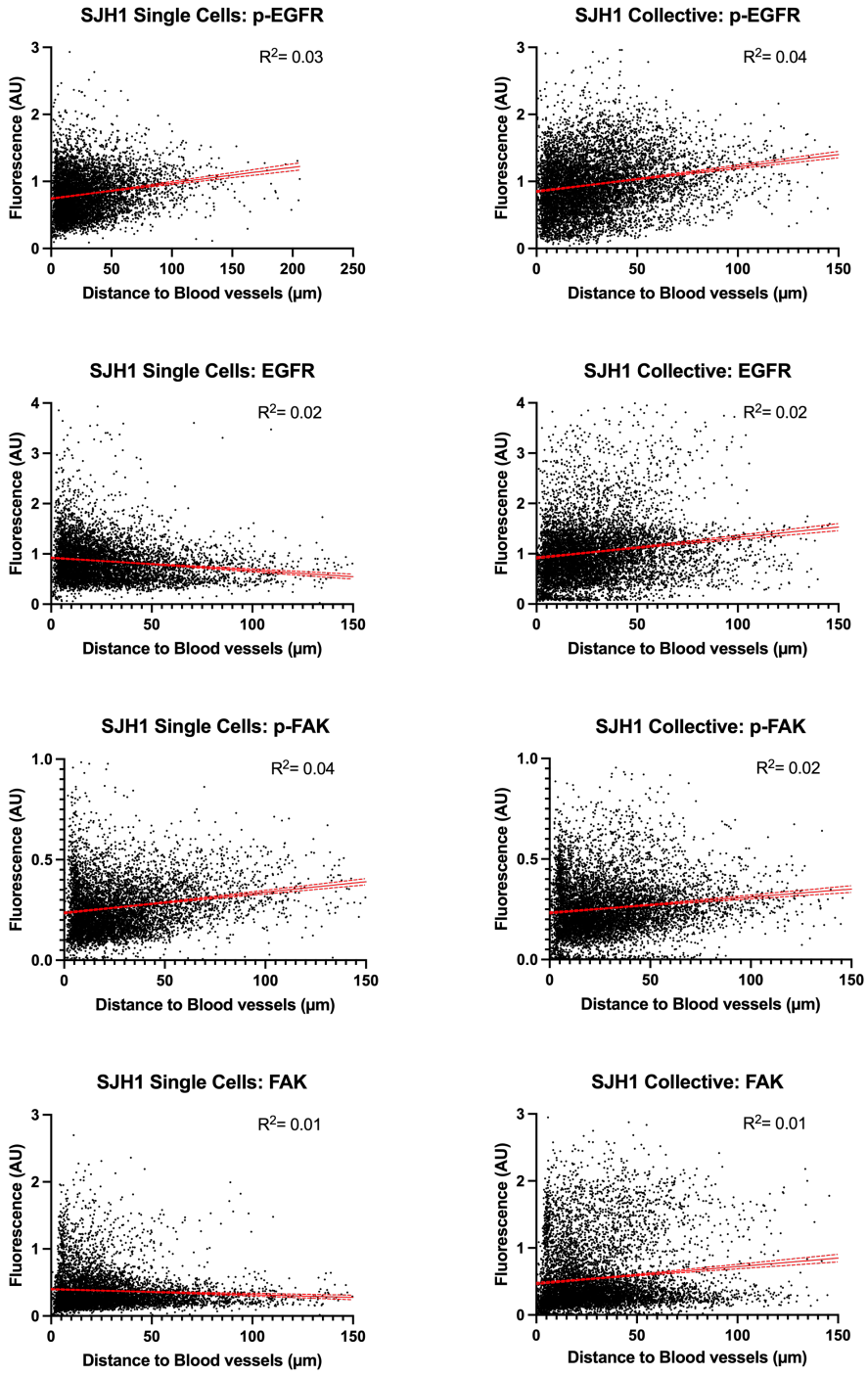

Figure 4.19: **Phosphorylation of EGFR and FAK in Human SJH1 GBM Xenograft in Relation to Distance from the GLUT-1 Positive Blood Vessels in the Mouse Brain, Segmented by Cells Found Individually and as Clusters**

IF staining was performed for p-EGFR, EGFR, p-FAK and FAK in HLA positive cells in 5 μm thick, whole brain sections of human GBM SJH1 cell lines. Cells were segmented into single-cells and clusters using nearest neighbour analysis. Fluorescence was measured as normalised counts (Fluorescent intensity normalised to the exposure value for each section). Individual values were plotted against the distance of the measured cell from the nearest GLUT-1 positive blood vessel. A linear regression analysis was performed to determine the line of best fit with the goodness of fit determined by the R^2 value.

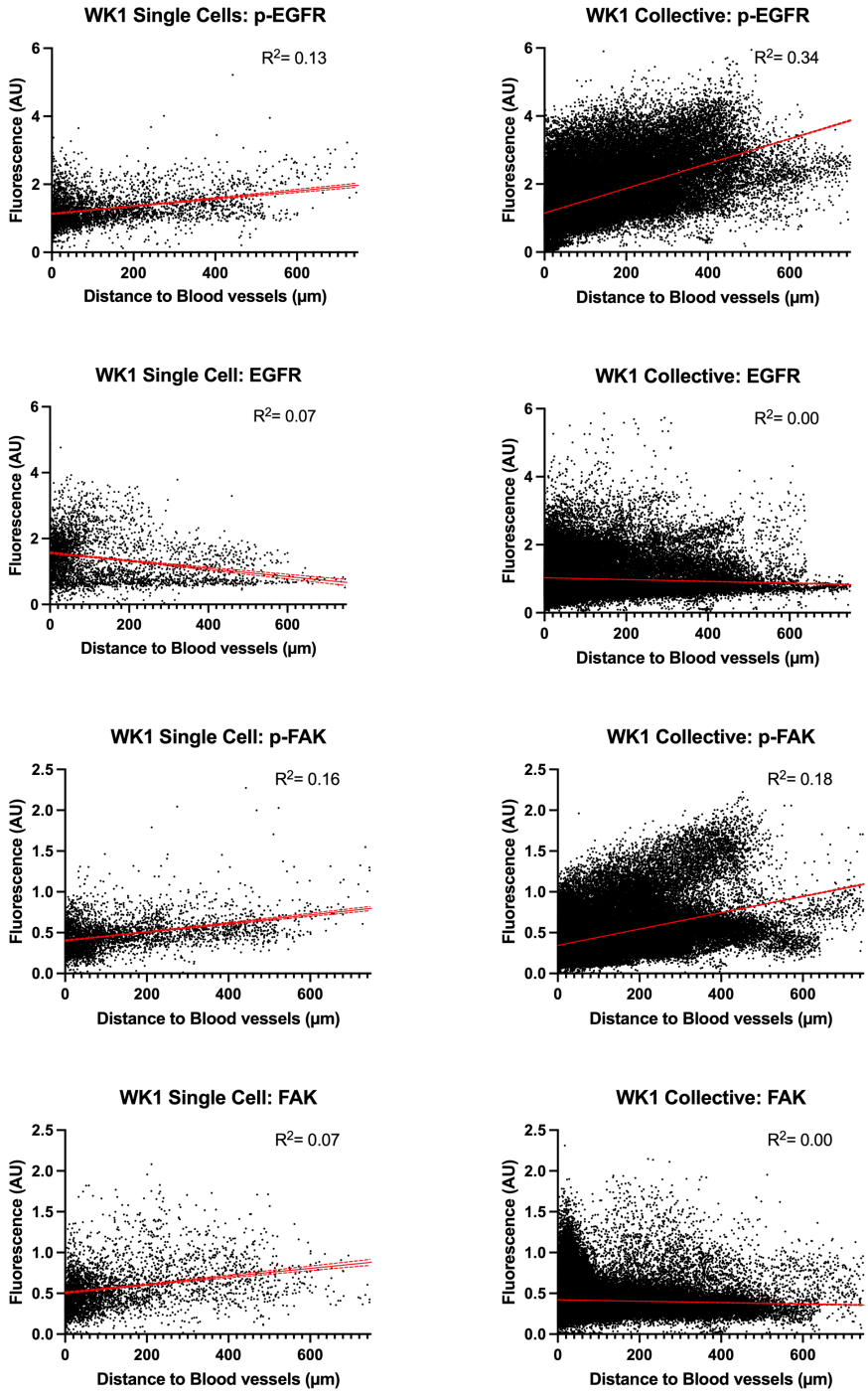

Figure 4.20: **Phosphorylation of EGFR and FAK in Human WK1 GBM Xenograft in Relation to Distance from the GLUT-1 Positive Blood Vessels in the Mouse Brain, Segmented by Cells Found Individually and as Clusters**

IF staining was performed for p-EGFR, EGFR, p-FAK and FAK in HLA positive cells in 5 μm thick, whole brain sections of human GBM WK1 cell lines. Cells were segmented into single-cells and clusters using nearest neighbour analysis. Fluorescence was measured as normalised counts (Fluorescent intensity normalised to the exposure value for each section). Individual values were plotted against the distance of the measured cell from the nearest GLUT-1 positive blood vessel. A linear regression analysis was performed to determine the line of best fit with the goodness of fit determined by the R^2 value.

4.2.11 The Correlation of FAK Phosphorylation to the Distance from Blood Vessels is Diminished in Single-Cell Migration in a Cell-Dependent Manner

Next, the relationship between FAK expression and phosphorylation in individual versus cell clusters with cell position relative to GLUT-1 positive blood vessels was analysed. For JK2 (Figure 4.17), RN1 (Figure 4.18), and SJH1 cell lines Figure (4.19), there is no correlation between FAK expression or FAK phosphorylation as a function of distance from GLUT-1 positive blood vessels in cells located as individuals or clusters.

In WK1 cells (Figure 4.20), following segmentation there continued to be no correlation between distance from blood vessels and FAK expression in clusters: R^2=0.00, with a minimal correlation in individual cells: R^2=0.07. However, there was a correlation between increased FAK phosphorylation and distance from blood vessels (clusters: R^2=0.18, individual cells: R^2=0.16). The data suggest that FAK phosphorylation increases with increased distance from GLUT-1 positive blood vessels in cells found as clusters. Although FAK phosphorylation in individual cells increases with increasing distance from GLUT-1 positive blood vessels (R^2=0.16), the correlation of FAK expression with GLUT-1 positive blood vessels (R^2=0.07), suggests that when compared to cells found as a group, there is a decreased influence of distance to GLUT-1 positive blood vessels on FAK phosphorylation in single cells.

4.3 Chapter Discussion

The movement and spread of glioma cells via the "Secondary Structures of Scherer" (Scherer [1938]) are influenced by mechanosensation, which involves integrins that engage with intracellular pathways such as EGFR and FAK (Buxboim et al. [2010], Rea et al. [2013], Sarker et al. [2020]). In this chapter, the relationship between EGFR and FAK phosphorylation in human GBM xenografts in mouse brain, was explored as a function of proximity to stiffer blood vessels in an otherwise soft brain parenchyma (Bellail et al. [2004], Reiter et al. [2023]).

4.3.1 The Difficulties of IF on Thick FFPE Sections

The use of thick histological sections is the ideal approach in studies exploring the spatial relationship between cells and structures in the surrounding parenchyma (Figure 4.1). A recent 3D reconstruction study by Ghose et al. [2023] exploring the relationship between immune cells in the skin and the vasculature found that there are significantly shorter distances between immune cells and vascular endothelial cells when measurements were taken in 3D reconstruction assays compared to 2D assays (56μm in 3D vs 108μmm in 2D) (Ghose et al. [2023]). Despite this, 2D spatial analysis continues to be the method of choice for most studies due to accessibility, cost, and technical ease. Studies as recent as 2023 by Lin et al. used whole slide 2D analysis to adequately quantify a range of cellular interactions and regions in colorectal cancer (Ghose et al. [2023], Lin et al. [2023]). Confocal imaging protocols routinely image depths 50-100 μm with imaging depths up

to 2mm being reported with customised clearing protocols (Ghose et al. [2023], Silvestri et al. [2016]. These protocols, however, are limited by the ability to multiplex only a small number of markers (Ghose et al. [2023]). Light-sheet microscopy complemented by tissue clearing methods has been employed to visualise brain tissue samples measuring 7cm^3 (Schueth et al. [2023]). Although Pesce et al. documented a greater number of multiplexed markers, light-sheet microscopy encounters limitations with lower cellular-level resolution (Ghose et al. [2023]).

Thick FFPE sections are also hampered by inherent AF, arising from many sources, including connective tissue components, cellular cytoplasmic contents, and fixatives and preservatives used to embed tissues (Davis et al. [2014]). Spectral analysis was performed on unstained sections of thick mouse brain tissue (Figure 4.2) to show that the emission profile of the unstained brain section is evident over a wider range of wavelengths compared to that of skin, colon, and heart tissue (Baharlou [2022]), corresponding to the commonly used excitation / emission spectra used in IF (Im et al. [2019]). Attempts to quench AF, using previously reported methods, were insufficient to improve image integrity (Figure 4.4) and hence not used (Erben et al. [2016], Oliveira et al. [2010]). In prior studies, unembedded 100 μm thick paraformaldehyde-fixed brain tissues were utilised to illustrate specific perivascular invasion and morphology of human GBM cell lines in mouse xenografts (Gupta et al. [2024]). Nevertheless, this thesis was limited to the use of FFPE tissues.

Due to additional issues with using thick FFPE sections, including the brittleness of the sections, the phenomenon of photobleaching when imaging thick sections, the

computing power required to analyse 3D sections, and poor penetration of antibodies into thick sections (Ciani et al. [2023], Smart et al. [2023], Taqi et al. [2018]), thin whole slide images were used in this thesis.

4.3.2 Single-Cells Cells Differ From Cells Which Cluster

The challenges of GBM are due to the diffuse invasion of tumour cells into the brain, which prevents complete surgical removal and leads to recurrence from cells beyond the resection margin (Cuddapah et al. [2014], Garcia-Diaz et al. [2023], Gupta et al. [2024]). GBM tumours exhibit significant inter- and intra-tumour heterogeneity (Brennan et al. [2013], Garcia-Diaz et al. [2023], Patel et al. [2014], Sottoriva et al. [2013], Verhaak et al. [2010]), yet current research predominantly focuses on the tumour bulk rather than the invasive cells responsible for recurrence (Gupta et al. [2024]). The micro-environments differ between the tumour core and the invasive edge, affecting the biological characteristics of cells in these regions (Brooks and Parrinello [2017], Garcia-Diaz et al. [2023], Glas et al. [2010], Venkataramani et al. [2022]). These differences may have important implications for the development of effective therapies for GBM (Garcia-Diaz et al. [2023]).

GBM exhibits the ability to infiltrate three-dimensional astrocyte models, mouse brain xenografts, and human tumour samples, both as solitary cells and in clusters (Gritsenko et al. [2017]). Specifically, GBM cells maintain their intercellular connections as they migrate along blood vessels and astrocyte-rich brain stroma, highlighting the importance of collective migration in HGG cell invasion into brain tissue (Cuddapah et al. [2014],

Farin et al. [2006], Gritsenko et al. [2017], Volovetz et al. [2020], Winkler et al. [2009]). Glioma cells have been observed to invade natural collagen scaffolds (Gritsenko et al. [2017], Grundy et al. [2016], Yang et al. [2010]). However, in the unmodified brain, collagen is predominantly found alongside blood vessels rather than in the broader brain parenchyma (Bellail et al. [2004], Gritsenko et al. [2012]), leaving the applicability of these observations for clarifying GBM migration patterns *in vivo* somewhat ambiguous (Gritsenko et al. [2017], Rape et al. [2014]).

In this chapter, primary-patient-derived GBM cells were segmented from mouse brain in xenograft mouse models using IF and HLA staining. Human GBM cells were then further segmented into single-cells, suggestive of individual migration, and those co-located with other GBM cells, suggesting collective migration, using Delaunay triangulation analysis (Gabriel and Sokal [1969], Goltsev et al. [2018]). In this analysis, inter-tumour differences were evident with a higher proportion of SJH1 cells (45%) appearing as individual cells compared to only 2% of WK1 cells located as single cells (Figure 4.11). Some of this difference may be explained by the location of the analysed section in relation to the site of initial tumour injection, with a section close to the tumour initiation site and tumour bulk potentially demonstrating a greater proportion of clustered GBM cells compared to a more distal tissue section. The influence of this was partially mitigated by the use and analysis of whole-sliding images to capture more spatial data. Despite this potential limitation, the data from Chapter 3 demonstrate that RN1 cells that migrated out of the spheroid bulk showed a strong preference to migrate as individuals while WK1 cells, representing the classical subtype, displayed a more diffuse migration in large

collections, which agree with results presented in this chapter using an ex vivo xenograft assay and previous studies on 2D cell culture (Figure 4.11) (Rosén et al. [2023]).

GBM cells have been suggested to use blood vessels for short-distance invasion, and the local recurrence seen after surgical removal of the tumour bulk may originate from these cells hiding along the peri-tumoral vasculature (Gupta et al. [2024]). Furthermore, the migration pattern of a given GBM cell line is reproducible and specific to the cell line when using patient-derived HGG cells, xenografted into a mouse brain model (Gupta et al. [2024]). In fact, this chapter suggests that the invasion and migration patterns of GBM tumour spheroids in PAHG explored in Chapter 3 are also observed in primary patient-derived xenograft models and highlight to an extent that the migration pattern is dictated by intrinsic mechanisms of glioma cells. Interestingly, data of cells migrating in 2D from spheroids explored in Chapter 3, suggest that SJH1 cells are very mechanosensitive in both single-cell and collective migration and showed a linear relationship between migration and underlying substrate stiffness (Figure. 3.5, Figure. 3.6 & Figure. 3.8). The closer distance of SJH1 cells that appear as single cells to GLUT-1 positive blood vessels may suggest that these cells use the stiffer perivascular space as a route of dissemination as suggested by Scherer (Reiter et al. [2023], Scherer [1938]. Data from Chapter 3 suggested that WK1 is mechano-insensitive during single-cell migration and mechano-sensitive when undergoing collective migration. This is in agreement with the data presented here with single WK1 cells further away from the GLUT-1 positive blood vessels compared to WK1 cells found as clusters (Figure 4.12). One hypothesis is that the mechano-insensitive single-cell migrating WK1 cells invade into the brain parenchyma

diffusely, while collectively migrating WK1 cells use blood vessels as a scaffold to migrate and invade. When considering the spatial relationship with GLUT-1 positive blood vessels, no significant differences emerged between single cells and clustered cells in the JK2 and SJH1 cell lines. It is important to note that the distance measurements of cells to GLUT-1 positive blood vessels in all xenograft sections exhibited considerable variability. This could be attributed to the sections' orientation as well as varying densities of cells and blood vessels in each section (Figure 4.1). Furthermore, the average survival time of the xenografts differed, ranging from 81 days for the RN1 cell line to 150 days for the WK1 cell line (Stringer et al. [2019]), suggesting that the duration of GBM invasion should be considered a potential contributing factor. Moreover, future research should aim to address the separation of angiogenesis impedance into tumour mass versus migration along pre-existing vascular. Finally, the roles of actively invading and senescent GBM cells should be investigated using morphological changes and biomarkers (Rossi and Abdelmohsen [2021]).

GSEA enrichment analysis in Chapter 3 revealed the enrichment of pathways associated with FA in SJH1 and WK1 cell lines, but not in RN1 or JK2 cell lines. Interestingly, when the differences between the association of GBM cells with GLUT-1 positive blood vessels were segmented by cell clustering (single cell versus collectives of cells), only SJH1 and WK1 cells demonstrated a significant difference between the two patterns suggesting a potential role of mechanobiology in the prediction of dissemination, potentially mediated by FAs.

As the EFGR and FAK pathways are involved in the migration and invasion of GBM

cells in the brain (Buxboim et al. [2010], Rea et al. [2013], Sarker et al. [2020]), the phosphorylation of these proteins was analysed as a function of distance from the stiffer blood vessels in an otherwise soft brain parenchyma (Bellail et al. [2004], Reiter et al. [2023]). Fascinatingly, WK1 cells, belonging to the classical subtype typified by *EGFR* amplification (Wang et al. [2017]), demonstrated an increase in EGFR and FAK phosphorylation with increasing distance from GLUT-1 positive blood vessels in cells appearing as clusters, which is diminished in single-cells. This contrasts with previous studies that have shown an increased phosphorylation of EGFR with increasing substrate stiffness in commercially available U-87 GBM cell lines (Umesh et al. [2014]). This may be due in part to molecular alterations in commercially available continuously cultured cell lines compared to patient-derived primary cell lines used in this study, which better represent tumours *in-vivo* (Pollard et al. [2009], Stringer et al. [2019]). Furthermore, a study by Garcia-Diaz et al. [2023] utilising single-cell RNA sequencing to profile GBM cells in a mouse xenograft model to reveal that cells at the tumour margin differ from the bulk of the tumour, supporting the current findings in the phosphorylation of signalling markers in cells appearing individually and those which appear in clusters. Alternatively, the observed findings may be due to biochemical factors in the microenvironment which vary with increasing distance from blood vessels such as hypoxia and availability of nutrients (Rademakers et al. [2019]). Observing a minimal correlation between proximity to blood vessels and expression of EGFR / FAK in the JK2, RN1, SJH1 cell lines prompts the question of whether additional components and pathways of ECM could affect migration patterns of GBM. Collagen, a predominant factor that contributes to ECM stiffness, is well researched, particularly regarding how cancer cells alter their mechanical properties,

such as pore size, density, stiffness, and viscoelasticity (Saraswathibhatla et al. [2023]). Increased collagen has been shown to trigger the AKT pathway in breast-cancer cell (Chen et al. [2013b]), with EGFR/FAK independent activation of the AKT pathway reported (Dobashi et al. [2009], Velling et al. [2004]), and so further studies may wish to explore this mechanism.

4.4 Concluding Remarks

In summary, the work in this chapter highlights a relationship between cell clusters that potentially reflect collective invasion versus individual cells that may reflect individual invasion, and distance from blood vessels. Furthermore, it suggests that the analysis of the tumour bulk alone may not reflect the entire tumour nor the invasive edge and that consideration of the entirety of the tumour would need to be taken into consideration when investigating future therapies for this devastating disease. Comparative profiling studies on a large number of cell lines with well-defined migration patterns and mechano-biology are likely to be informative.

Chapter 5

Mechanical Properties of Brain Tumours and Normal Brain

The soft mechanical characteristics of the brain environment affect cellular behaviours (Budday et al. [2015, 2020], Pillai and Franze [2024]), which has consequences for high-grade glioma (HGG) therapies (Pillai and Franze [2024], Sarker et al. [2020], Sohrabi et al. [2023]). Therapies deemed successful in preclinical tests in rigid cell cultures often fail in clinical trials (Cruz Da Silva et al. [2021], Gunjur et al. [2022], Oster et al. [2023]), underscoring the need to define brain stiffness and its changes during treatments such as surgery, chemotherapy and radiation. Understanding brain stiffness could lead to the identification of new therapeutic targets and the optimisation of treatment timing.

Due to inconsistency in the reported values obtained for *in-vivo* brain tissue from MRE in the literature (Budday et al. [2020], Chatelin et al. [2010], Manduca et al. [2021]), a systematic review was performed here to methodically evaluate the published literature on

brain stiffness over a range of transducer frequencies, brain locations, and reported stiffness modality. This chapter aimed to determine the changes in the stiffness of the tumour mass and the surrounding brain parenchyma induced by radiotherapy, chemotherapy, and surgical intervention compared to a healthy brain to inform the future development of models that truly reflect the brain parenchyma and consequently lead to improved preclinical development of successful therapies.

5.1 Literature Search

Systematic review was conducted in accordance with the Preferred Reporting Items for Systematic Reviews and Meta-Analysis (PRISMA) guidelines (Page et al. [2021]). Ovid MEDLINE, Ovid Embase, PubMed, Web of Science and Google Scholar were searched on 11 July 2024. Combined database-specific subject headings with free text terms in the title, abstract and keyword fields for “Brain”, “Tumour”, “Cancer” , “MRE” and “Magnetic Resonance Elastography” were used. Articles with the term “review” in the title and keyword field were excluded. 2 reviewers evaluated studies based on the following criteria:

1. **Inclusion Criteria**

    (a) Publications in English

    (b) Peer-Reviewed Journal Articles

    (c) Full-Text Articles

    (d) MRE on entirely normal healthy human brain with and without comparison

to human subjects with brain tumours OR MRE in animal models reporting on results of tumours in the brain with and without comparison to healthy controls

2. **Exclusion Criteria**

   (a) Literature Review, Systematic reviews/Meta-analyses , Conference Abstracts, Thesis, Pre-Print Articles

   (b) Studies not reporting quantitative data

   (c) Studies without a statement of Ethics

Study selection was performed using Covidence (Covidence systematic review software, Veritas Health Innovation, Melbourne, Australia. Available at www.covidence.org.) which is a web-based collaboration software platform that streamlines the production of systematic reviews and other reviews of the literature.

2,203 studies were identified from database searching with 1,000 studies identified from Ovid MEDLINE, 511 studies identified from PubMed, 408 studies identified from Ovid Embase, 212 studies from Web Of Science and 72 identified from Google Scholar. 866 duplicate records were removed by Covidence. 1,337 abstracts were screened and 1,229 were removed for failing to meet all inclusion criteria or meeting an exclusion criteria. Full-text review was performed for the remaining 202 studies. The reasons for exclusion are presented in Figure 5.1.

A total of 90 studies were included in this chapter for systematic review.

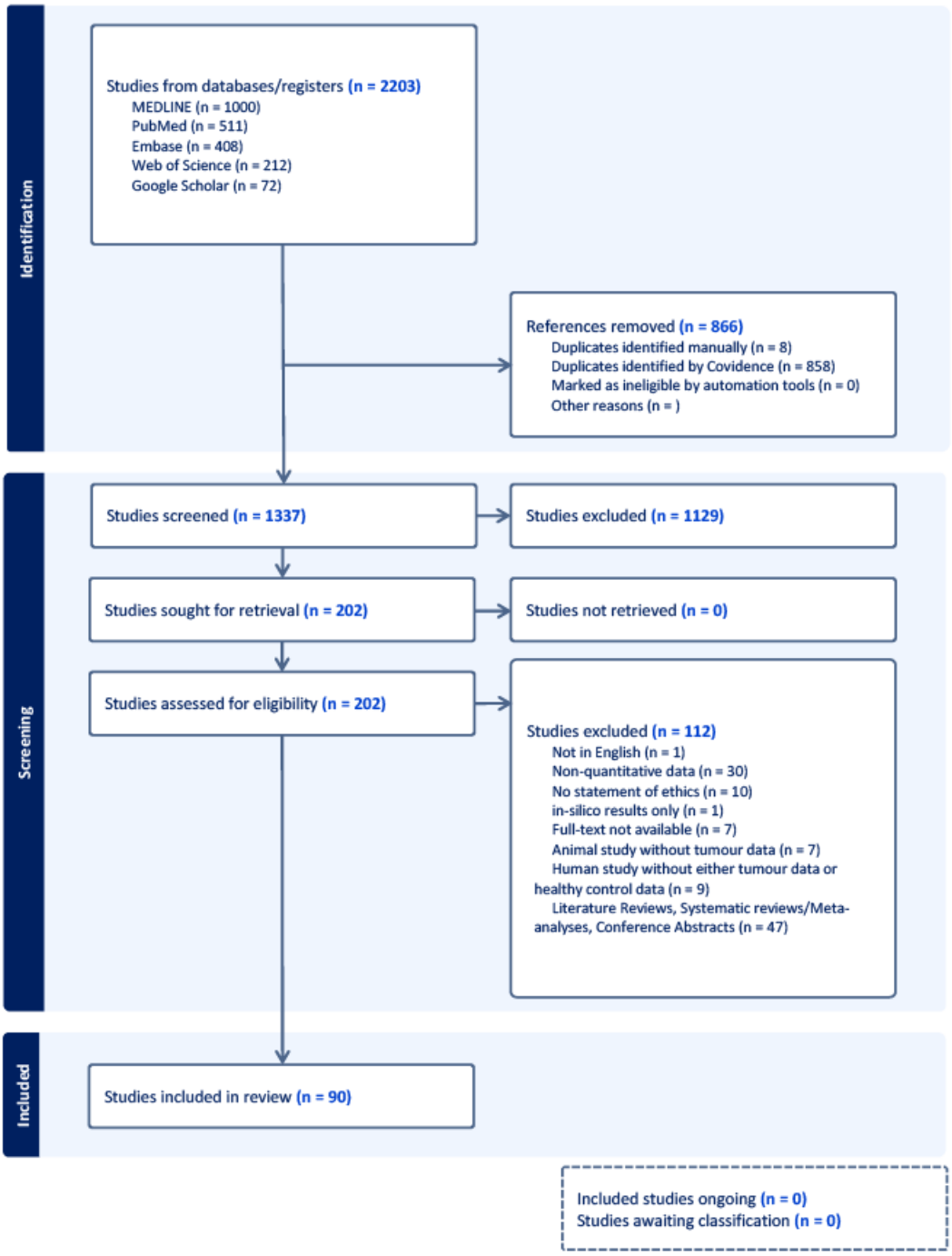

Figure 5.1: **PRSIMA Flow Diagram describing article screening and selection process.**

5.2 Data Extraction

The following data was extracted from the selected studies:

1. **Study Characteristics**
   (a) First Author
   (b) Year of Publication
   (c) Sample Size
2. **Clinical Characterisation**
   (a) Age
   (b) Sex
   (c) Tumour Type (if applicable)
3. **MRE Parameters**
   (a) Resolution
   (b) Analysis Algorithm
   (c) Transducer Frequency
   (d) Measurement Location
4. **Outcomes**
   (a) Estimate and Modality of Stiffness Measurements

The appendices were also reviewed for data. Data were summarised as mean estimates of G', G'', $\mid G^* \mid$ and "shear stiffness" with standard deviation estimates also collected. The "shear stiffness" was defined as a separate modality in this thesis, as it has been inconsistently reported in the past to represent the complex shear modulus or to the density$X$wave speed^2 (Manduca et al. [2021]).

Where data were only presented as graphical data, PlotDigitizer (https://plotdigitizer.com) was used to extract the data. PlotDigitizer is a Java-supported programme that allows the extraction of raw data from X-Y-type scatter or line plots (Aydin and Yassikaya [2022], Jelicic Kadic et al. [2016]).

Where data were not presented as mean and standard deviation, methods previously described by Wan et al. and Chi et al. were used to obtain estimates of the mean and standard deviation of the data presented in the studies (Chi et al. [2023], Wan et al. [2014]).

5.3 Data Analysis

As factors such as transducer frequency and brain subregion (Figure 5.2) influence the measured stiffness reported (Manduca et al. [2021], Pillai and Franze [2024]), the data were segmented by these two factors and a subgroup analysis was performed. The methods described by Neyeloff et al. were used to estimate the population mean of G' and G'', $\mid G^* \mid$ and the shear stiffness for each of the brain regions reported at each reported frequency. This method allows for the meta-analysis of data using a Microsoft Excel

spreadsheet, using either fixed-effects or random-effects model. Where random-effects modelling could not be used due to a single study sample, a fixed effects model was used to estimate the mean and errors of the population (Neyeloff et al. [2012]). The test for intra-study heterogeneity was measured using the Cochran Q test (Q) and I^2. Q is calculated as the weighted sum of squared differences between the effects of the individual study and the pooled effect between the studies (Neyeloff et al. [2012]). I^2 is expressed as a percentage of total variability in a set of effect sizes due to heterogeneity, with higher values indicating more heterogeneity between studies. (Melsen et al. [2014], Neyeloff et al. [2012]).

Linear regression analysis was then performed to compare white and grey matter using Graphpad Prism. G' and G'', $\mid G^* \mid$ and the shear stiffness of various brain tumours were compared to the normal brain using a Z-test with $\alpha = 0.05$.

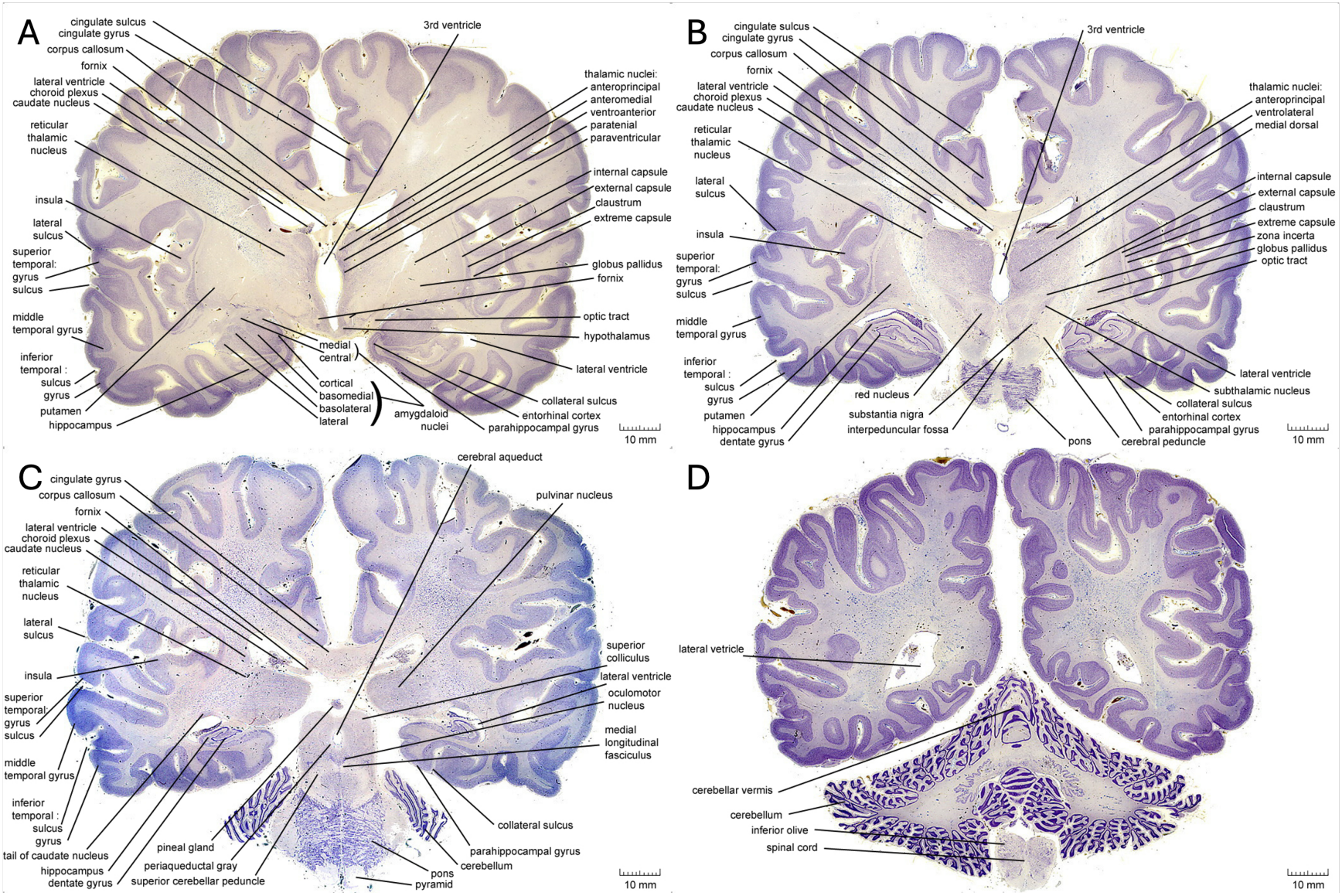

Figure 5.2: **Human Whole Brain Coronal Sections**

Sequential coronal sections of human whole brain stained with hematoxylin and eosin. Images are presented sequentially from most anterior **(A)** to most posterior **(D)**. The images are reproduced with permission from the Michigan State University Brain Biodiversity Bank. https://brains.anatomy.msu.edu/

5.4 Storage Modulus of Normal Brain

17 studies, with 354 subjects in total, reported on G' of the normal brain using shear waves induced at frequencies of 25 (5 studies), 30 (1 study), 37.5 (5 studies), 40 (2 studies), 50 (9 studies), 60 (3 studies), 62.5 (5 studies), 80 (3 studies), 83 (1 study) and 90 Hz (2 studies) (Table 5.1). Linear regression analysis was performed to compare G' of the grey and white matter with the transducer frequency (Figure 5.3). There were no differences in the slopes of the curve (P = 0.15); however, there is a significant difference in the y-intercepts (P=0.0003) suggesting that white matter is stiffer than grey matter.

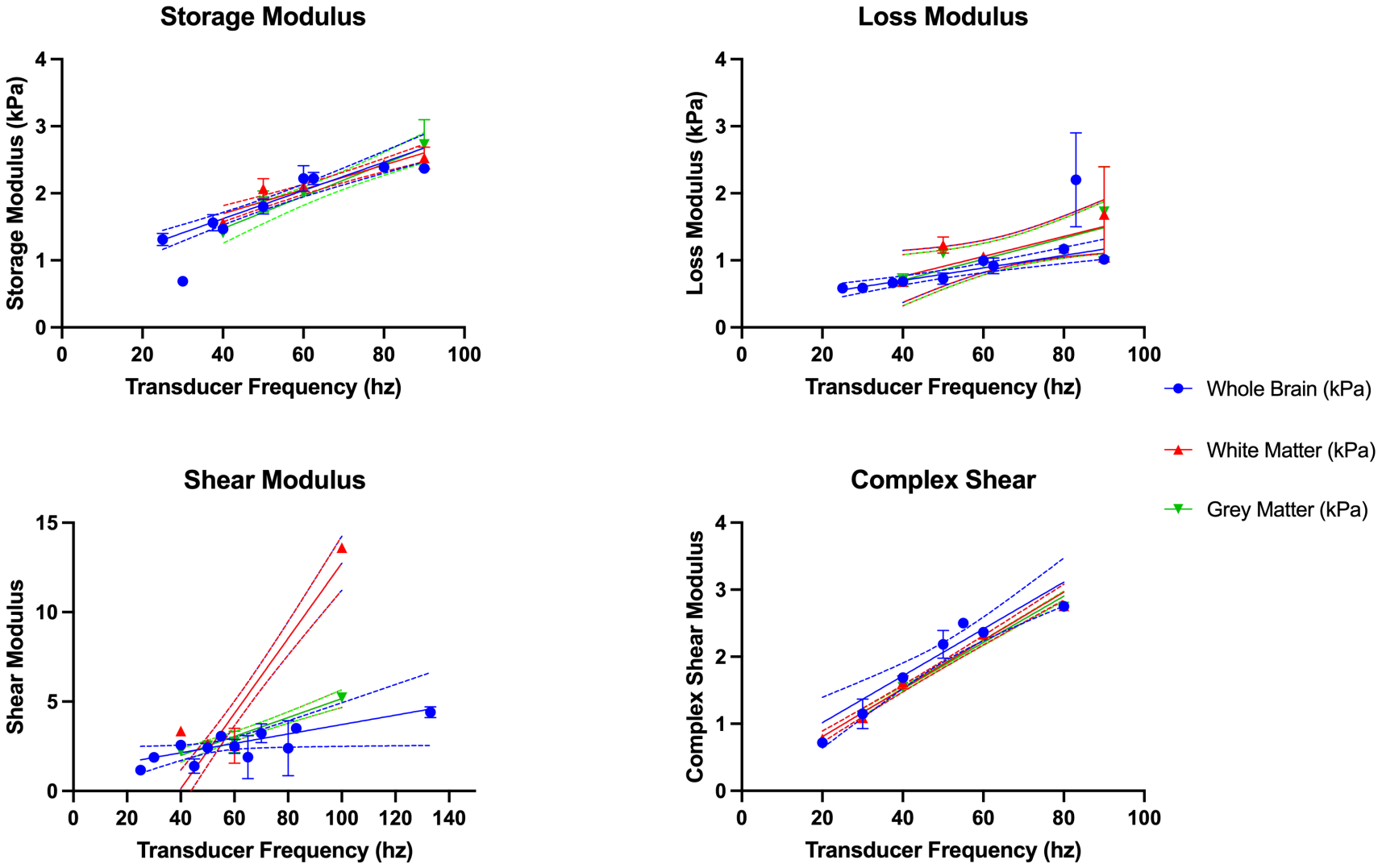

Figure 5.3: **Population estimates for storage, loss, shear and complex shear modulus of human whole brain, white matter and grey matter was determined by meta-analysis of published MRE studies in human subjects.**

Population estimates were plotted against the induction shear frequency used in MRE. Data presented as mean +/- SEM

Table 5.1: **Population estimates for storage modulus of human brain and sub-regions** .

Location	Frequency (Hz)	Studies (n)	Subjects (n)	Mean (kPa)	95% CI (kPa)	Q	I^2
Amygdala	40	1	46	1.84 +/- 0.06	1.72-1.96	0	
	60	1	46	2.3 +/- 0.05	2.2-2.39	0	
	80	1	46	2.52 +/- 0.05	2.43-2.62	0	
	90	1	46	2.53 +/- 0.05	2.43-2.64	0	
Brainstem	50	1	3	3.01 +/- 0.32	2.38-3.64	0	
Caudate Nucleus	40	1	46	1.47 +/- 0.05	1.38-1.57	0	
	50	2	32	1.21 +/- 0.28	0.66-1.76	130	99.23
	60	1	46	2.05 +/- 0.04	1.96-2.13	0	
	80	1	46	2.49 +/- 0.04	2.41-2.57	0	
	90	1	46	2.37 +/- 0.05	2.27-2.46	0	
Corona Radiata	50	2	8	2.78 +/- 0.14	-2.04-6.85	0	
Corpus Callosum	50	2	8	3.09 +/- 0.15	2.8-3.38	0	
Frontal Lobe	50	2	32	1.44 +/- 0.21	1.03-1.85	88	98.87
Grey Mattter	40	2	72	1.41 +/- 0.06	1.29-1.53	8	88.16
	50	3	27	1.88 +/- 0.16	1.57-2.19	57	96.51
	60	2	72	2.01 +/- 0.06	1.89-2.13	14	92.80
	80	3	80	2.36 +/- 0.02	2.31-2.4	2	18.21
	90	2	51	2.73 +/- 0.37	2.01-3.45	184	99.46
Hippocampus	40	1	46	1.46 +/- 0.04	1.38-1.55	0	

Table 5.1 Population estimates for storage modulus of human brain and sub-regions - ***continued from previous page***

Location	Frequency (Hz)	Studies (n)	Subjects (n)	Mean (kPa)	95% CI (kPa)	Q	I^2
	50	2	32	1.52 +/- 0.31	0.91-2.13	68	98.54
	60	1	46	2.23 +/- 0.03	2.16-2.3	0	
	80	1	46	2.86 +/- 0.05	2.75-2.97	0	
	90	1	46	0.63 +/- 0.03	0.57-0.68	0	
Occipital Lobe	50	2	32	1.28 +/- 0.16	0.96-1.59	18	94.55
Pallidum	40	1	46	1.77 +/- 0.05	1.68-1.87	0	
	60	1	46	2.22 +/- 0.05	2.12-2.32	0	
	80	1	46	2.32 +/- 0.04	2.24-2.4	0	
	90	1	46	2.16 +/- 0.04	2.08-2.25	0	
Parietal Lobe	50	2	32	1.53 +/- 0.21	1.11-1.94	30	96.67
Putamen	40	1	46	1.85 +/- 0.04	1.76-1.93	0	
	50	2	32	1.5 +/- 0.28	0.95-2.05	99	98.99
	60	1	46	2.27 +/- 0.03	2.2-2.34	0	
	80	1	46	2.53 +/- 0.04	2.45-2.61	0	
	90	1	46	2.34 +/- 0.05	2.24-2.44	0	
Subcortical Grey Matter	40	1	46	1.48 +/- 0.03	1.41-1.55	0	
	60	1	46	2.01 +/- 0.03	1.95-2.06	0	
	80	1	46	2.31 +/- 0.03	2.25-2.36	0	
	90	1	46	2.23 +/- 0.04	2.15-2.3	0	
Temporal Lobe	50	2	32	1.58 +/- 0.23	1.13-2.03	73	98.64

Table 5.1 Population estimates for storage modulus of human brain and sub-regions - *continued from previous page*

Location	Frequency (Hz)	Studies (n)	Subjects (n)	Mean (kPa)	95% CI (kPa)	Q	I^2
Thalamus	40	1	46	1.23 +/- 0.04	1.15-1.31	0	
	50	2	32	1.17 +/- 0.23	0.72-1.62	194	99.48
	60	1	46	2 +/- 0.03	1.93-2.07	0	
	80	1	46	2.36 +/- 0.04	2.28-2.44	0	
	90	1	46	2.2 +/- 0.05	2.1-2.29	0	
White Matter	40	2	72	1.56 +/- 0.05	1.46-1.65	6	82.15
	50	6	50	2.07 +/- 0.15	1.78-2.36	290	98.28
	60	2	72	2.1 +/- 0.04	2.03-2.18	6	83.59
	80	3	80	2.43 +/- 0.02	2.39-2.47	1	0.00
	90	2	51	2.53 +/- 0.16	2.21-2.86	35	97.18
Whole Brain	25	5	181	1.31 +/- 0.09	1.13-1.49	324	98.77
	30	1	9	0.69 +/- 0.02	0.65-0.73	0	
	37.5	5	181	1.56 +/- 0.12	1.33-1.8	261	98.47
	40	2	72	1.47 +/- 0.04	1.4-1.54	3	65.47
	50	7	197	1.8 +/- 0.11	1.58-2.01	516	98.84
	60	3	117	2.22 +/- 0.19	1.84-2.6	484	99.59
	62.5	5	181	2.22 +/- 0.09	2.04-2.4	178	97.75
	80	2	72	2.39 +/- 0.01	2.36-2.41	0	0.00
	90	1	46	2.37 +/- 0.03	2.31-2.43	0	

5.5 Loss Modulus of Normal Brain

15 studies, with 310 subjects in total reported on the G'' of normal brain using shear waves induced at frequencies of 25 (5 studies), 30 (1 study), 37.5 (5 studies), 40 (2 studies), 50 (8 studies), 60 (2 studies), 62.5 (5 studies), 80 (3 studies), 83 (1 study) and 90 Hz (2 studies) (Table 5.2). When linear regression analysis is performed to compare the G'' of grey and white matter with the transducer frequency (Figure 5.3), there is no difference in the slope of the curves (P = 0.93); however, there is a significant difference in the y-intercepts (P=0.0005) suggesting that white matter is stiffer than grey matter.

Table 5.2: **Population estimates for loss modulus of human brain and sub-regions** .

Location	Frequency (Hz)	Studies (n)	Subjects (n)	Loss Modulus (kPa)	95% CI (kPa)	Q	I^2
Amygdala	40	1	46	0.68+/-0.03	0.62-0.75	0	
	60	1	46	1.05+/-0.04	0.97-1.14	0	
	80	1	46	1.07+/-0.04	0.98-1.15	0	
	90	1	46	0.82+/-0.05	0.73-0.92	0	
Caudate Nucleus	40	1	46	0.59+/-0.03	0.53-0.65	0	
	50	1	17	0.84+/-0.04	0.76-0.92	0	
	60	1	46	0.8+/-0.03	0.74-0.85	0	
	80	1	46	0.91+/-0.03	0.84-0.97	0	
	90	1	46	0.68+/-0.03	0.62-0.75	0	
Corona Radiata	50	1	7	1.97+/-0.05	1.88-2.06	0	
Corpus Callosum	50	1	7	1.23+/-0.1	1.04-1.42	0	

Table 5.2 Population estimates for loss modulus of human brain and sub-regions - *continued from previous page*

Location	Frequency (Hz)	Studies (n)	Subjects (n)	Loss Modulus (kPa)	95% CI (kPa)	Q	I^2
Frontal Lobe	50	1	17	1.14+/-0.03	1.09-1.19	0	
Grey Matter	40	2	72	0.71+/-0.09	0.52-0.89	62	98.39
	50	3	27	1.1+/-0.05	1-1.21	7	70.69
	60	2	72	0.96+/-0.04	0.89-1.04	17	94.14
	80	3	80	1.15+/-0.02	1.1-1.19	13	84.29
	90	2	51	1.72+/-0.67	-1.27-3.05	207	99.52
Hippocampus	40	1	46	0.91+/-0.02	0.87-0.95	0	
	50	1	17	0.96+/-0.03	0.91-1.01	0	
	60	1	46	1.2+/-0.03	1.15-1.26	0	
	80	1	46	1.09+/-0.04	1.01-1.17	0	
	90	1	46	1.44+/-0.04	1.36-1.51	0	
Occipital Lobe	50	1	17	1.17+/-0.03	1.11-1.23	0	
Pallidum	40	1	46	0.67+/-0.03	0.61-0.73	0	
	60	1	46	1.09+/-0.04	1.01-1.18	0	
	80	1	46	0.86+/-0.04	0.77-0.94	0	
	90	1	46	0.52+/-0.03	0.46-0.57	0	
Parietal Lobe	50	1	17	1.23+/-0.02	1.18-1.28	0	
Putamen	40	1	46	0.87+/-0.04	0.8-0.95	0	
	50	1	17	1.11+/-0.05	1.01-1.21	0	
	60	1	46	1.14+/-0.04	1.07-1.21	0	

Table 5.2 Population estimates for loss modulus of human brain and sub-regions - ***continued from previous page***

Location	Frequency (Hz)	Studies (n)	Subjects (n)	Loss Modulus (kPa)	95% CI (kPa)	Q	I^2
	80	1	46	1.07+/-0.04	1-1.15	0	
	90	1	46	0.72+/-0.04	0.65-0.79	0	
Subcortical Grey Matter	40	1	46	0.58+/-0.02	0.54-0.62	0	
	60	1	46	0.88+/-0.02	0.83-0.92	0	
	80	1	46	0.9+/-0.03	0.84-0.95	0	
	90	1	46	0.67+/-0.03	0.61-0.72	0	
Temporal Lobe	50	1	17	1.32+/-0.03	1.27-1.37	0	
Thalamus	40	1	46	0.35+/-0.02	0.31-0.38	0	
	50	1	17	0.73+/-0.03	0.67-0.79	0	
	60	1	46	0.69+/-0.02	0.66-0.73	0	
	80	1	46	0.72+/-0.02	0.67-0.77	0	
	90	1	46	0.49+/-0.03	0.44-0.55	0	
White Matter	40	2	72	0.68+/-0.01	0.66-0.7	0	0.00
	50	4	34	1.23+/-0.12	0.99-1.46	185	98.38
	60	2	72	1.05+/-0.06	0.95-1.16	22	95.46
	80	3	80	1.18+/-0.02	1.15-1.22	0	0.00
	90	2	51	1.69+/-0.71	0.29-3.08	230	99.57
Whole Brain	25	5	181	0.58+/-0.05	0.48-0.68	302	98.68
	30	1	9	0.59+/-0.02	0.55-0.62	0	
	37.5	5	181	0.66+/-0.07	-0.6-1.57	384	98.96

Table 5.2 Population estimates for loss modulus of human brain and sub-regions - *continued from previous page*

Location	Frequency (Hz)	Studies (n)	Subjects (n)	Loss Modulus (kPa)	95% CI (kPa)	Q	I^2
	40	2	72	0.69+/-0.04	0.62-0.76	9	89.04
	50	5	181	0.73+/-0.09	0.56-0.9	659	99.39
	60	2	72	1+/-0.03	0.93-1.06	11	91.05
	62.5	5	181	0.92+/-0.12	0.69-1.15	922	99.57
	80	2	72	1.17+/-0	1.16-1.18	0	0.00
	83	1	1	2.2+/-0.7	0.83-3.57	0	
	90	1	46	1.02+/-0.03	0.96-1.07	0	

5.6 Shear Modulus of Normal Brain

28 studies, with 433 subjects in total reported on the "shear stiffness" of normal brain using shear waves induced at frequencies of 25 (1 study), 30 (1 study), 40 (1 studies), 45 (1 study), 50 (19 studies), 55 (1 study), 60 (5 studies), 65 (1 studies), 70 (2 studies), 80 (1 studies), 83 (1 study), 100 (1 studies), and 113 Hz (1 study) (Table 5.3). When linear regression analysis is performed to compare the shear stiffness of grey and white matter with increasing transducer frequency (Figure 5.3), there is a significant difference in the slope of the curves ($P < 0.0001$) suggesting that grey matter may have a higher "shear stiffness" at lower frequencies and a lower "shear stiffness" at higher frequencies compared to white matter. When the single study that reported shear stiffness values at 100 Hz is identified and removed using Grubb's test for outliers, the slopes of the linear

regression analysis curves are not significantly different (P=0.53), however, there is a significant difference in the intercepts (P=0.0369) suggesting that white matter is stiffer than grey matter.

Table 5.3: **Population estimates for shear modulus of human brain and sub-regions**

Location	Frequency (Hz)	Studies (n)	Subjects (n)	Shear Modulus (kPa)	95% CI (kPa)	Q	I^2
Amygdala	50	3	45	3.49+/-0.21	3.07-3.91	32	93.74
Caudate Nucleus	50	3	45	2.96+/-0.43	2.12-3.8	219	99.09
Corona Radiata	50	2	17	2.68+/-0.06	2.57-2.79	0	
Corpus Callosum	50	3	22	2.55+/-0.39	1.79-3.31	372	99.46
Globus Pallidus	50	2	24	3.32+/-0.27	2.78-3.86	17	93.95
Grey Matter	40	1	10	2.24+/-0.04	2.15-2.33	0	
	50	4	41	2.53+/-0.21	2.13-2.94	241	98.75
	60	2	14	2.74+/-0.6	1.56-3.92	44	97.74
	100	1	25	5.22+/-0.05	5.13-5.31	0	
Hippocampus	50	9	236	3.04+/-0.09	2.87-3.22	137	94.15
Pallidum	50	1	21	3.84+/-0.06	3.73-3.95	0	
Putamen	50	3	45	3.63+/-0.16	-4.44-10.18	62	96.77
Subcortical Grey Matter	50	1	12	2.73+/-0.07	2.6-2.86	0	
Thalamus	50	3	45	3.31+/-0.3	2.73-3.89	114	98.24
White Matter	40	1	10	3.36+/-0.03	3.29-3.43	0	
	50	6	54	2.64+/-0.2	2.25-3.02	389	98.71
	60	3	42	2.53+/-0.98	0.61-4.44	2376	99.92

Table 5.3 Population estimates for shear modulus of human brain and sub-regions- ***continued from previous page***

Location	Frequency (Hz)	Studies (n)	Subjects (n)	Shear Modulus (kPa)	95% CI (kPa)	Q	I^2
	100	1	25	13.6+/-0.08	13.45-13.75	0	
Whole Brain	25	1	6	1.17+/-0.01	1.15-1.19	0	
	30	1	8	1.88+/-0.07	1.74-2.01	0	
	40	1	10	2.57+/-0.01	2.55-2.59	0	
	45	1	1	1.4+/-0.4	0.62-2.18	0	
	50	11	97	2.42+/-0.18	2.07-2.78	2302	99.57
	55	1	10	3.07+/-0.16	2.75-3.39	0	
	60	4	58	2.5+/-0.39	1.73-3.27	1860	99.84
	65	1	1	1.89+/-1.2	-0.46-4.24	0	
	70	2	11	3.23+/-0.53	2.2-4.26	58	98.27
	80	1	1	2.4+/-1.54	-0.62-5.42	0	
	83	1	1	3.5+/-0.02	3.47-3.53	0	
	133	1	1	4.4+/-0.3	3.81-4.99	0	

5.7 Complex Shear Modulus of Normal Brain

25 studies, with 579 subjects in total reported on the $\mid G^* \mid$ of normal brain using shear waves induced at frequencies of 20 (2 studies), 30 (3 studies), 40 (2 studies), 50 (6 studies), 55 (1 study), 60 (4 studies) and 80 Hz (1 study). 11 studies investigated $\mid G^* \mid$ of the normal brain using a multi-frequency technique (Table 5.4). When linear regression

analysis is performed to compare the $\mid G^* \mid$ of grey and white matter with the transducer frequency (Figure 5.3), it is found that there is no difference in the slope of the curve (P = 0.51), however, there is a significant difference in the intercepts (P=0.0076) suggesting that white matter is stiffer than grey matter.

Table 5.4: **Population estimates for complex shear modulus of human brain and sub-regions**

Location	Frequency (Hz)	Studies (n)	Participants (n)	Complex Shear Modulus (kPa)	95% CI (kPa)	Q	I^2
Amygdala	Multi-Frequency	1	14	1.07+/-0.03	1-1.14	0	
Basal Ganglia	20	1	42	0.69+/-0.02	0.66-0.73	0	
Capsula Interna	Multi-Frequency	1	12	1.29+/-0.04	-0.28-2.29	0	
Caudate Nucleus	50	1	15	2.98+/-0.1	2.79-3.17	0	
	Multi-Frequency	2	35	0.69+/-0.08	0.53-0.85	4	74.01
Cerebellum	60	2	56	1.77+/-0.03	1.71-1.82	2	53.85
Corpus Callosum	Multi-Frequency	1	23	1.13+/-0.04	1.05-1.21	0	
Crus Cerebri	Multi-Frequency	1	12	1.64+/-0.08	1.49-1.79	0	
Frontal Lobe	20	1	4	1.04+/-0.02	1-1.08	0	
	50	1	15	2.25+/-0.05	2.15-2.35	0	
	60	2	56	2.35+/-0.13	2.1-2.59	28	96.42
	Multi-Frequency	2	29	1.28+/-0.13	1.03-1.53	12	91.65
Globus Pallidus	Multi-Frequency	1	14	1.19+/-0.07	1.05-1.33	0	
Grey matter	30	1	44	1.08+/-0	1.08-1.08	0	
	40	2	70	1.54+/-0.04	1.46-1.63	0	
	60	2	70	2.3+/-0.02	2.26-2.34	0	
	80	1	26	2.74+/-0.03	2.68-2.8	0	
	Multi-Frequency	1	5	1.03+/-0.02	0.99-1.07	0	
Hippocampus	50	1	26	3.06+/-0.05	2.96-3.17	0	
	Multi-Frequency	2	35	1.03+/-0.04	0.96-1.11	2	55.27
Leniform Nucleus	50	1	18	2.21+/-0.05	2.12-2.3	0	
Mesencephalic Nucleus	Multi-Frequency	1	12	0.96+/-0.02	0.91-1.01	0	

Table 5.4 Population estimates for complex shear modulus of human brain and sub-regions- ***continued from previous page***

Location	Frequency (Hz)	Studies (n)	Participants (n)	Complex Shear Modulus (kPa)	95% CI (kPa)	Q	I^2
Nucleus Accumbens	50	1	44	2.94+/-0.05	2.83-3.05	0	
	Multi-Frequency	1	14	1.41+/-0.03	1.35-1.47	0	
Occipital Lobe	20	1	4	0.96+/-0.03	0.91-1.01	0	
	50	1	15	2.75+/-0.05	2.65-2.85	0	
	60	2	56	2.5+/-0.07	2.36-2.65	4	76.46
	Multi-Frequency	1	12	1.45+/-0.05	1.36-1.54	0	
Orbitofrontal Cortex	50	1	44	2.75+/-0.03	2.69-2.81	0	
Parietal Lobe	50	1	15	2.23+/-0.09	2.05-2.41	0	
	60	2	56	2.21+/-0.08	2.04-2.37	6	84.43
Pons	Multi-Frequency	1	12	0.97+/-0.02	0.92-1.02	0	
Putamen	20	1	4	0.94+/-0.09	0.76-1.12	0	
	50	1	15	3.6+/-0.09	3.43-3.77	0	
Putamen	Multi-Frequency	1	14	1.58+/-0.06	1.45-1.71	0	
Striatum	Multi-Frequency	1	12	1.24+/-0.09	1.06-1.42	0	
Temporal Lobe	50	1	15	2.7+/-0.05	2.6-2.8	0	
	60	2	56	2.61+/-0.02	2.57-2.66	0	0.00
Thalamus	20	1	42	0.55+/-0.14	0.27-0.83	0	
	50	1	15	2.42+/-0.07	2.28-2.56	0	
	Multi-Frequency	5	87	1.16+/-0.08	1-1.31	63	93.60
Ventromedial Prefrontal Cortex	50	1	44	2.97+/-0.03	2.9-3.04	0	
White Matter	20	1	42	0.78+/-0.01	0.75-0.8	0	
	30	2	77	1.09+/-0.03	1.03-1.15	0	
	40	2	70	1.62+/-0.1	1.43-1.8	0	
	60	2	70	2.33+/-0.02	2.3-2.37	0	
	80	1	26	2.76+/-0.04	2.68-2.84	0	
	Multi-Frequency	4	78	1.4+/-0.12	1.16-1.63	105	97.13
Whole Brain	20	1	4	0.72+/-0.02	0.69-0.75	0	
	30	2	50	1.15+/-0.22	-0.19-2.51	0	

Table 5.4 Population estimates for complex shear modulus of human brain and sub-regions- ***continued from previous page***

Location	Frequency (Hz)	Studies (n)	Participants (n)	Complex Shear Modulus (kPa)	95% CI (kPa)	Q	I^2
	40	1	36	1.69+/-0.03	1.64-1.74	0	
	50	4	116	2.18+/-0.21	1.78-2.59	242	98.76
	55	1	48	2.5+/-0.01	2.49-2.51	2	7.50
	60	3	82	2.37+/-0.02	2.33-2.4	0	
	80	1	26	2.75+/-0.03	2.68-2.82	0	
	Multi-Frequency	7	127	1.39+/-0.09	1.22-1.56	247	97.57

5.8 MRE of Human Brain Tumours

To date, there are limited numbers of studies that have been performed using MRE to investigate the mechanical characteristics of brain tumours. In total, 11 studies were identified with 142 subjects that investigated G' (2 studies), G'' (2 studies) and $\mid G^* \mid$ (7 studies) of glioblastoma (6 studies), gliomas excluding glioblastoma (4 studies), meningioma (8 studies), B-cell lymphoma (1 study) and brain metastasis (3 studies).

G' of glioblastoma at 50 Hz was compared with the G' of the whole brain at 50 Hz using a two-tailed unpaired t-test with no significant differences observed between the two (P = 0.4147). Similarly, the G'' at 50 Hz was not significantly different between the two (P=0.8555). Other conditions in which G', G'' and $\mid G^* \mid$ were obtained for glioblastoma could not be compared with normal brain due to the lack of comparator values in the published literature.

$\mid G^* \mid$ of gliomas other than glioblastoma is also not significantly different from

normal whole brain measurements at 60 Hz (P= 0.0689). In contrast, the complex shear modulus of meningiomas is significantly higher than that of the normal whole brain at 60 Hz ($P < 0.0001$).

When analysing the $\mid G^* \mid$ values obtained from multi-frequency analysis, compared to normal analysis of the whole brain, glioblastoma is not significantly different (P = 0.5151), nor are other gliomas (P = 0.8909), meningioma (P = 0.3266) or metastasis (P = 0.8225).

Table 5.5: **Population estimates for storage, loss, and complex shear modulus of human brain tumours in published MRE studies**

Tumour	Stiffness Modality	Frequency (Hz)	Studies (n)	Participants (n)	Stiffness (kPa)	95 % CI (kPa)	Q	I^2
B-Cell Lymphoma	Complex Shear Modulus	45	1	1	1.4			
Glioblastoma	Complex Shear Modulus	45	1	3	1.24+/-0.18	0.89-1.59	0.00	
		30-60	4	45	1.29+/-0.04	1.19-1.37	4.36	31.21
	Loss	50	1	10	0.66+/-0.02	0.62-0.70	0.00	
		30-60	1	3	0.63+/-0.07	0.48-0.77	0.00	
	Storage	50	1	10	1.4+/-0.04	1.32-1.48	0.00	
		30-60	1	3	1.09+/-0.09	0.91-1.26	0.00	
Gliomas other than Glioblastoma	Complex Shear Modulus	45	1	7	1.3+/-0.1	1.11-1.49	0.00	
		60	1	18	2.2+/-0.16	1.88-2.52	0.00	

Table 5.5 Population estimates for storage, loss, and complex shear modulus of human brain tumours - *continued from previous page*

Tumour	Stiffness Modality	Frequency (Hz)	Studies (n)	Participants (n)	Stiffness (kPa)	95 % CI (kPa)	Q	I^2
		30-60	2	4	1.46+/-0.1	1.26-1.65	0.47	0.00
	Loss	30-60	1	1	0.77+/-0.39	0.00- 1.54	0.00	
	Storage	30-60	1	1	0.76+/-0.46	0.00- 1.67	0.00	
Meningioma	Complex Shear Modulus	45	1	2	2.09+/-0.04	2.02-2.17	0.00	
		60	1	18	3.12+/-0.29	2.55-3.69	0.00	
		30-60	3	19	1.62+/-0.03	1.57-1.68	1.15	0.00
	Loss	30-60	1	3	1.19+/-0.1	0.99-1.39	0.00	
	Storage	30-60	1	3	1.19+/-0.08	1.03-1.35	0.00	
Metastasis	Complex Shear Modulus	45	1	3	1.25+/-0.14	0.97-1.54	0.00	

Table 5.5 Population estimates for storage, loss, and complex shear modulus of human brain tumours - ***continued from previous page***

Tumour	Stiffness Modality	Frequency (Hz)	Studies (n)	Participants (n)	Stiffness (kPa)	95 % CI (kPa)	Q	I^2
		30-60	2	6	1.84+/-0.17	0.95-1.62	0.02	0.00
	Loss	30-60	1	1	0.61+/-0.32	0.00-1.24	0.00	
	Storage	30-60	1	1	1.06+/-0.21	0.66-1.47	0.00	

5.9 MRE on Animal Brain

Given the small number of studies of human brain tumours, studies that have investigated the mechanical features of brain tumours in mouse models were therefore included. 5 studies used MRE to measure the stiffness of brain tumour animal models with (1 study) or without (4 studies) healthy controls . All studies used glioblastoma as the tumour of interest and were performed in mouse models. Data from 52 mice with glioblastoma (orthotopic xenografts) were included and compared with 6 healthy control mice. G' (1 study), G'' (2 studies) and $\mid G^* \mid$ (2 studies) was investigated at frequencies of 900 (1 study), 1000 (3 studies) and 1800 Hz (1 study).

The G' of glioblastoma at 1000 Hz in a mouse model (1 study) was softer than that of the healthy mouse brain (1 study) (P = 0.0043) as was the G'' of glioblastoma at 1000 Hz in a mouse model (1 study) compared to that of the healthy mouse brain (1 study) (P=0.0001).

Table 5.6: **Population estimates for storage, loss, and complex shear modulus of animal brain tumours with or without healthy controls**

Animal	Tumour	Stiffness Modality	Frequency (Hz)	Studies (n)	Animals (n)	Stiffness (kPa)	95 % CI (kPa)	Q	I squared
Mouse	Glioblastoma	Complex Shear	900	1	20	5.34 +/- Unk		0	
			1000	2	10	5.71 +/- 0.57	4.60 - 6.83	13.218063	92.4345953
		Loss	1000	1	20	2.52 +/- 0.16	2.19 - 2.84	0	
			1800	1	12	3.24 +/- 0.53	2.21 - 4.27	0	
		Storage	1000	1	20	4.25 +/- 0.28	3.70 - 4.80	0	
	Healthy Control	Loss	1000	1	6	4.36 +/- 0.07	4.22 - 4.50	0	
		Storage	1000	1	6	5.89 +/- 0.07	5.75 - 6.03	0	

5.10 Chapter Discussion

5.10.1 Stiffness Values are Influenced by Measurement Modality

Understanding the mechanical properties of the brain is essential to develop effective treatments (Mai et al. [2024], Sarker et al. [2020], Seker-Polat et al. [2022]). This chapter sought to methodically review the published literature using meta-analysis to better define the mechanical environment of the brain parenchyma, specifically focussing on data from MRE studies. The brain demonstrates viscoelasticity, combining both elastic and viscous characteristics, and numerous metrics such as G', G'', $\mid G^* \mid$, and "shear stiffness" are available to evaluate its stiffness (Franze [2013], Manduca et al. [2021], Pillai and Franze [2024]). Furthermore, the measured stiffness values are influenced by the frequency of the applied shear waves. A prior systematic review sought to mitigate differences in data acquisition methodologies between studies by evaluating the stiffness of tumours relative to contralateral normal white matter. However, it did not account for the effects of the transducer frequency on the metrics G', G'', $\mid G^* \mid$, and "shear stiffness" (Bunevicius et al. [2020]). Consequently, in this chapter, the results for these measurements are further segmented by the frequency of the transducer used in MRE. This was validated by examining G', G'', $\mid G^* \mid$, and "shear stiffness" across the whole brain, white matter, and grey matter, all of which increased with higher transducer frequencies, as shown

in Figure 5.3. This observation aligns with earlier studies (Braun et al. [2014], Franze et al. [2013], Guo et al. [2013], Pillai and Franze [2024], Weickenmeier et al. [2018]). Similarly, differences in G' and G'', $\mid G^* \mid$ and "shear stiffness" are seen in various regions of the brain (Sections 5.4-5.7). When comparing white and grey matter using linear regression, it was found that white matter is stiffer than grey matter in the reported values of G' and G'', $\mid G^* \mid$ and "shear stiffness" which is consistent with previously reported MRE data (Budday et al. [2020], Guo et al. [2013], Weickenmeier et al. [2018]) and consistent with rheometric analysis data (Budday et al. [2015], Weickenmeier et al. [2016]).

As seen in tables 5.1-5.4 very few studies report on the mechanical properties of the brain with the same stiffness modality, transducer frequency, and region of interest. Of the 202 estimates of the mechanical properties of the brain presented in tables 5.1-5.4, 92 estimates were from single-study samples. The shear modulus of the normal human whole brain at 50 Hz had the highest number of studies that contributed to the estimation of the population mean with 11 studies. Even with this number of studies, there was a high degree of heterogeneity between studies with an I^2 of 99.57. Similarly, the shear modulus of the normal human hippocampus at 50 Hz had the highest number of subjects who contributed to the estimation of the population mean with 236 participants. Despite this, there was still a high degree of heterogeneity between studies with an I^2 of 94.15, suggesting a substantial contribution from intra-study differences including; patient population characteristics, study methodology, and analysis methods used (Higgins et al. [2003], von Hippel [2015]). Multiple MRE studies have reported the effects of ageing on

brain stiffness, with a decrease in stiffness reported with age (Arani et al. [2015], Coelho and Sousa [2022], Delgorio et al. [2021], Hiscox et al. [2018], Kalra et al. [2019], Lv et al. [2020], Sack et al. [2009, 2011]). The sexual dimorphism of the mechanical properties of the brain is more controversial with Arani et al. [2015], Lv et al. [2020], and Sack et al. [2009] showing a difference between males and females; however, later studies by Sack et al. [2011] and Takamura et al. [2020] did not demonstrate statistically significant sexual dimorphism. Johnson et al. [2014] evaluated the impact of MRE resolution on G' and G'' by comparing an isotropic resolution of 1.6 mm with 2.0 mm on healthy human controls to demonstrate a higher G' and G'' in the brainstem with higher resolution scans. However, this finding was not demonstrated in other regions of the brain (Johnson et al. [2014]). Guo et al. [2013] demonstrated that the use of the MDEV inversion algorithm produced discrepancies in the values for G'', but not G', in studies of healthy phantom human brain and phantom brain compared to Helmholtz equation inversion analysis (Guo et al. [2013], Streitberger et al. [2014]). Finally, the ultra-soft mechanical properties of the brain push the mechanical testing and force sensors to their sensitivity limits and, as a result, earlier studies demonstrated higher stiffness values compared to more recent studies (Budday et al. [2020]).

With factors such as patient population, MRE imaging parameters, and data analysis method influencing the reported values of G' and G'', $\mid G^* \mid$ and "shear stiffness", it is imperative to establish a consensus on the standard acquisition, analysis, and reporting of MRE data to allow for a ready comparison of studies and to better build an atlas of human brain stiffness (Budday et al. [2020], Chatelin et al. [2010], Guo et al. [2013], Manduca

et al. [2021]). This chapter served to highlight that this unfortunately is not the case currently and more work is required to better understand the mechanical characteristics of the human brain *in-vivo*.

5.10.2 Brain Tumours

MRE has been used to investigate brain parenchyma in disorders such as Parkinson's Disease, Cerebral Palsy, Alzheimer's Disease and Multiple Sclerosis, demonstrating reduced brain stiffness in these conditions (Chaze et al. [2019], Lipp et al. [2018, 2013], Murphy et al. [2011, 2016], Pillai and Franze [2024], Streitberger et al. [2012], Wuerfel et al. [2010]). In these diseases, MRE changes correlate with histological tissue changes such as decreased cell number, inflammation, and loss of connectivity, suggesting that the viscoelastic properties of the brain represent the underlying microstructure. (Guo et al. [2019], Munder et al. [2018], Murphy et al. [2016], Sack et al. [2013], Silva et al. [2021a], Yin et al. [2018]).

GBM are distinguished histologically by the presence of a focal necrotic core, surrounded by layers of tumour cells that move away from the necrotic core called pseudopalisades (Brat et al. [2004], Rong et al. [2006]). During the growth and expansion of GBM tumours, compressive forces are generated due to the confines of the cranium (Pillai and Franze [2024]). Historically, malignant brain tumours were believed to be stiffer than healthy brain tissue (Northcott et al. [2018], Northey et al. [2017]). However, more recently, there has been a suggestion that GBM are mechanically softer compared to healthy brain controls(Jamin et al. [2015], Janas et al. [2024], Pillai and Franze [2024],

Streitberger et al. [2014]). In this chapter, when data from the pooled literature was analysed, there was no discernible difference in G', G'' or $\mid G^* \mid$ for glioblastoma compared to healthy brain tissue (Section 5.8), however, this analysis is limited by a small sample size in the glioblastoma cohort and a high degree of heterogeneity in the normal brain cohort. Furthermore, Streitberger et al. [2014] and Reiss-Zimmermann et al. [2015] demonstrated intra- and intra-tumour heterogeneity in $\mid G^* \mid$ in patients with GBM, with some patients showing decreased and others increased values of $\mid G^* \mid$ compared to healthy brain controls, citing intra-tumour heterogeneity caused by solid mass, cystic structures, and necrotic regions within the tumour (Reiss-Zimmermann et al. [2015], Streitberger et al. [2014]).

When the analysis is performed with pooled MRE data on other brain tumours, no differences in $\mid G^* \mid$ of gliomas other than GBM at 60Hz were found, compared to healthy control brains. In contrast, $\mid G^* \mid$ of meningiomas at 60 Hz is significantly stiffer compared to the normal healthy brain. This mimics the recent finding of Duhon et al. [2024] showing increased meningiomas stiffness and that the MRE findings were correlated with the intraoperative evaluation of stiffness by operating surgeons. Tumour stiffness is among a key characteristic that is considered in planning resection surgery with softer tumours requiring less invasive, endoscopic procedure, whilst firm tumours may require more open surgical approaches. (Arani et al. [2021], Zada et al. [2013]).

Overall, this chapter serves to highlight the paucity and inconsistencies of data on the mechanical properties of brain tumours which has hindered the development of pre-clinical models of HGG and hence successful therapies.

5.10.3 Modelling in the Murine brain

Animal studies are useful pre-clinical models of human disease, with murine models commonly used to model GBM (Gómez-Oliva et al. [2021], Haddad et al. [2021], Loewa et al. [2023], McGonigle and Ruggeri [2014], Mukherjee et al. [2022]). Despite this, GBM allograft cell line models in immunocompetent mice do not fully replicate the features of human GBM, and likewise, patient-derived GBM xenograft models in immunosuppressed mice models do not allow the study of the role of the immune system (Gómez-Oliva et al. [2021], Haddad et al. [2021], Jin et al. [2021]). In this review on the use of MRE in animal models of brain tumours, we find that the 5 identified studies used GBM in a mouse model for MRE evaluation. In contrast to the findings in human experiments reported in section 5.8 which reported no significant differences in the stiffness of GBM in human subjects compared to healthy controls, there is the suggestion that GBM in a mouse model is softer in terms of G' and G'' compared to normal mouse brain. This may be due to the low number of published studies identified or due to possible better experimental control in animal studies, resulting in lower variability intra- and inter-studies, which would otherwise have reduced the power of statistical analysis (Altman and Krzywinski [2015], Haddad et al. [2021], Loewa et al. [2023], McGonigle and Ruggeri [2014], Mukherjee et al. [2022], Neyeloff et al. [2012], von Hippel [2015]).

Despite the value of MRE in preclinical studies of HGG, these studies are hindered by the time it takes to scan the brains of mice (Janas et al. [2024]). Clinical MRE in humans can be completed in 2 minutes with a single transducer driving frequency, while MRE in murine brains can exceed 30 minutes (Bertalan et al. [2019]), and many studies

compromise the image resolution and number of transducer frequencies used to minimise the total scan times (Papazoglou et al. [2012]). Unfortunately, these limitations preclude meaningful longitudinal studies with a large number of animals investigating the impact of radiotherapy, chemotherapy, and surgery on the mechanical properties of the brain. As such, more human MRE studies are required.

5.10.4 Future Directions

Future MRE studies to investigate longitudinal studies that detail changes with therapy would be required to better determine not only the new targets but also the ideal timing of therapies at various stages of the treatment pathway. MRE has been demonstrated to delineate *IDH1* mutation status with softer tumours being indicative of a wild type *IDH1*, which has been associated with a poorer outcome (Bunevicius et al. [2020], Pepin et al. [2018], Yan et al. [2009]).

Surgical interventions on the brain significantly influence its mechanical environment, triggering processes such as blood clotting, inflammation, cell proliferation, and tissue restructuring. Unlike scars developed in other mammalian tissues, physical insult to CNS tissue results in marked softening of the glial scar (Moeendarbary et al. [2017]). Currently, the efficacy of brain tumour therapies is measured by changes of tumour size (James et al. [1999], Macdonald et al. [1990]), however, changes in tumour size do not reflect changes in internal properties of the tumours, and therefore it has been suggested that MRE could potentially be used as a biomarker for treatment response (Feng et al. [2016], Schregel et al. [2020]). A study using a mouse model of GBM testing anti-VEGF therapy

found increased $\mid G^* \mid$, increased tumour size and longer survival in therapy exposed tumours compared to untreated controls (Schregel et al. [2020]). MRE was used to assess the after-effects of radiation therapy treatment in a murine brain GBM model and did not demonstrate any change in the mechanical properties of the contralateral hemisphere in the treated group, however, an increase in G' was observed in the untreated group over time (Feng et al. [2016]). This is important as differentiation of GBM progression from radiation necrosis remains a challenge using conventional imaging techniques and is imperative in clinical decision making (Bunevicius et al. [2020]).

In cancer research, orthotopic xenotransplantation models are regarded as the benchmark for examining human cancer cell biology *in vivo*. Despite this, due to graft vs. host immune conflicts, these models require immunocompromised hosts. Although they provide clinically relevant insights, these models do not adequately address the significant role of the immune system in tumour progression (Semenkow et al. [2017]). Inflammation after therapeutic intervention and surrounding the tumour mass is associated with vascular leakage and immune cell infiltration that, in themselves, can alter the mechanical properties of tissues such as the brain (Meyer et al. [2024], Silva et al. [2021b], Streitberger et al. [2014]). Furthermore, radiation therapy and chemotherapy methods, and dosing regime are different in humans, so studies in humans are required to realise the clinical impact of MRE.

This chapter also highlights the lack of consistent reporting and study methodology, which restricts meaningful data comparison. In addition, it further highlights the impact of the frequency of the transducer on the reported results. Although the amplitude of

vibrations is extremely small, on the order of 100 μm or less, with frequencies of 20-100 Hz being used (Bunevicius et al. [2020]), this is not consistent with the frequency and amplitude of cell mechanosensation with the loading and deformation of the tissues of interest which goes beyond physiological conditions, which in itself may cause damage to the tissue itself (Budday et al. [2020]). In conclusion, MRE faces several challenges and limitations in clinical use, mainly due to its scarcity and the need for costly specialised equipment and experimental scan sequences (Bresnahan et al. [2023], Jamshidi et al. [2024]). Currently, there is no established standard protocol for this diagnostic approach, and previous studies have used various protocols and imaging conditions. Therefore, future research might focus on more accurately simulating the amplitudes and frequencies at which cells perceive their environment and employing standardised imaging protocols.

5.11 Chapter Conclusions

In this chapter, a systematic review of the use of MRE to evaluate the mechanical properties of the brain in health and disease was performed. The use of MRE was chosen, as this technique has a distinct advantage over other traditional methods of rheometric analysis, including, the evaluation of *in-vivo* tissues, higher resolution and deeper penetration of tissue analysis (Christ et al. [2010], Koser et al. [2016], Pillai and Franze [2024], Thompson et al. [2019]). Although great efforts have been made to model the mechanical properties of the brain, contradictory results and variations in study techniques have hindered progress and prevented meaningful comparison of data (Budday et al. [2020], Chatelin et al. [2010]). Furthermore, this chapter serves to highlight the lack

of longitudinal data on changes in the mechanical properties of the brain with therapies, which is required to deliver novel and more targeted therapies for HGG (Mai et al. [2024], Seker-Polat et al. [2022]).

Chapter 6

Conclusions and Outlook

Glioblastoma multiforme (GBM), a WHO grade IV glioma, is the most common malignant primary brain tumour in adults and accounts for 15% of all primary tumours and 45% of all primary brain tumours (Ostrom et al. [2013, 2015], Rosenthal et al. [2006]) with an extremely poor prognosis and survival time of just under 15 months (Gan et al. [2015], Stupp et al. [2005]). This poor prognosis highlights the need to better understand the biology of GBM to improve existing treatment protocols (Gupta et al. [2024], Pillai and Franze [2024], Stupp et al. [2005]).

It has been increasingly recognised that the mechanical properties of the tumour microenvironment (TME) influence the signalling, protein expression, and migration of GBM (Budday et al. [2020], Pillai and Franze [2024], Sarker et al. [2020], Umesh et al. [2014]). As such, in order to generate successful therapies *in-vitro* the mechanical environment must be defined *in-vivo*.

The data presented in this thesis sought to investigate the role of the TME in GBM migration and invasion using biologically relevant models. Tumour spheroids of primary patient-derived GBM cells plated on mechanically tunable polyacrylamide hydrogels (PAHG) allowed for the investigation of the influence of cell-cell interactions on mechano-sensitive migration. Mouse xenograft models with the same primary patient-derived GBM cell lines were then used to correlate the role of epithelial growth factor receptor (EGFR) signalling and focal adhesion kinase (FAK) signalling with mechanosensation, during both collective migration and when cells migrate as individuals. Finally, stiffness of the brain *in-vivo* during health, disease and treatment was analysed using a systematic review of the literature. Importantly, this study allows for more accurate modelling of the brain parenchyma, taking into consideration the influence of the mechanical environment of the TME, the heterogeneity in stiffness due to penetrating structures such as blood vessels and the role of surround cells.

6.1 Cell-Cell Interactions Modulate Mechanosensation

The resistance of GBM to curative intent surgery and chemoradiation is due to the highly invasive nature of GBM (Cuddapah et al. [2014], Garcia-Diaz et al. [2023], Gupta et al. [2024]). Much of our understanding of GBM biology is obtained from single-cell 2D culture assays which fail to capture the role of cell-cell interactions which are present in GBM invasion (Gritsenko et al. [2017], Grundy et al. [2016], Osswald et al. [2015]).

When spheroids were plated on PAHG, some cell lines showed little migration from

the spheroids onto the PAHG while others revealed extensive migration from the spheroid onto the substrate. Those cell lines with extensive migration onto the substrate had spindle-shaped cell bodies, reflective of a more "mesenchymal" type of migration. In contrast, cell lines with little migration from the spheroids onto the PAHG had rounded cell bodies on soft substrates, reflective of a more "amoeboid" type of migration, and spindle-shaped cell bodies on stiffer substrates. This helps define stiffness-sensitive and stiffness-insensitive morphologies in primary patient-derived cell lines. Interestingly, the classification of one of the cell lines used, WK1, is in contrast with Grundy et al., who had defined mechano-sensitive and -insensitive morphologies in cell lines on 2D cultures of single cells (Grundy et al. [2016]). This could result from interactions among cells within the bulk of the spheroids, which modify mechanosensation pathways before they arise on the PAHGs. Alternatively, it has been proposed that the inclusion of cell-cell interactions in an spheroid culture, combined with cell-substrate interactions, might exert selective pressure on which cells exit the spheroid.

When patterns of migration are queried in the spheroid model, all cell lines were representative of stiffness-sensitive phenotypes when cells migrate as individuals and as collectives. It was further shown that the observed monotonic relationship between substrate stiffness and migration in cells migrating individually was disrupted in those migrating as clusters. This suggests that there is an influence of cell-cell interactions on the migration behaviours of GBM.

To underpin a potential genetic basis for the behaviours seen, gene set enrichment analysis (GSEA) was performed on publicly available RNA sequencing data for the cell

lines used, to demonstrate enrichment of gene sets responsible for focal adhesions (FA) in cell lines which demonstrated varying mechanical sensitivities in morphology, individual cell migration, and during collective migration. This observation is consistent with earlier studies that showed HGG cells form elongated focal adhesions (FAs) on stiff surfaces, while these FAs tend to decrease on more pliable substrates (Liu et al. [2015], Ulrich et al. [2009]). The lack of FA prompts mesenchymal cells to transition into a fast-moving amoeboid phenotype (Liu et al. [2015], Ulrich et al. [2009]).

6.2 EGFR and FAK Signalling May Direct Routes of Dissemination

The brain's soft parenchyma is a distinctive bodily structure characterised by a low Young's modulus (E) in the range of 0.1-1 kPa (Budday et al. [2015], Butcher et al. [2009], Christ et al. [2010], Elkin et al. [2007], Taylor and Miller [2004]), making it significantly softer than rigid tissues such as bone, which has an E valued at approximately 100 kPa (Engler et al. [2006]). This parenchyma is mechanically diverse, comprising grey matter, white matter fibre tracts, and the infiltrating vasculature, all contributing to the tissue's mechanical microenvironment (Budday et al. [2020], Hrapko et al. [2008], Scherer [1938]).

Using formalin-fixed human xenografts in a whole brain slice mouse model with the same primary patient-derived cell lines as the spheroid model, the data revealed that migration patterns seen in the spheroid model were largely conserved in the *ex-vivo* xenograft model. Cell lines exhibiting mechanosensitive migration patterns both as individual and collective entities in spheroid models were in closer proximity with

the firmer blood vessels in the xenograft model than cell lines with diverse mechanical responses in morphology, single-cell movement, and collective migration within the spheroid model. Interestingly, the WK1 cell line, which was mechano-insensitive in individual cell migration and mechano-sensitive when migrating as groups on the spheroid model, demonstrated subpopulations with different migration phenotypes. Cells appearing as groups, were in closer proximity to blood vessels, compared to single-cells in the xenograft model. One hypothesis is that the mechano-insensitive single-cell cells invade into the brain parenchyma diffusely, while mechano-sensitive collectively migrating cells use blood vessels as a scaffold to migrate and invade. This cell line demonstrated a strong enrichment in FA associated genes in GSEA analysis. Fascinatingly, this cell line also demonstrated an increase in EGFR and FAK phosphorylation with increasing distance from blood vessels in cells migrating as groups, the effect of which is diminished in individually migrating cells. The correlation of FAK and EGFR phosphorylation as a function of distance from blood vessels was not demonstrated in cell lines that did not demonstrate differences in mechanosensitive migration patterns in individually and collectively migrating cells.

Overall, this suggests that GBM cells are heterogeneous with inter- and intra- tumoural differences. Moreover, data suggest that cell-cell interactions potentially modulate the FA / EGFR / FAK-associated mechanosensation pathways in a cell-line dependent manner to form sub-population of cells. This is clinically significant, as much of our understanding of GBM biology originates from examining clusters of cells of the tumour bulk, rather than investigating the invasive single marginal cells responsible for tumour

recurrence (Garcia-Diaz et al. [2023]).

6.3 MRE Stiffness Values are Influenced by Measurement Modality, Transducer Frequency and Region of Interest

An inadequate understanding of the role of the mechanical environment within TME might partially elucidate why therapies deemed successful in preclinical trials using rigid cell culture plates often fail to translate into effective treatments for patients (Cruz Da Silva et al. [2021], Gunjur et al. [2022], Oster et al. [2023]). Therefore, to create effective treatments for targeting HGGs *in-vivo*, it is essential to first determine the stiffness of the human brain parenchyma *in-vivo* and understand how this stiffness changes throughout treatment involving surgery, chemotherapy, and radiation therapy.

Data presented report on a systematic review performed to methodically evaluate the published literature on brain stiffness segmented by transducer frequencies, brain locations, and reported stiffness modality, since all influence reports of brain stiffness (Manduca et al. [2021], Pillai and Franze [2024]).

Differences in experimental methods, patient population traits, and analysis techniques led to significant heterogeneity among studies. Additionally, the necessity to categorise stiffness estimates by variables like stiffness modality and transducer frequency resulted in 92 out of 202 estimates of the normal brain's mechanical properties being derived from single-sample studies. Variations in MRE measurement methods and a limited sample size in existing studies further complicate estimates of GBM stiffness,

hindering the resolution of the debate over whether GBM is stiffer or softer compared to normal brain tissue. (Jamin et al. [2015], Janas et al. [2024], Northcott et al. [2018], Northey et al. [2017], Pillai and Franze [2024], Streitberger et al. [2014]).

In summary, despite significant attempts to measure the mechanical properties of the brain, differing outcomes and diverse research methods have impeded advances and limited the ability to compare results effectively. Furthermore, the data presented underscore the absence of longitudinal studies on how therapies affect the mechanical properties of the brain, which is essential for developing new and well-timed treatments for HGG.

6.4 Conclusion

In summary, the findings of this thesis underscore the significance of replicating the mechanical characteristics of the TME through biologically relevant models. This approach helps to understand how tumour-TME and tumour-tumour interactions influence GBM invasion pathways. The data opens up new possibilities for improving mechanical TME modelling, which is crucial for understanding tumour cell biology and crafting innovative strategies to tackle this truly devastating disease.

Literature Cited

Agnihotri, S., Burrell, K. E., Wolf, A., Jalali, S., Hawkins, C., Rutka, J. T., and Zadeh, G. (2013). Glioblastoma, a brief review of history, molecular genetics, animal models and novel therapeutic strategies. *Archivum immunologiae et therapiae experimentalis*, 61(1):25–41.

Agnihotri, S. and Zadeh, G. (2016). Metabolic reprogramming in glioblastoma: the influence of cancer metabolism on epigenetics and unanswered questions. *Neuro-oncology*, 18(2):160–72.

Ah-Pine, F., Khettab, M., Bedoui, Y., Slama, Y., Daniel, M., Doray, B., and Gasque, P. (2023). On the origin and development of glioblastoma: multifaceted role of perivascular mesenchymal stromal cells. *Acta Neuropathologica Communications*, 11(1):104.

Ahmed, T. (2023). Biomaterial-based in vitro 3D modeling of glioblastoma multiforme. *Cancer Pathogenesis and Therapy*, 1(3):177–194.

Alifieris, C. and Trafalis, D. T. (2015). Glioblastoma multiforme: Pathogenesis and treatment. *Pharmacology & Therapeutics*, 152:63–82.

Allaway, R. J., Fischer, D. A., de Abreu, F. B., Gardner, T. B., Gordon, S. R., Barth, R. J., Colacchio, T. A., Wood, M., Kacsoh, B. Z., Bouley, S. J., Cui, J., Hamilton, J., Choi, J. A., Lange, J. T., Peterson, J. D., Padmanabhan, V., Tomlinson, C. R., Tsongalis, G. J., Suriawinata, A. A., Greene, C. S., Sanchez, Y., and Smith, K. D. (2016). Genomic characterization of patient-derived xenograft models established from fine needle aspirate biopsies of a primary pancreatic ductal adenocarcinoma and from patient-matched metastatic sites. *Oncotarget*, 7(13):17087–17102.

Allen, M., Bjerke, M., Edlund, H., Nelander, S., and Westermark, B. (2016). Origin of the U87MG glioma cell line: Good news and bad news. *Science Translational Medicine*, 8(354).

Altman, N. and Krzywinski, M. (2015). Sources of variation. *Nature Methods*, 12(1):5–6.

Ananthanarayanan, B., Kim, Y., and Kumar, S. (2011). Elucidating the mechanobiology of malignant brain tumors using a brain matrix-mimetic hyaluronic acid hydrogel platform. *Biomaterials*, 32(31):7913–7923.

Arani, A., Manduca, A., Ehman, R. L., and Huston III, J. (2021). Harnessing brain waves: a review of brain magnetic resonance elastography for clinicians and scientists entering the field. *The British Journal of Radiology*, 94(1119).

Arani, A., Murphy, M. C., Glaser, K. J., Manduca, A., Lake, D. S., Kruse, S. A., Jack, C. R., Ehman, R. L., and Huston, J. (2015). Measuring the effects of aging and sex on regional brain stiffness with MR elastography in healthy older adults. *NeuroImage*, 111:59–64.

Arora, R., Cao, C., Kumar, M., Sinha, S., Chanda, A., McNeil, R., Samuel, D., Arora, R. K., Matthews, T. W., Chandarana, S., Hart, R., Dort, J. C., Biernaskie, J., Neri, P., Hyrcza, M. D., and Bose, P. (2023). Spatial transcriptomics reveals distinct and conserved tumor core and edge architectures that predict survival and targeted therapy response. *Nature Communications*, 14(1):5029.

Aum, D. J., Kim, D. H., Beaumont, T. L., Leuthardt, E. C., Dunn, G. P., and Kim, A. H. (2014). Molecular and cellular heterogeneity: the hallmark of glioblastoma. *Neurosurgical focus*, 37(6):E11.

Aydin, O. and Yassikaya, M. Y. (2022). Validity and Reliability Analysis of the PlotDigitizer Software Program for Data Extraction from Single-Case Graphs. *Perspectives on Behavior Science*, 45(1):239–257.

Baharlou, H. (2022). *The role of Anogenital Mononuclear Phagocytes in HIV transmission*. PhD thesis, The University of Sydney, Sydney, NSW, Australia.

Baker, A.-M., Bird, D., Lang, G., Cox, T. R., and Erler, J. T. (2013). Lysyl oxidase enzymatic function increases stiffness to drive colorectal cancer progression through FAK. *Oncogene*, 32(14):1863–1868.

Balss, J., Meyer, J., Mueller, W., Korshunov, A., Hartmann, C., and von Deimling, A. (2008). Analysis of the IDH1 codon 132 mutation in brain tumors. *Acta neuropathologica*, 116(6):597–602.

Bankhead, P., Loughrey, M. B., Fernández, J. A., Dombrowski, Y., McArt, D. G., Dunne,

P. D., McQuaid, S., Gray, R. T., Murray, L. J., Coleman, H. G., James, J. A., Salto-Tellez, M., and Hamilton, P. W. (2017). QuPath: Open source software for digital pathology image analysis. *Scientific Reports*, 7(1):16878.

Barnes, J. M., Kaushik, S., Bainer, R. O., Sa, J. K., Woods, E. C., Kai, F., Przybyla, L., Lee, M., Lee, H. W., Tung, J. C., Maller, O., Barrett, A. S., Lu, K. V., Lakins, J. N., Hansen, K. C., Obernier, K., Alvarez-Buylla, A., Bergers, G., Phillips, J. J., Nam, D.-H., Bertozzi, C. R., and Weaver, V. M. (2018). A tension-mediated glycocalyx–integrin feedback loop promotes mesenchymal-like glioblastoma. *Nature Cell Biology*, 20(10):1203–1214.

Barnes, J. M., Przybyla, L., and Weaver, V. M. (2017). Tissue mechanics regulate brain development, homeostasis and disease. *Journal of cell science*, 130(1):71–82.

Bazellières, E., Conte, V., Elosegui-Artola, A., Serra-Picamal, X., Bintanel-Morcillo, M., Roca-Cusachs, P., Muñoz, J. J., Sales-Pardo, M., Guimerà, R., and Trepat, X. (2015). Control of cell–cell forces and collective cell dynamics by the intercellular adhesome. *Nature Cell Biology*, 17(4):409–420.

Beauchesne, P. (2011). Extra-neural metastases of malignant gliomas: myth or reality? *Cancers*, 3(1):461–77.

Behnan, J., Stangeland, B., Hosainey, S. A. M., Joel, M., Olsen, T. K., Micci, F., Glover, J. C., Isakson, P., and Brinchmann, J. E. (2017). Differential propagation of stroma and cancer stem cells dictates tumorigenesis and multipotency. *Oncogene*, 36(4):570–584.

Bell, S., Redmann, A.-L., and Terentjev, E. M. (2019). Universal Kinetics of the Onset of

Cell Spreading on Substrates of Different Stiffness. *Biophysical journal*, 116(3):551–559.

Bellail, A. C., Hunter, S. B., Brat, D. J., Tan, C., and Van Meir, E. G. (2004). Microregional extracellular matrix heterogeneity in brain modulates glioma cell invasion. *The international journal of biochemistry & cell biology*, 36(6):1046–69.

Berrier, A. L. and Yamada, K. M. (2007). Cell-matrix adhesion. *Journal of cellular physiology*, 213(3):565–73.

Bershadsky, A. D., Ballestrem, C., Carramusa, L., Zilberman, Y., Gilquin, B., Khochbin, S., Alexandrova, A. Y., Verkhovsky, A. B., Shemesh, T., and Kozlov, M. M. (2006). Assembly and mechanosensory function of focal adhesions: experiments and models. *European Journal of Cell Biology*, 85(3-4):165–173.

Bertalan, G., Guo, J., Tzschätzsch, H., Klein, C., Barnhill, E., Sack, I., and Braun, J. (2019). Fast tomoelastography of the mouse brain by multifrequency single-shot MR elastography. *Magnetic Resonance in Medicine*, 81(4):2676–2687.

Bhargav, A. G., Domino, J. S., Chamoun, R., and Thomas, S. M. (2022). Mechanical Properties in the Glioma Microenvironment: Emerging Insights and Theranostic Opportunities. *Frontiers in Oncology*, 11.

Biernat, W., Kleihues, P., Yonekawa, Y., and Ohgaki, H. (1997). Amplification and overexpression of MDM2 in primary (de novo) glioblastomas. *Journal of neuropathology and experimental neurology*, 56(2):180–5.

Blacher, S., Erpicum, C., Lenoir, B., Paupert, J., Moraes, G., Ormenese, S., Bullinger, E., and Noel, A. (2014). Cell Invasion in the Spheroid Sprouting Assay: A Spatial Organisation Analysis Adaptable to Cell Behaviour. *PLoS ONE*, 9(5):e97019.

Bonnans, C., Chou, J., and Werb, Z. (2014). Remodelling the extracellular matrix in development and disease. *Nature Reviews Molecular Cell Biology*, 15(12):786–801.

Bordignon, K. C., Neto, M. C., Ramina, R., de Meneses, M. S., Zazula, A. D., and de Almeida, L. G. M. P. (2006). Patterns of neuroaxis dissemination of gliomas: suggestion of a classification based on magnetic resonance imaging findings. *Surgical neurology*, 65(5):472–7.

Brábek, J., Mierke, C. T., Rösel, D., Veselý, P., and Fabry, B. (2010). The role of the tissue microenvironment in the regulation of cancer cell motility and invasion. *Cell Communication and Signaling*, 8(1):22.

Bradbury, P. M., Turner, K., Mitchell, C., Griffin, K. R., Middlemiss, S., Lau, L., Dagg, R., Taran, E., Cooper-White, J., Fabry, B., and O'Neill, G. M. (2017). The focal adhesion targeting domain of p130Cas confers a mechanosensing function. *Journal of cell science*, 130(7):1263–1273.

Brat, D. J., Castellano-Sanchez, A. A., Hunter, S. B., Pecot, M., Cohen, C., Hammond, E. H., Devi, S. N., Kaur, B., and Van Meir, E. G. (2004). Pseudopalisades in glioblastoma are hypoxic, express extracellular matrix proteases, and are formed by an actively migrating cell population. *Cancer research*, 64(3):920–7.

Braun, J., Guo, J., Lützkendorf, R., Stadler, J., Papazoglou, S., Hirsch, S., Sack,

I., and Bernarding, J. (2014). High-resolution mechanical imaging of the human brain by three-dimensional multifrequency magnetic resonance elastography at 7T. *NeuroImage*, 90:308–14.

Brennan, C. W., Verhaak, R. G. W., McKenna, A., Campos, B., Noushmehr, H., Salama, S. R., Zheng, S., Chakravarty, D., Sanborn, J. Z., Berman, S. H., Beroukhim, R., Bernard, B., Wu, C.-J., Genovese, G., Shmulevich, I., Barnholtz-Sloan, J., Zou, L., Vegesna, R., Shukla, S. A., Ciriello, G., Yung, W. K., Zhang, W., Sougnez, C., Mikkelsen, T., Aldape, K., Bigner, D. D., Van Meir, E. G., Prados, M., Sloan, A., Black, K. L., Eschbacher, J., Finocchiaro, G., Friedman, W., Andrews, D. W., Guha, A., Iacocca, M., O'Neill, B. P., Foltz, G., Myers, J., Weisenberger, D. J., Penny, R., Kucherlapati, R., Perou, C. M., Hayes, D. N., Gibbs, R., Marra, M., Mills, G. B., Lander, E., Spellman, P., Wilson, R., Sander, C., Weinstein, J., Meyerson, M., Gabriel, S., Laird, P. W., Haussler, D., Getz, G., Chin, L., and TCGA Research Network (2013). The somatic genomic landscape of glioblastoma. *Cell*, 155(2):462–77.

Bresnahan, R., Duarte, R., Mahon, J., Beale, S., Chaplin, M., Bhattacharyya, D., Houten, R., Edwards, K., Nevitt, S., Maden, M., and Boland, A. (2023). Diagnostic accuracy and clinical impact of MRI-based technologies for patients with non-alcoholic fatty liver disease: systematic review and economic evaluation. *Health Technology Assessment*, pages 1–115.

Brooks, L. J. and Parrinello, S. (2017). Vascular regulation of glioma stem-like cells: a balancing act. *Current Opinion in Neurobiology*, 47:8–15.

Budday, S., Nay, R., de Rooij, R., Steinmann, P., Wyrobek, T., Ovaert, T. C., and Kuhl,

E. (2015). Mechanical properties of gray and white matter brain tissue by indentation. *Journal of the mechanical behavior of biomedical materials*, 46:318–30.

Budday, S., Ovaert, T. C., Holzapfel, G. A., Steinmann, P., and Kuhl, E. (2020). Fifty Shades of Brain: A Review on the Mechanical Testing and Modeling of Brain Tissue. *Archives of Computational Methods in Engineering*, 27(4):1187–1230.

Bunevicius, A., Schregel, K., Sinkus, R., Golby, A., and Patz, S. (2020). REVIEW: MR elastography of brain tumors. *NeuroImage. Clinical*, 25:102109.

Burgess, A., Matar, E., Neuen, B., and Fox, G. J. (2019). A longitudinal faculty development program: supporting a culture of teaching. *BMC Medical Education*, 19(1):400.

Burgess, A. W., Cho, H.-S., Eigenbrot, C., Ferguson, K. M., Garrett, T. P., Leahy, D. J., Lemmon, M. A., Sliwkowski, M. X., Ward, C. W., and Yokoyama, S. (2003). An Open-and-Shut Case? Recent Insights into the Activation of EGF/ErbB Receptors. *Molecular Cell*, 12(3):541–552.

Burridge, K., Fath, K., Kelly, T., Nuckolls, G., and Turner, C. (1988). Focal Adhesions: Transmembrane Junctions Between the Extracellular Matrix and the Cytoskeleton. *Annual Review of Cell Biology*, 4(1):487–525.

Butcher, D. T., Alliston, T., and Weaver, V. M. (2009). A tense situation: forcing tumour progression. *Nature reviews. Cancer*, 9(2):108–22.

Buxboim, A., Rajagopal, K., Brown, A. E. X., and Discher, D. E. (2010). How

deeply cells feel: methods for thin gels. *Journal of Physics: Condensed Matter*, 22(19):194116.

Canel, M., Serrels, A., Miller, D., Timpson, P., Serrels, B., Frame, M. C., and Brunton, V. G. (2010). Quantitative In vivo Imaging of the Effects of Inhibiting Integrin Signaling via Src and FAK on Cancer Cell Movement: Effects on E-cadherin Dynamics. *Cancer Research*, 70(22):9413–9422.

Canny, J. (1986). A Computational Approach to Edge Detection. *IEEE Transactions on Pattern Analysis and Machine Intelligence*, PAMI-8(6):679–698.

Case, L. B. and Waterman, C. M. (2015). Integration of actin dynamics and cell adhesion by a three-dimensional, mechanosensitive molecular clutch. *Nature Cell Biology*, 17(8):955–963.

Cavallaro, U. and Christofori, G. (2001). Cell adhesion in tumor invasion and metastasis: loss of the glue is not enough. *Biochimica et Biophysica Acta (BBA) - Reviews on Cancer*, 1552(1):39–45.

Chang, F., Levengood, S. L., Cho, N., Chen, L., Wang, E., Yu, J. S., and Zhang, M. (2018). Crosslinked Chitosan-PEG Hydrogel for Culture of Human Glioblastoma Cell Spheroids and Drug Screening. *Advanced Therapeutics*, 1(7).

Chatelin, S., Constantinesco, A., and Willinger, R. (2010). Fifty years of brain tissue mechanical testing: From in vitro to in vivo investigations. *Biorheology*, 47(5-6):255–276.

Chauvet, D., Imbault, M., Capelle, L., Demene, C., Mossad, M., Karachi, C., Boch, A.-L., Gennisson, J.-L., and Tanter, M. (2016). In Vivo Measurement of Brain Tumor Elasticity Using Intraoperative Shear Wave Elastography. *Ultraschall in der Medizin*, 37(6):584–590.

Chaze, C. A., McIlvain, G., Smith, D. R., Villermaux, G. M., Delgorio, P. L., Wright, H. G., Rogers, K. J., Miller, F., Crenshaw, J. R., and Johnson, C. L. (2019). Altered brain tissue viscoelasticity in pediatric cerebral palsy measured by magnetic resonance elastography. *NeuroImage. Clinical*, 22:101750.

Chen, E. Y., Tan, C. M., Kou, Y., Duan, Q., Wang, Z., Meirelles, G. V., Clark, N. R., and Ma'ayan, A. (2013a). Enrichr: interactive and collaborative HTML5 gene list enrichment analysis tool. *BMC bioinformatics*, 14(1):128.

Chen, H. and Nalbantoglu, J. (2014). Ring cell migration assay identifies distinct effects of extracellular matrix proteins on cancer cell migration. *BMC Research Notes*, 7(1):183.

Chen, J., McKay, R., and Parada, L. (2012). Malignant Glioma: Lessons from Genomics, Mouse Models, and Stem Cells. *Cell*, 149(1):36–47.

Chen, J. E., Pedron, S., and Harley, B. A. C. (2017a). The Combined Influence of Hydrogel Stiffness and Matrix-Bound Hyaluronic Acid Content on Glioblastoma Invasion. *Macromolecular Bioscience*, 17(8).

Chen, P., Cescon, M., and Bonaldo, P. (2013b). Collagen VI in cancer and its biological mechanisms.

Chen, R., Smith-Cohn, M., Cohen, A. L., and Colman, H. (2017b). Glioma Subclassifications and Their Clinical Significance. *Neurotherapeutics*, 14(2):284–297.

Chi, K.-Y., Li, M.-Y., Chen, C., and Kang, E. (2023). Ten circumstances and solutions for finding the sample mean and standard deviation for meta-analysis. *Systematic Reviews*, 12(1):62.

Christ, A. F., Franze, K., Gautier, H., Moshayedi, P., Fawcett, J., Franklin, R. J. M., Karadottir, R. T., and Guck, J. (2010). Mechanical difference between white and gray matter in the rat cerebellum measured by scanning force microscopy. *Journal of biomechanics*, 43(15):2986–92.

Ciani, C., Pistorio, G., Mearelli, M., and Falcone, C. (2023). Immunofluorescence protocol for localizing protein targets in brain tissue from diverse model and non-model mammals. *STAR Protocols*, 4(3):102482.

Cisneros Castillo, L. R., Oancea, A.-D., Stüllein, C., and Régnier-Vigouroux, A. (2016). A Novel Computer-Assisted Approach to evaluate Multicellular Tumor Spheroid Invasion Assay. *Scientific reports*, 6:35099.

Claes, A., Idema, A. J., and Wesseling, P. (2007). Diffuse glioma growth: a guerilla war. *Acta neuropathologica*, 114(5):443–58.

Coelho, A. and Sousa, N. (2022). Magnetic resonance elastography of the ageing brain in normal and demented populations: A systematic review. *Human Brain Mapping*, 43(13):4207–4218.

Costa, E. C., Moreira, A. F., de Melo-Diogo, D., Gaspar, V. M., Carvalho, M. P., and Correia, I. J. (2016). 3D tumor spheroids: an overview on the tools and techniques used for their analysis. *Biotechnology advances*, 34(8):1427–1441.

Cross, S. E., Jin, Y.-S., Rao, J., and Gimzewski, J. K. (2007). Nanomechanical analysis of cells from cancer patients. *Nature Nanotechnology*, 2(12):780–783.

Cruz Da Silva, E., Mercier, M.-C., Etienne-Selloum, N., Dontenwill, M., and Choulier, L. (2021). A Systematic Review of Glioblastoma-Targeted Therapies in Phases II, III, IV Clinical Trials. *Cancers*, 13(8):1795.

Cuddapah, V. A., Robel, S., Watkins, S., and Sontheimer, H. (2014). A neurocentric perspective on glioma invasion. *Nature reviews. Neuroscience*, 15(7):455–65.

Cukierman, E., Pankov, R., Stevens, D. R., and Yamada, K. M. (2001). Taking Cell-Matrix Adhesions to the Third Dimension. *Science*, 294(5547):1708–1712.

D'Alessandro, G., Antonangeli, F., Marrocco, F., Porzia, A., Lauro, C., Santoni, A., and Limatola, C. (2020). Gut microbiota alterations affect glioma growth and innate immune cells involved in tumor immunosurveillance in mice. *European Journal of Immunology*, 50(5):705–711.

Dandy, W. E. (1928). Removal Of Right Cerebral Hemisphere For Certain Tumors With Hemiplegia. *Journal of the American Medical Association*, 90(11):823.

Darnell, M., Gu, L., and Mooney, D. (2018). RNA-seq reveals diverse effects of substrate stiffness on mesenchymal stem cells. *Biomaterials*, 181:182–188.

David, L., Dulong, V., Le Cerf, D., Chauzy, C., Norris, V., Delpech, B., Lamacz, M., and Vannier, J.-P. (2004). Reticulated hyaluronan hydrogels: a model for examining cancer cell invasion in 3D. *Matrix Biology*, 23(3):183–193.

Davis, A. S., Richter, A., Becker, S., Moyer, J. E., Sandouk, A., Skinner, J., and Taubenberger, J. K. (2014). Characterizing and Diminishing Autofluorescence in Formalin-fixed Paraffin-embedded Human Respiratory Tissue. *Journal of Histochemistry & Cytochemistry*, 62(6):405–423.

Delgorio, P. L., Hiscox, L. V., Daugherty, A. M., Sanjana, F., Pohlig, R. T., Ellison, J. M., Martens, C. R., Schwarb, H., McGarry, M. D. J., and Johnson, C. L. (2021). Effect of Aging on the Viscoelastic Properties of Hippocampal Subfields Assessed with High-Resolution MR Elastography. *Cerebral Cortex*, 31(6):2799–2811.

Demuth, T. and Berens, M. E. (2004). Molecular mechanisms of glioma cell migration and invasion. *Journal of neuro-oncology*, 70(2):217–28.

Dickinson, R. B., Caro, L., and Purich, D. L. (2004). Force Generation by Cytoskeletal Filament End-Tracking Proteins. *Biophysical Journal*, 87(4):2838–2854.

Dobashi, Y., Suzuki, S., Sato, E., Hamada, Y., Yanagawa, T., and Ooi, A. (2009). EGFR-dependent and independent activation of Akt/mTOR cascade in bone and soft tissue tumors. *Modern Pathology*, 22(10):1328–1340.

Dobes, M., Khurana, V. G., Shadbolt, B., Jain, S., Smith, S. F., Smee, R., Dexter, M., and Cook, R. (2011). Increasing incidence of glioblastoma multiforme and meningioma,

and decreasing incidence of Schwannoma (2000-2008): Findings of a multicenter Australian study. *Surgical neurology international*, 2:176.

D'Souza, R. C. J., Offenhäuser, C., Straube, J., Baumgartner, U., Kordowski, A., Li, Y., Stringer, B. W., Alexander, H., Lwin, Z., Inglis, P.-L., Jeffree, R. L., Johns, T. G., Boyd, A. W., and Day, B. W. (2020). Q-Cell Glioblastoma Resource: Proteomics Analysis Reveals Unique Cell-States are Maintained in 3D Culture. *Cells*, 9(2):267.

Duhon, B. H., Thompson, K., Fisher, M., Kaul, V. F., Nguyen, H. T., Harris, M. S., Varadarajan, V., Adunka, O. F., Prevedello, D. M., Kolipaka, A., and Ren, Y. (2024). Tumor biomechanical stiffness by magnetic resonance elastography predicts surgical outcomes and identifies biomarkers in vestibular schwannoma and meningioma. *Scientific Reports*, 14(1):14561.

Earnest, F., Kelly, P. J., Scheithauer, B. W., Kall, B. A., Cascino, T. L., Ehman, R. L., Forbes, G. S., and Axley, P. L. (1988). Cerebral astrocytomas: histopathologic correlation of MR and CT contrast enhancement with stereotactic biopsy. *Radiology*, 166(3):823–7.

Eikenberry, S. E., Sankar, T., Preul, M. C., Kostelich, E. J., Thalhauser, C. J., and Kuang, Y. (2009). Virtual glioblastoma: growth, migration and treatment in a three-dimensional mathematical model. *Cell proliferation*, 42(4):511–28.

Elkin, B. S., Azeloglu, E. U., Costa, K. D., and Morrison, B. (2007). Mechanical heterogeneity of the rat hippocampus measured by atomic force microscope indentation. *Journal of neurotrauma*, 24(5):812–22.

Elosegui-Artola, A., Trepat, X., and Roca-Cusachs, P. (2018). Control of Mechanotransduction by Molecular Clutch Dynamics. *Trends in Cell Biology*, 28(5):356–367.

Emery, I. F., Gopalan, A., Wood, S., Chow, K.-h., Battelli, C., George, J., Blaszyk, H., Florman, J., and Yun, K. (2017). Expression and function of ABCG2 and XIAP in glioblastomas. *Journal of Neuro-Oncology*, 133(1):47–57.

Engelhardt, B. and Ransohoff, R. M. (2012). Capture, crawl, cross: the T cell code to breach the blood-brain barriers. *Trends in immunology*, 33(12):579–89.

Engler, A. J., Sen, S., Sweeney, H. L., and Discher, D. E. (2006). Matrix elasticity directs stem cell lineage specification. *Cell*, 126(4):677–89.

Erben, T., Ossig, R., Naim, H. Y., and Schnekenburger, J. (2016). What to do with high autofluorescence background in pancreatic tissues – an efficient Sudan black B quenching method for specific immunofluorescence labelling. *Histopathology*, 69(3):406–422.

Erickson, A. E., Lan Levengood, S. K., Sun, J., Chang, F., and Zhang, M. (2018). Fabrication and Characterization of Chitosan–Hyaluronic Acid Scaffolds with Varying Stiffness for Glioblastoma Cell Culture. *Advanced Healthcare Materials*, 7(15).

Fang, Z., Liu, X., and Peltz, G. (2023). GSEApy: a comprehensive package for performing gene set enrichment analysis in Python. *Bioinformatics*, 39(1).

Faria, E. C., Ma, N., Gazi, E., Gardner, P., Brown, M., Clarke, N. W., and Snook, R. D.

(2008). Measurement of elastic properties of prostate cancer cells using AFM. *The Analyst*, 133(11):1498.

Farin, A., Suzuki, S. O., Weiker, M., Goldman, J. E., Bruce, J. N., and Canoll, P. (2006). Transplanted glioma cells migrate and proliferate on host brain vasculature: A dynamic analysis. *Glia*, 53(8):799–808.

Fedele, M., Cerchia, L., Pegoraro, S., Sgarra, R., and Manfioletti, G. (2019). Proneural-Mesenchymal Transition: Phenotypic Plasticity to Acquire Multitherapy Resistance in Glioblastoma. *International Journal of Molecular Sciences*, 20(11):2746.

Feng, Y., Clayton, E. H., Okamoto, R. J., Engelbach, J., Bayly, P. V., and Garbow, J. R. (2016). A longitudinal magnetic resonance elastography study of murine brain tumors following radiation therapy. *Physics in medicine and biology*, 61(16):6121–31.

Fife, C. M., McCarroll, J. A., and Kavallaris, M. (2014). Movers and shakers: cell cytoskeleton in cancer metastasis. *British Journal of Pharmacology*, 171(24):5507–5523.

Fletcher, D. A. and Mullins, R. D. (2010). Cell mechanics and the cytoskeleton. *Nature*, 463(7280):485–492.

Florczyk, S. J., Wang, K., Jana, S., Wood, D. L., Sytsma, S. K., Sham, J. G., Kievit, F. M., and Zhang, M. (2013). Porous chitosan-hyaluronic acid scaffolds as a mimic of glioblastoma microenvironment ECM. *Biomaterials*, 34(38):10143–10150.

Franze, K. (2013). The mechanical control of nervous system development. *Development (Cambridge, England)*, 140(15):3069–77.

Franze, K., Janmey, P. A., and Guck, J. (2013). Mechanics in Neuronal Development and Repair. *Annual Review of Biomedical Engineering*, 15(1):227–251.

Friedl, P. and Alexander, S. (2011). Cancer invasion and the microenvironment: plasticity and reciprocity. *Cell*, 147(5):992–1009.

Friedl, P., Sahai, E., Weiss, S., and Yamada, K. M. (2012). New dimensions in cell migration. *Nature reviews. Molecular cell biology*, 13(11):743–7.

Friedl, P. and Wolf, K. (2003). Tumour-cell invasion and migration: diversity and escape mechanisms. *Nature reviews. Cancer*, 3(5):362–74.

Friedl, P. and Wolf, K. (2010). Plasticity of cell migration: a multiscale tuning model. *The Journal of cell biology*, 188(1):11–9.

Fritz-Laylin, L. K., Prochnik, S. E., Ginger, M. L., Dacks, J. B., Carpenter, M. L., Field, M. C., Kuo, A., Paredez, A., Chapman, J., Pham, J., Shu, S., Neupane, R., Cipriano, M., Mancuso, J., Tu, H., Salamov, A., Lindquist, E., Shapiro, H., Lucas, S., Grigoriev, I. V., Cande, W. Z., Fulton, C., Rokhsar, D. S., and Dawson, S. C. (2010). The Genome of Naegleria gruberi Illuminates Early Eukaryotic Versatility. *Cell*, 140(5):631–642.

Furnari, F. B., Fenton, T., Bachoo, R. M., Mukasa, A., Stommel, J. M., Stegh, A., Hahn, W. C., Ligon, K. L., Louis, D. N., Brennan, C., Chin, L., DePinho, R. A., and Cavenee, W. K. (2007). Malignant astrocytic glioma: genetics, biology, and paths to treatment. *Genes & development*, 21(21):2683–710.

Gabriel, K. R. and Sokal, R. R. (1969). A New Statistical Approach to Geographic Variation Analysis. *Systematic Zoology*, 18(3):259.

Gan, H. K., Rosenthal, M. A., Cher, L., Dally, M., Drummond, K., Murphy, M., and Thursfield, V. (2015). Management of glioblastoma in Victoria, Australia (2006-2008). *Journal of Clinical Neuroscience*, 22(9):1462–6.

Ganslandt, O., Stadlbauer, A., Fahlbusch, R., Kamada, K., Buslei, R., Blumcke, I., Moser, E., and Nimsky, C. (2005). Proton magnetic resonance spectroscopic imaging integrated into image-guided surgery: correlation to standard magnetic resonance imaging and tumor cell density. *Neurosurgery*, 56(2 Suppl):291–8.

Garcia-Diaz, C., Pöysti, A., Mereu, E., Clements, M. P., Brooks, L. J., Galvez-Cancino, F., Castillo, S. P., Tang, W., Beattie, G., Courtot, L., Ruiz, S., Roncaroli, F., Yuan, Y., Marguerat, S., Quezada, S. A., Heyn, H., and Parrinello, S. (2023). Glioblastoma cell fate is differentially regulated by the microenvironments of the tumor bulk and infiltrative margin. *Cell Reports*, 42(5):112472.

Gautier, H. O., Thompson, A. J., Achouri, S., Koser, D. E., Holtzmann, K., Moeendarbary, E., and Franze, K. (2015). Atomic force microscopy-based force measurements on animal cells and tissues. In *Methods in Cell Biology*, volume 125, pages 211–235.

Ghose, S., Ju, Y., McDonough, E., Ho, J., Karunamurthy, A., Chadwick, C., Cho, S., Rose, R., Corwin, A., Surrette, C., Martinez, J., Williams, E., Sood, A., Al-Kofahi, Y., Falo, L. D., Börner, K., and Ginty, F. (2023). 3D reconstruction of skin and spatial mapping of immune cell density, vascular distance and effects of sun exposure and aging. *Communications Biology*, 6(1):718.

Giese, A., Bjerkvig, R., Berens, M. E., and Westphal, M. (2003). Cost of migration:

invasion of malignant gliomas and implications for treatment. *Journal of Clinical Oncology*, 21(8):1624–36.

Glas, M., Rath, B. H., Simon, M., Reinartz, R., Schramme, A., Trageser, D., Eisenreich, R., Leinhaas, A., Keller, M., Schildhaus, H., Garbe, S., Steinfarz, B., Pietsch, T., Steindler, D. A., Schramm, J., Herrlinger, U., Brüstle, O., and Scheffler, B. (2010). Residual tumor cells are unique cellular targets in glioblastoma. *Annals of Neurology*, 68(2):264–269.

Goltsev, Y., Samusik, N., Kennedy-Darling, J., Bhate, S., Hale, M., Vazquez, G., Black, S., and Nolan, G. P. (2018). Deep Profiling of Mouse Splenic Architecture with CODEX Multiplexed Imaging. *Cell*, 174(4):968–981.

Gómez-Oliva, R., Domínguez-García, S., Carrascal, L., Abalos-Martínez, J., Pardillo-Díaz, R., Verástegui, C., Castro, C., Nunez-Abades, P., and Geribaldi-Doldán, N. (2021). Evolution of Experimental Models in the Study of Glioblastoma: Toward Finding Efficient Treatments. *Frontiers in Oncology*, 10.

González, V., Brell, M., Fuster, J., Moratinos, L., Alegre, D., López, S., and Ibáñez, J. (2022). Analyzing the role of reoperation in recurrent glioblastoma: a 15-year retrospective study in a single institution. *World Journal of Surgical Oncology*, 20(1):384.

Gritsenko, P., Leenders, W., and Friedl, P. (2017). Recapitulating in vivo-like plasticity of glioma cell invasion along blood vessels and in astrocyte-rich stroma. *Histochemistry and Cell Biology*, 148(4):395–406.

Gritsenko, P. G., Ilina, O., and Friedl, P. (2012). Interstitial guidance of cancer invasion. *The Journal of pathology*, 226(2):185–99.

Grundy, T. J. (2019). *Mechanoregulation of glioblastoma by extracellular biophysical stimuli*. PhD thesis, The University of Sydney, Sydney, NSW, Australia.

Grundy, T. J., De Leon, E., Griffin, K. R., Stringer, B. W., Day, B. W., Fabry, B., Cooper-White, J., and O'Neill, G. M. (2016). Differential response of patient-derived primary glioblastoma cells to environmental stiffness. *Scientific reports*, 6(1):23353.

Grundy, T. J., Orcheston-Findlay, L., de Silva, E., Jegathees, T., Prior, V., Sarker, F. A., and O'Neill, G. M. (2022). Mechanosensitive expression of the mesenchymal subtype marker connective tissue growth factor in glioblastoma. *Scientific Reports*, 12(1):14982.

Gunjur, A., Balasubramanian, A., Hafeez, U., Menon, S., Cher, L., Parakh, S., and Gan, H. K. (2022). Poor correlation between preclinical and patient efficacy data for tumor targeted monotherapies in glioblastoma: the results of a systematic review. *Journal of Neuro-Oncology*, 159(3):539–549.

Guo, J., Bertalan, G., Meierhofer, D., Klein, C., Schreyer, S., Steiner, B., Wang, S., Vieira da Silva, R., Infante-Duarte, C., Koch, S., Boehm-Sturm, P., Braun, J., and Sack, I. (2019). Brain maturation is associated with increasing tissue stiffness and decreasing tissue fluidity. *Acta Biomaterialia*, 99:433–442.

Guo, J., Hirsch, S., Fehlner, A., Papazoglou, S., Scheel, M., Braun, J., and Sack, I. (2013). Towards an Elastographic Atlas of Brain Anatomy. *PLoS ONE*, 8(8):e71807.

Gupta, R. K., Niklasson, M., Bergström, T., Segerman, A., Betsholtz, C., and Westermark, B. (2024). Tumor-specific migration routes of xenotransplanted human glioblastoma cells in mouse brain. *Scientific Reports*, 14(1):864.

Gzell, C., Back, M., Wheeler, H., Bailey, D., and Foote, M. (2017). Radiotherapy in Glioblastoma: the Past, the Present and the Future. *Clinical oncology (Royal College of Radiologists (Great Britain))*, 29(1):15–25.

Haddad, A. F., Young, J. S., Amara, D., Berger, M. S., Raleigh, D. R., Aghi, M. K., and Butowski, N. A. (2021). Mouse models of glioblastoma for the evaluation of novel therapeutic strategies. *Neuro-Oncology Advances*, 3(1).

Haeger, A., Wolf, K., Zegers, M. M., and Friedl, P. (2015). Collective cell migration: guidance principles and hierarchies. *Trends in Cell Biology*, 25(9):556–566.

Hambardzumyan, D., Gutmann, D. H., and Kettenmann, H. (2016). The role of microglia and macrophages in glioma maintenance and progression. *Nature neuroscience*, 19(1):20–7.

Han, S. J., Kwon, S., and Kim, K. S. (2021). Challenges of applying multicellular tumor spheroids in preclinical phase. *Cancer cell international*, 21(1):152.

Han, Y. L., Pegoraro, A. F., Li, H., Li, K., Yuan, Y., Xu, G., Gu, Z., Sun, J., Hao, Y., Gupta, S. K., Li, Y., Tang, W., Kang, H., Teng, L., Fredberg, J. J., and Guo, M. (2020). Cell swelling, softening and invasion in a three-dimensional breast cancer model. *Nature Physics*, 16(1):101–108.

Hanahan, D. (2022). Hallmarks of Cancer: New Dimensions. *Cancer Discovery*, 12(1):31–46.

Hanahan, D. and Weinberg, R. A. (2000). The hallmarks of cancer. *Cell*, 100(1):57–70.

Hanahan, D. and Weinberg, R. A. (2011). Hallmarks of cancer: the next generation. *Cell*, 144(5):646–74.

Hao, J., Zhang, Y., Ye, R., Zheng, Y., Zhao, Z., and Li, J. (2013). Mechanotransduction in cancer stem cells. *Cell Biology International*, 37(9):888–891.

Hecht, I., Bar-El, Y., Balmer, F., Natan, S., Tsarfaty, I., Schweitzer, F., and Ben-Jacob, E. (2015). Tumor Invasion Optimization by Mesenchymal-Amoeboid Heterogeneity. *Scientific Reports*, 5(1):10622.

Hegi, M. E., Diserens, A.-C., Gorlia, T., Hamou, M.-F., de Tribolet, N., Weller, M., Kros, J. M., Hainfellner, J. A., Mason, W., Mariani, L., Bromberg, J. E. C., Hau, P., Mirimanoff, R. O., Cairncross, J. G., Janzer, R. C., and Stupp, R. (2005). MGMT gene silencing and benefit from temozolomide in glioblastoma. *The New England journal of medicine*, 352(10):997–1003.

Higgins, J. P. T., Thompson, S. G., Deeks, J. J., and Altman, D. G. (2003). Measuring inconsistency in meta-analyses. *BMJ (Clinical research ed.)*, 327(7414):557–60.

Hiscox, L. V., Johnson, C. L., McGarry, M. D., Perrins, M., Littlejohn, A., van Beek, E. J., Roberts, N., and Starr, J. M. (2018). High-resolution magnetic resonance elastography reveals differences in subcortical gray matter viscoelasticity between young and healthy older adults. *Neurobiology of Aging*, 65:158–167.

Hrapko, M., van Dommelen, J. A. W., Peters, G. W. M., and Wismans, J. S. H. M. (2008). The influence of test conditions on characterization of the mechanical properties of brain tissue. *Journal of biomechanical engineering*, 130(3):031003.

Im, K., Mareninov, S., Diaz, M. F. P., and Yong, W. H. (2019). An Introduction to Performing Immunofluorescence Staining. *Methods in molecular biology (Clifton, N.J.)*, 1897:299–311.

Isomursu, A., Park, K.-Y., Hou, J., Cheng, B., Mathieu, M., Shamsan, G. A., Fuller, B., Kasim, J., Mahmoodi, M. M., Lu, T. J., Genin, G. M., Xu, F., Lin, M., Distefano, M. D., Ivaska, J., and Odde, D. J. (2022). Directed cell migration towards softer environments. *Nature Materials*, 21(9):1081–1090.

James, K., Eisenhauer, E., Christian, M., Terenziani, M., Vena, D., Muldal, A., and Therasse, P. (1999). Measuring Response in Solid Tumors: Unidimensional Versus Bidimensional Measurement. *JNCI Journal of the National Cancer Institute*, 91(6):523–528.

Jamin, Y., Boult, J. K. R., Li, J., Popov, S., Garteiser, P., Ulloa, J. L., Cummings, C., Box, G., Eccles, S. A., Jones, C., Waterton, J. C., Bamber, J. C., Sinkus, R., and Robinson, S. P. (2015). Exploring the biomechanical properties of brain malignancies and their pathologic determinants in vivo with magnetic resonance elastography. *Cancer research*, 75(7):1216–1224.

Jamshidi, M. H., Karami, A., Keshavarz, A., Fatemi, A., and Ghanavati, S. (2024). Magnetic Resonance Elastography for Breast Cancer Diagnosis Through

the Assessment of Tissue Biomechanical Properties. *Health Science Reports*, 7(12):e70253.

Janas, A., Jordan, J., Bertalan, G., Meyer, T., Bukatz, J., Sack, I., Senger, C., Nieminen-Kelhä, M., Brandenburg, S., Kremenskaia, I., Krantchev, K., Al-Rubaiey, S., Mueller, S., Koch, S. P., Boehm-Sturm, P., Reiter, R., Zips, D., Vajkoczy, P., and Acker, G. (2024). In vivo characterization of brain tumor biomechanics: magnetic resonance elastography in intracranial B16 melanoma and GL261 glioma mouse models. *Frontiers in oncology*, 14:1402578.

Janiszewska, M., Primi, M. C., and Izard, T. (2020). Cell adhesion in cancer: Beyond the migration of single cells. *Journal of Biological Chemistry*, 295(8):2495–2505.

Jelicic Kadic, A., Vucic, K., Dosenovic, S., Sapunar, D., and Puljak, L. (2016). Extracting data from figures with software was faster, with higher interrater reliability than manual extraction. *Journal of Clinical Epidemiology*, 74:119–123.

Jin, F., Jin-Lee, H. J., and Johnson, A. J. (2021). Mouse Models of Experimental Glioblastoma. In *Gliomas*, pages 15–46. Exon Publications.

Johnson, C. L., Holtrop, J. L., McGarry, M. D., Weaver, J. B., Paulsen, K. D., Georgiadis, J. G., and Sutton, B. P. (2014). 3D multislab, multishot acquisition for fast, whole-brain MR elastography with high signal-to-noise efficiency. *Magnetic Resonance in Medicine*, 71(2):477–485.

Jones, T. S. and Holland, E. C. (2011). Molecular Pathogenesis of Malignant Glial Tumors. *Toxicologic Pathology*, 39(1):158–166.

Jue, T. R. and McDonald, K. L. (2016). The challenges associated with molecular targeted therapies for glioblastoma. *Journal of neuro-oncology*, 127(3):427–34.

Kalra, P., Raterman, B., Mo, X., and Kolipaka, A. (2019). Magnetic resonance elastography of brain: Comparison between anisotropic and isotropic stiffness and its correlation to age. *Magnetic resonance in medicine*, 82(2):671–679.

Kechagia, J. Z., Ivaska, J., and Roca-Cusachs, P. (2019). Integrins as biomechanical sensors of the microenvironment. *Nature Reviews Molecular Cell Biology*, 20(8):457–473.

Khalil, A. A. and Friedl, P. (2010). Determinants of leader cells in collective cell migration. *Integrative Biology*, 2(11-12):568.

Kim, J. Y., Hong, S. M., and Ro, J. Y. (2017). Recent updates on grading and classification of neuroendocrine tumors. *Ann Diagn Pathol*, 29:11–16.

Kleihues, P. and Ohgaki, H. (1999). Primary and secondary glioblastomas: from concept to clinical diagnosis. *Neuro-oncology*, 1(1):44–51.

Kleinman, H. K. and Martin, G. R. (2005). Matrigel: Basement membrane matrix with biological activity. *Seminars in Cancer Biology*, 15(5):378–386.

Kondapaneni, R. V., Gurung, S. K., Nakod, P. S., Goodarzi, K., Yakati, V., Lenart, N. A., and Rao, S. S. (2024). Glioblastoma mechanobiology at multiple length scales. *Biomaterials Advances*, 160:213860.

Koo, S., Martin, G. S., Schulz, K. J., Ronck, M., and Toussaint, L. G. (2012). Serial

selection for invasiveness increases expression of miR-143/miR-145 in glioblastoma cell lines. *BMC cancer*, 12(1):143.

Koser, D. E., Thompson, A. J., Foster, S. K., Dwivedy, A., Pillai, E. K., Sheridan, G. K., Svoboda, H., Viana, M., Costa, L. d. F., Guck, J., Holt, C. E., and Franze, K. (2016). Mechanosensing is critical for axon growth in the developing brain. *Nature Neuroscience*, 19(12):1592–1598.

Krishnan, R., Park, J.-A., Seow, C. Y., Lee, P. V.-S., and Stewart, A. G. (2016). Cellular Biomechanics in Drug Screening and Evaluation: Mechanopharmacology. *Trends in Pharmacological Sciences*, 37(2):87–100.

Krishnan, S., Szabo, E., Burghardt, I., Frei, K., Tabatabai, G., and Weller, M. (2015). Modulation of cerebral endothelial cell function by TGF-β in glioblastoma: VEGF-dependent angiogenesis versus endothelial mesenchymal transition. *Oncotarget*, 6(26):22480–95.

Kumar, S., Kapoor, A., Desai, S., Inamdar, M. M., and Sen, S. (2016). Proteolytic and non-proteolytic regulation of collective cell invasion: tuning by ECM density and organization. *Scientific reports*, 6(1):19905.

Lau, L. W., Cua, R., Keough, M. B., Haylock-Jacobs, S., and Yong, V. W. (2013). Pathophysiology of the brain extracellular matrix: a new target for remyelination. *Nature Reviews Neuroscience*, 14(10):722–729.

Ledur, P. F., Onzi, G. R., Zong, H., and Lenz, G. (2017). Culture conditions defining

glioblastoma cells behavior: what is the impact for novel discoveries? *Oncotarget*, 8(40):69185–69197.

Lee, J., Jo, D. H., Kim, J. H., Cho, C. S., Han, J. E., Kim, Y., Park, H., Yoo, S. H., Yu, Y. S., Moon, H. E., Park, H. R., Kim, D. G., Kim, J. H., and Paek, S. H. (2019). Development of a patient-derived xenograft model of glioblastoma via intravitreal injection in mice. *Experimental & Molecular Medicine*, 51(4):1–9.

Lee, J., Kotliarova, S., Kotliarov, Y., Li, A., Su, Q., Donin, N. M., Pastorino, S., Purow, B. W., Christopher, N., Zhang, W., Park, J. K., and Fine, H. A. (2006). Tumor stem cells derived from glioblastomas cultured in bFGF and EGF more closely mirror the phenotype and genotype of primary tumors than do serum-cultured cell lines. *Cancer Cell*, 9(5):391–403.

Lekka, M., Pogoda, K., Gostek, J., Klymenko, O., Prauzner-Bechcicki, S., Wiltowska-Zuber, J., Jaczewska, J., Lekki, J., and Stachura, Z. (2012). Cancer cell recognition – Mechanical phenotype. *Micron*, 43(12):1259–1266.

Lenting, K., Verhaak, R., ter Laan, M., Wesseling, P., and Leenders, W. (2017). Glioma: experimental models and reality. *Acta Neuropathologica*, 133(2):263–282.

Levental, I., Georges, P. C., and Janmey, P. A. (2007). Soft biological materials and their impact on cell function. *Soft Matter*, 3(3):299–306.

Li, C. I., Anderson, B. O., Daling, J. R., and Moe, R. E. (2003). Trends in Incidence Rates of Invasive Lobular and Ductal Breast Carcinoma. *JAMA*, 289(11):1421.

Li, R., Li, H., Yan, W., Yang, P., Bao, Z., Zhang, C., Jiang, T., and You, Y. (2015). Genetic and clinical characteristics of primary and secondary glioblastoma is associated with differential molecular subtype distribution. *Oncotarget*, 6(9):7318–24.

Lin, J.-R., Wang, S., Coy, S., Chen, Y.-A., Yapp, C., Tyler, M., Nariya, M. K., Heiser, C. N., Lau, K. S., Santagata, S., and Sorger, P. K. (2023). Multiplexed 3D atlas of state transitions and immune interaction in colorectal cancer. *Cell*, 186(2):363–381.

Lintz, M., Muñoz, A., and Reinhart-King, C. A. (2017). The Mechanics of Single Cell and Collective Migration of Tumor Cells. *Journal of biomechanical engineering*, 139(2):0210051–9.

Lipp, A., Skowronek, C., Fehlner, A., Streitberger, K.-J., Braun, J., and Sack, I. (2018). Progressive supranuclear palsy and idiopathic Parkinson's disease are associated with local reduction of in vivo brain viscoelasticity. *European Radiology*, 28(8):3347–3354.

Lipp, A., Trbojevic, R., Paul, F., Fehlner, A., Hirsch, S., Scheel, M., Noack, C., Braun, J., and Sack, I. (2013). Cerebral magnetic resonance elastography in supranuclear palsy and idiopathic Parkinson's disease. *NeuroImage: Clinical*, 3:381–387.

Liu, Y.-J., Le Berre, M., Lautenschlaeger, F., Maiuri, P., Callan-Jones, A., Heuzé, M., Takaki, T., Voituriez, R., and Piel, M. (2015). Confinement and low adhesion induce fast amoeboid migration of slow mesenchymal cells. *Cell*, 160(4):659–672.

Llinares-Benadero, C. and Borrell, V. (2019). Deconstructing cortical folding: genetic, cellular and mechanical determinants. *Nature Reviews Neuroscience*, 20(3):161–176.

Loewa, A., Feng, J. J., and Hedtrich, S. (2023). Human disease models in drug development. *Nature Reviews Bioengineering*, 1(8):545–559.

Lomakin, A. J., Cattin, C. J., Cuvelier, D., Alraies, Z., Molina, M., Nader, G. P. F., Srivastava, N., Sáez, P. J., Garcia-Arcos, J. M., Zhitnyak, I. Y., Bhargava, A., Driscoll, M. K., Welf, E. S., Fiolka, R., Petrie, R. J., De Silva, N. S., González-Granado, J. M., Manel, N., Lennon-Duménil, A. M., Müller, D. J., and Piel, M. (2020). The nucleus acts as a ruler tailoring cell responses to spatial constraints. *Science*, 370(6514).

Louis, D. N., Perry, A., Reifenberger, G., von Deimling, A., Figarella-Branger, D., Cavenee, W. K., Ohgaki, H., Wiestler, O. D., Kleihues, P., and Ellison, D. W. (2016). The 2016 World Health Organization Classification of Tumors of the Central Nervous System: a summary. *Acta neuropathologica*, 131(6):803–20.

Louis, D. N., Perry, A., Wesseling, P., Brat, D. J., Cree, I. A., Figarella-Branger, D., Hawkins, C., Ng, H. K., Pfister, S. M., Reifenberger, G., Soffietti, R., von Deimling, A., and Ellison, D. W. (2021). The 2021 WHO Classification of Tumors of the Central Nervous System: a summary. *Neuro-Oncology*, 23(8):1231–1251.

Lu, C.-L., Qin, L., Liu, H.-C., Candas, D., Fan, M., and Li, J. J. (2015). Tumor cells switch to mitochondrial oxidative phosphorylation under radiation via mTOR-mediated hexokinase II inhibition–a Warburg-reversing effect. *PloS one*, 10(3):e0121046.

Lu, P., Ruan, D., Huang, M., Tian, M., Zhu, K., Gan, Z., and Xiao, Z. (2024). Harnessing the potential of hydrogels for advanced therapeutic applications: current achievements and future directions. *Signal Transduction and Targeted Therapy*, 9(1):166.

Lun, M., Lok, E., Gautam, S., Wu, E., and Wong, E. T. (2011). The natural history of extracranial metastasis from glioblastoma multiforme. *Journal of neuro-oncology*, 105(2):261–73.

Luu, N., Zhang, S., Lam, R. H., and Chen, W. (2024). Mechanical constraints in tumor guide emergent spatial patterns of glioblastoma cancer stem cells. *Mechanobiology in Medicine*, 2(1):100027.

Lv, H., Kurt, M., Zeng, N., Ozkaya, E., Marcuz, F., Wu, L., Laksari, K., Camarillo, D. B., Pauly, K. B., Wang, Z., and Wintermark, M. (2020). MR elastography frequency–dependent and independent parameters demonstrate accelerated decrease of brain stiffness in elder subjects. *European Radiology*, 30(12):6614–6623.

Macdonald, D. R., Cascino, T. L., Schold, S. C., and Cairncross, J. G. (1990). Response criteria for phase II studies of supratentorial malignant glioma. *Journal of Clinical Oncology*, 8(7):1277–1280.

Magaki, S., Hojat, S. A., Wei, B., So, A., and Yong, W. H. (2019). An Introduction to the Performance of Immunohistochemistry. *Methods in molecular biology*, 1897:289–298.

Mai, Z., Lin, Y., Lin, P., Zhao, X., and Cui, L. (2024). Modulating extracellular matrix stiffness: a strategic approach to boost cancer immunotherapy. *Cell Death & Disease*, 15(5):307.

Mair, D. B., Ames, H. M., and Li, R. (2018). Mechanisms of invasion and motility of high-grade gliomas in the brain. *Molecular Biology of the Cell*, 29(21):2509–2515.

Majd, N. K., Vo, H. H., Moran, C. A., Weathers, S.-P., Song, I.-W., Williford, G. L., Rodon, J., Fu, S., and Tsimberidou, A.-M. (2024). Metastatic extraneural glioblastoma diagnosed with molecular testing. *The Oncologist*, 29(9):811–816.

Manduca, A., Bayly, P. V., Ehman, R. L., Kolipaka, A., Royston, T. J., Sack, I., Sinkus, R., and Van Beers, B. E. (2021). MR elastography: Principles, guidelines, and terminology. *Magnetic Resonance in Medicine*, 85(5):2377–2390.

Manini, I., Caponnetto, F., Bartolini, A., Ius, T., Mariuzzi, L., Di Loreto, C., Beltrami, A. P., and Cesselli, D. (2018). Role of Microenvironment in Glioma Invasion: What We Learned from In Vitro Models. *International journal of molecular sciences*, 19(1).

Mariappan, Y. K., Glaser, K. J., and Ehman, R. L. (2010). Magnetic resonance elastography: a review. *Clinical anatomy*, 23(5):497–511.

Mark, C., Grundy, T. J., Strissel, P. L., Böhringer, D., Grummel, N., Gerum, R., Steinwachs, J., Hack, C. C., Beckmann, M. W., Eckstein, M., Strick, R., O'Neill, G. M., and Fabry, B. (2020). Collective forces of tumor spheroids in three-dimensional biopolymer networks. *eLife*, 9.

Mayor, R. and Etienne-Manneville, S. (2016). The front and rear of collective cell migration. *Nature Reviews Molecular Cell Biology*, 17(2):97–109.

McGonigle, P. and Ruggeri, B. (2014). Animal models of human disease: Challenges in enabling translation. *Biochemical Pharmacology*, 87(1):162–171.

Melsen, W., Bootsma, M., Rovers, M., and Bonten, M. (2014). The effects of clinical and

statistical heterogeneity on the predictive values of results from meta-analyses. *Clinical Microbiology and Infection*, 20(2):123–129.

Meyer, T., Castelein, J., Schattenfroh, J., Sophie Morr, A., Vieira da Silva, R., Tzschätzsch, H., Reiter, R., Guo, J., and Sack, I. (2024). Magnetic resonance elastography in a nutshell: Tomographic imaging of soft tissue viscoelasticity for detecting and staging disease with a focus on inflammation. *Progress in Nuclear Magnetic Resonance Spectroscopy*, 144-145:1–14.

Miroshnikova, Y. A., Mouw, J. K., Barnes, J. M., Pickup, M. W., Lakins, J., Kim, Y., Lobo, K., Persson, A. I., Reis, G. F., McKnight, T. R., Holland, E., Phillips, J. J., and Weaver, V. M. (2016). Tissue mechanics promote IDH1-dependent HIF1α–tenascin C feedback to regulate glioblastoma aggression. *Nature Cell Biology*, 18(12):1336–1345.

Miroshnikova, Y. A., Rozenberg, G. I., Cassereau, L., Pickup, M., Mouw, J. K., Ou, G., Templeman, K. L., Hannachi, E.-I., Gooch, K. J., Sarang-Sieminski, A. L., García, A. J., and Weaver, V. M. (2017). $\alpha 5\beta 1$-Integrin promotes tension-dependent mammary epithelial cell invasion by engaging the fibronectin synergy site. *Molecular Biology of the Cell*, 28(22):2958–2977.

Moeendarbary, E., Weber, I. P., Sheridan, G. K., Koser, D. E., Soleman, S., Haenzi, B., Bradbury, E. J., Fawcett, J., and Franze, K. (2017). The soft mechanical signature of glial scars in the central nervous system. *Nature Communications*, 8(1):14787.

Mohiuddin, E. and Wakimoto, H. (2021). Extracellular matrix in glioblastoma:

opportunities for emerging therapeutic approaches. *American journal of cancer research*, 11(8):3742–3754.

Møller, H. G., Rasmussen, A. P., Andersen, H. H., Johnsen, K. B., Henriksen, M., and Duroux, M. (2013). A systematic review of microRNA in glioblastoma multiforme: micro-modulators in the mesenchymal mode of migration and invasion. *Molecular neurobiology*, 47(1):131–44.

Mukherjee, P., Roy, S., Ghosh, D., and Nandi, S. K. (2022). Role of animal models in biomedical research: a review. *Laboratory Animal Research*, 38(1):18.

Munder, T., Pfeffer, A., Schreyer, S., Guo, J., Braun, J., Sack, I., Steiner, B., and Klein, C. (2018). MR elastography detection of early viscoelastic response of the murine hippocampus to amyloid β accumulation and neuronal cell loss due to Alzheimer's disease. *Journal of Magnetic Resonance Imaging*, 47(1):105–114.

Murphy, M. C., Huston, J., Jack, C. R., Glaser, K. J., Manduca, A., Felmlee, J. P., and Ehman, R. L. (2011). Decreased brain stiffness in Alzheimer's disease determined by magnetic resonance elastography. *Journal of magnetic resonance imaging : JMRI*, 34(3):494–8.

Murphy, M. C., Jones, D. T., Jack, C. R., Glaser, K. J., Senjem, M. L., Manduca, A., Felmlee, J. P., Carter, R. E., Ehman, R. L., and Huston, J. (2016). Regional brain stiffness changes across the Alzheimer's disease spectrum. *NeuroImage. Clinical*, 10((Murphy, Jones, Jack, Glaser, Senjem, Felmlee, Ehman, Huston) Department of Radiology, Mayo Clinic College of Medicine, 200 First Street SW, Rochester,

MN 55905, United States(Jones) Department of Neurology, Mayo Clinic College of Medicine, 200 First Stre):283–90.

Muthupillai, R., Lomas, D. J., Rossman, P. J., Greenleaf, J. F., Manduca, A., and Ehman, R. L. (1995). Magnetic resonance elastography by direct visualization of propagating acoustic strain waves. *Science*, 269(5232):1854–7.

Nakada, M., Nambu, E., Furuyama, N., Yoshida, Y., Takino, T., Hayashi, Y., Sato, H., Sai, Y., Tsuji, T., Miyamoto, K.-i., Hirao, A., and Hamada, J.-i. (2013). Integrin $\alpha 3$ is overexpressed in glioma stem-like cells and promotes invasion. *British Journal of Cancer*, 108(12):2516–2524.

Nakamura, M., Yang, F., Fujisawa, H., Yonekawa, Y., Kleihues, P., and Ohgaki, H. (2000). Loss of heterozygosity on chromosome 19 in secondary glioblastomas. *Journal of neuropathology and experimental neurology*, 59(6):539–43.

Nakamura, M., Yonekawa, Y., Kleihues, P., and Ohgaki, H. (2001). Promoter hypermethylation of the RB1 gene in glioblastomas. *Laboratory investigation; a journal of technical methods and pathology*, 81(1):77–82.

Nath, S. and Devi, G. R. (2016). Three-dimensional culture systems in cancer research: Focus on tumor spheroid model. *Pharmacology & therapeutics*, 163:94–108.

Navab, R., Strumpf, D., To, C., Pasko, E., Kim, K. S., Park, C. J., Hai, J., Liu, J., Jonkman, J., Barczyk, M., Bandarchi, B., Wang, Y. H., Venkat, K., Ibrahimov, E., Pham, N.-A., Ng, C., Radulovich, N., Zhu, C.-Q., Pintilie, M., Wang, D., Lu, A., Jurisica, I., Walker, G. C., Gullberg, D., and Tsao, M.-S. (2016). Integrin $\alpha 11\beta 1$ regulates cancer stromal

stiffness and promotes tumorigenicity and metastasis in non-small cell lung cancer. *Oncogene*, 35(15):1899–1908.

Neyeloff, J. L., Fuchs, S. C., and Moreira, L. B. (2012). Meta-analyses and Forest plots using a microsoft excel spreadsheet: step-by-step guide focusing on descriptive data analysis. *BMC Research Notes*, 5(1):52.

Nobusawa, S., Watanabe, T., Kleihues, P., and Ohgaki, H. (2009). IDH1 mutations as molecular signature and predictive factor of secondary glioblastomas. *Clinical Cancer Research*, 15(19):6002–7.

Northcott, J. M., Dean, I. S., Mouw, J. K., and Weaver, V. M. (2018). Feeling Stress: The Mechanics of Cancer Progression and Aggression. *Frontiers in Cell and Developmental Biology*, 6(FEB).

Northey, J. J., Przybyla, L., and Weaver, V. M. (2017). Tissue Force Programs Cell Fate and Tumor Aggression. *Cancer Discovery*, 7(11):1224–1237.

Nunes, A. S., Barros, A. S., Costa, E. C., Moreira, A. F., and Correia, I. J. (2019). 3D tumor spheroids as in vitro models to mimic in vivo human solid tumors resistance to therapeutic drugs. *Biotechnology and bioengineering*, 116(1):206–226.

Nuñez, R. E., del Valle, M. M., Ortiz, K., Almodovar, L., and Kucheryavykh, L. (2021). Microglial Cytokines Induce Invasiveness and Proliferation of Human Glioblastoma through Pyk2 and FAK Activation. *Cancers*, 13(24):6160.

Nyberg, K. D., Hu, K. H., Kleinman, S. H., Khismatullin, D. B., Butte, M. J., and Rowat,

A. C. (2017). Quantitative Deformability Cytometry: Rapid, Calibrated Measurements of Cell Mechanical Properties. *Biophysical Journal*, 113(7):1574–1584.

Ogneva, I. V., Lebedev, D. V., and Shenkman, B. S. (2010). Transversal Stiffness and Young's Modulus of Single Fibers from Rat Soleus Muscle Probed by Atomic Force Microscopy. *Biophysical Journal*, 98(3):418–424.

Ohgaki, H., Dessen, P., Jourde, B., Horstmann, S., Nishikawa, T., Di Patre, P.-L., Burkhard, C., Schüler, D., Probst-Hensch, N. M., Maiorka, P. C., Baeza, N., Pisani, P., Yonekawa, Y., Yasargil, M. G., Lütolf, U. M., and Kleihues, P. (2004). Genetic pathways to glioblastoma: a population-based study. *Cancer research*, 64(19):6892–9.

Ohgaki, H. and Kleihues, P. (2005). Population-based studies on incidence, survival rates, and genetic alterations in astrocytic and oligodendroglial gliomas. *Journal of neuropathology and experimental neurology*, 64(6):479–89.

Ohgaki, H. and Kleihues, P. (2007). Genetic pathways to primary and secondary glioblastoma. *The American journal of pathology*, 170(5):1445–53.

Ohgaki, H. and Kleihues, P. (2013). The definition of primary and secondary glioblastoma. *Clinical Cancer Research*, 19(4):764–72.

Oliveira, V. C., Carrara, R. C. V., Simoes, D. L. C., Saggioro, F. P., Carlotti, C. G., Covas, D. T., and Neder, L. (2010). Sudan Black B treatment reduces autofluorescence and improves resolution of in situ hybridization specific fluorescent signals of brain sections. *Histology and histopathology*, 25(8):1017–24.

Olson, R. A., Brastianos, P. K., and Palma, D. A. (2011). Prognostic and predictive value of epigenetic silencing of MGMT in patients with high grade gliomas: a systematic review and meta-analysis. *Journal of neuro-oncology*, 105(2):325–35.

Omidvar, R., Tafazzoli-shadpour, M., Shokrgozar, M. A., and Rostami, M. (2014). Atomic force microscope-based single cell force spectroscopy of breast cancer cell lines: An approach for evaluating cellular invasion. *Journal of Biomechanics*, 47(13):3373–3379.

Osswald, M., Jung, E., Sahm, F., Solecki, G., Venkataramani, V., Blaes, J., Weil, S., Horstmann, H., Wiestler, B., Syed, M., Huang, L., Ratliff, M., Karimian Jazi, K., Kurz, F. T., Schmenger, T., Lemke, D., Gömmel, M., Pauli, M., Liao, Y., Häring, P., Pusch, S., Herl, V., Steinhäuser, C., Krunic, D., Jarahian, M., Miletic, H., Berghoff, A. S., Griesbeck, O., Kalamakis, G., Garaschuk, O., Preusser, M., Weiss, S., Liu, H., Heiland, S., Platten, M., Huber, P. E., Kuner, T., von Deimling, A., Wick, W., and Winkler, F. (2015). Brain tumour cells interconnect to a functional and resistant network. *Nature*, 528(7580):93–98.

Oster, C., Schmidt, T., Agkatsev, S., Lazaridis, L., Kleinschnitz, C., Sure, U., Scheffler, B., Kebir, S., and Glas, M. (2023). Are we providing best-available care to newly diagnosed glioblastoma patients? Systematic review of phase III trials in newly diagnosed glioblastoma 2005–2022. *Neuro-Oncology Advances*, 5(1).

Ostrom, Q. T., Bauchet, L., Davis, F. G., Deltour, I., Fisher, J. L., Langer, C. E., Pekmezci,

M., Schwartzbaum, J. A., Turner, M. C., Walsh, K. M., Wrensch, M. R., and Barnholtz-Sloan, J. S. (2014). The epidemiology of glioma in adults: a "state of the science" review. *Neuro-oncology*, 16(7):896–913.

Ostrom, Q. T., Gittleman, H., Farah, P., Ondracek, A., Chen, Y., Wolinsky, Y., Stroup, N. E., Kruchko, C., and Barnholtz-Sloan, J. S. (2013). CBTRUS statistical report: Primary brain and central nervous system tumors diagnosed in the United States in 2006-2010. *Neuro-oncology*, 15 Suppl 2(Suppl 2):1–56.

Ostrom, Q. T., Gittleman, H., Fulop, J., Liu, M., Blanda, R., Kromer, C., Wolinsky, Y., Kruchko, C., and Barnholtz-Sloan, J. S. (2015). CBTRUS Statistical Report: Primary Brain and Central Nervous System Tumors Diagnosed in the United States in 2008-2012. *Neuro-oncology*, 17 Suppl 4(Suppl 4):iv1–iv62.

Otsu, N. (1979). A Threshold Selection Method from Gray-Level Histograms. *IEEE Transactions on Systems, Man, and Cybernetics*, 9(1):62–66.

Padmanaban, V., Krol, I., Suhail, Y., Szczerba, B. M., Aceto, N., Bader, J. S., and Ewald, A. J. (2019). E-cadherin is required for metastasis in multiple models of breast cancer. *Nature*, 573(7774):439–444.

Page, M. J., McKenzie, J. E., Bossuyt, P. M., Boutron, I., Hoffmann, T. C., Mulrow, C. D., Shamseer, L., Tetzlaff, J. M., Akl, E. A., Brennan, S. E., Chou, R., Glanville, J., Grimshaw, J. M., Hróbjartsson, A., Lalu, M. M., Li, T., Loder, E. W., Mayo-Wilson, E., McDonald, S., McGuinness, L. A., Stewart, L. A., Thomas, J., Tricco, A. C., Welch,

V. A., Whiting, P., and Moher, D. (2021). The PRISMA 2020 statement: an updated guideline for reporting systematic reviews. *BMJ (Clinical research ed.)*, 372:n71.

Panková, K., Rösel, D., Novotný, M., and Brábek, J. (2010). The molecular mechanisms of transition between mesenchymal and amoeboid invasiveness in tumor cells. *Cellular and molecular life sciences : CMLS*, 67(1):63–71.

Paolillo, M., Comincini, S., and Schinelli, S. (2021). In Vitro Glioblastoma Models: A Journey into the Third Dimension. *Cancers*, 13(10):2449.

Papazoglou, S., Hirsch, S., Braun, J., and Sack, I. (2012). Multifrequency inversion in magnetic resonance elastography. *Physics in Medicine and Biology*, 57(8):2329–2346.

Parakh, S., Thursfield, V., Cher, L., Dally, M., Drummond, K., Murphy, M., Rosenthal, M. A., and Gan, H. K. (2016). Recurrent glioblastoma: Current patterns of care in an Australian population. *Journal of Clinical Neuroscience*, 24:78–82.

Parra, E. R., Uraoka, N., Jiang, M., Cook, P., Gibbons, D., Forget, M.-A., Bernatchez, C., Haymaker, C., Wistuba, I. I., and Rodriguez-Canales, J. (2017). Validation of multiplex immunofluorescence panels using multispectral microscopy for immune-profiling of formalin-fixed and paraffin-embedded human tumor tissues. *Scientific Reports*, 7(1):13380.

Parsons, D. W., Jones, S., Zhang, X., Lin, J. C.-H., Leary, R. J., Angenendt, P., Mankoo, P., Carter, H., Siu, I.-M., Gallia, G. L., Olivi, A., McLendon, R., Rasheed, B. A., Keir, S., Nikolskaya, T., Nikolsky, Y., Busam, D. A., Tekleab, H., Diaz, L. A., Hartigan, J., Smith, D. R., Strausberg, R. L., Marie, S. K. N., Shinjo, S. M. O., Yan, H., Riggins,

G. J., Bigner, D. D., Karchin, R., Papadopoulos, N., Parmigiani, G., Vogelstein, B., Velculescu, V. E., and Kinzler, K. W. (2008). An integrated genomic analysis of human glioblastoma multiforme. *Science*, 321(5897):1807–12.

Paschos, K. A., Canovas, D., and Bird, N. C. (2009). The role of cell adhesion molecules in the progression of colorectal cancer and the development of liver metastasis. *Cellular Signalling*, 21(5):665–674.

Pasquier, B., Pasquier, D., N'golet, A., Panh, M. H., and Couderc, P. (1980). Extraneural metastases of astrocytomas and glioblastomas clinicopathological study of two cases and review of literature. *Cancer*, 45(1):112–125.

Paszek, M. J., Zahir, N., Johnson, K. R., Lakins, J. N., Rozenberg, G. I., Gefen, A., Reinhart-King, C. A., Margulies, S. S., Dembo, M., Boettiger, D., Hammer, D. A., and Weaver, V. M. (2005). Tensional homeostasis and the malignant phenotype. *Cancer cell*, 8(3):241–54.

Patel, A. P., Tirosh, I., Trombetta, J. J., Shalek, A. K., Gillespie, S. M., Wakimoto, H., Cahill, D. P., Nahed, B. V., Curry, W. T., Martuza, R. L., Louis, D. N., Rozenblatt-Rosen, O., Suvà, M. L., Regev, A., and Bernstein, B. E. (2014). Single-cell RNA-seq highlights intratumoral heterogeneity in primary glioblastoma. *Science*, 344(6190):1396–1401.

Pawlizak, S., Fritsch, A. W., Grosser, S., Ahrens, D., Thalheim, T., Riedel, S., Kießling, T. R., Oswald, L., Zink, M., Manning, M. L., and Käs, J. A. (2015). Testing the

differential adhesion hypothesis across the epithelialmesenchymal transition. *New Journal of Physics*, 17(8):083049.

Pedron, S., Becka, E., and Harley, B. A. (2013). Regulation of glioma cell phenotype in 3D matrices by hyaluronic acid. *Biomaterials*, 34(30):7408–7417.

Pepin, K. M., McGee, K. P., Arani, A., Lake, D. S., Glaser, K. J., Manduca, A., Parney, I. F., Ehman, R. L., and Huston, J. (2018). MR Elastography Analysis of Glioma Stiffness and IDH1-Mutation Status. *AJNR. American journal of neuroradiology*, 39(1):31–36.

Pesce, L., Scardigli, M., Gavryusev, V., Laurino, A., Mazzamuto, G., Brady, N., Sancataldo, G., Silvestri, L., Destrieux, C., Hof, P. R., Costantini, I., and Pavone, F. S. (2022). 3D molecular phenotyping of cleared human brain tissues with light-sheet fluorescence microscopy. *Communications Biology*, 5(1):447.

Phillips, H. S., Kharbanda, S., Chen, R., Forrest, W. F., Soriano, R. H., Wu, T. D., Misra, A., Nigro, J. M., Colman, H., Soroceanu, L., Williams, P. M., Modrusan, Z., Feuerstein, B. G., and Aldape, K. (2006). Molecular subclasses of high-grade glioma predict prognosis, delineate a pattern of disease progression, and resemble stages in neurogenesis. *Cancer cell*, 9(3):157–73.

Pibuel, M. A., Poodts, D., Díaz, M., Hajos, S. E., and Lompardía, S. L. (2021). The scrambled story between hyaluronan and glioblastoma. *Journal of Biological Chemistry*, 296:100549.

Piccirilli, M., Brunetto, G. M. F., Rocchi, G., Giangaspero, F., and Salvati, M. (2008).

Extra Central Nervous System Metastases from Cerebral Glioblastoma Multiforme in Elderly Patients. Clinico-Pathological Remarks on our Series of Seven Cases and Critical Review of the Literature. *Tumori Journal*, 94(1):40–51.

Pietschmann, S., von Bueren, A. O., Kerber, M. J., Baumert, B. G., Kortmann, R. D., and Müller, K. (2015). An Individual Patient Data Meta-Analysis on Characteristics, Treatments and Outcomes of Glioblastoma/ Gliosarcoma Patients with Metastases Outside of the Central Nervous System. *PLOS ONE*, 10(4):e0121592.

Pillai, E. K. and Franze, K. (2024). Mechanics in the nervous system: From development to disease. *Neuron*, 112(3):342–361.

Pollard, S. M., Yoshikawa, K., Clarke, I. D., Danovi, D., Stricker, S., Russell, R., Bayani, J., Head, R., Lee, M., Bernstein, M., Squire, J. A., Smith, A., and Dirks, P. (2009). Glioma Stem Cell Lines Expanded in Adherent Culture Have Tumor-Specific Phenotypes and Are Suitable for Chemical and Genetic Screens. *Cell Stem Cell*, 4(6):568–580.

Preusser, M., Charles Janzer, R., Felsberg, J., Reifenberger, G., Hamou, M.-F., Diserens, A.-C., Stupp, R., Gorlia, T., Marosi, C., Heinzl, H., Hainfellner, J. A., and Hegi, M. (2008). Anti-O6-methylguanine-methyltransferase (MGMT) immunohistochemistry in glioblastoma multiforme: observer variability and lack of association with patient survival impede its use as clinical biomarker. *Brain pathology (Zurich, Switzerland)*, 18(4):520–32.

Quiñones-Hinojosa, A., Sanai, N., Gonzalez-Perez, O., and Garcia-Verdugo, J. M. (2007).

The Human Brain Subventricular Zone: Stem Cells in This Niche and Its Organization. *Neurosurgery Clinics of North America*, 18(1):15–20.

Rademakers, T., Horvath, J. M., Blitterswijk, C. A., and LaPointe, V. L. (2019). Oxygen and nutrient delivery in tissue engineering: Approaches to graft vascularization. *Journal of Tissue Engineering and Regenerative Medicine*, 13(10):1815–1829.

Rao, S. S., Lannutti, J. J., Viapiano, M. S., Sarkar, A., and Winter, J. O. (2014). Toward 3D Biomimetic Models to Understand the Behavior of Glioblastoma Multiforme Cells. *Tissue Engineering Part B: Reviews*, 20(4):314–327.

Rape, A., Ananthanarayanan, B., and Kumar, S. (2014). Engineering strategies to mimic the glioblastoma microenvironment. *Advanced Drug Delivery Reviews*, 79-80:172–183.

Rea, K., Sensi, M., Anichini, A., Canevari, S., and Tomassetti, A. (2013). EGFR/MEK/ERK/CDK5-dependent integrin-independent FAK phosphorylated on serine 732 contributes to microtubule depolymerization and mitosis in tumor cells. *Cell Death & Disease*, 4(10):e815–e815.

Reifenberger, G., Wirsching, H.-G., Knobbe-Thomsen, C. B., and Weller, M. (2017). Advances in the molecular genetics of gliomas - implications for classification and therapy. *Nature reviews. Clinical oncology*, 14(7):434–452.

Reiss-Zimmermann, M., Streitberger, K.-J., Sack, I., Braun, J., Arlt, F., Fritzsch, D., and Hoffmann, K.-T. (2015). High Resolution Imaging of Viscoelastic Properties of

Intracranial Tumours by Multi-Frequency Magnetic Resonance Elastography. *Clinical neuroradiology*, 25(4):371–8.

Reiter, N., Paulsen, F., and Budday, S. (2023). Mechanisms of mechanical load transfer through brain tissue. *Scientific Reports*, 13(1):8703.

Rho, J. Y., Ashman, R. B., and Turner, C. H. (1993). Young's modulus of trabecular and cortical bone material: Ultrasonic and microtensile measurements. *Journal of Biomechanics*, 26(2):111–119.

Rivera, A. L., Pelloski, C. E., Gilbert, M. R., Colman, H., De La Cruz, C., Sulman, E. P., Bekele, B. N., and Aldape, K. D. (2010). MGMT promoter methylation is predictive of response to radiotherapy and prognostic in the absence of adjuvant alkylating chemotherapy for glioblastoma. *Neuro-oncology*, 12(2):116–21.

Rojiani, A. M. and Dorovini-Zis, K. (1996). Glomeruloid vascular structures in glioblastoma multiforme: an immunohistochemical and ultrastructural study. *Journal of neurosurgery*, 85(6):1078–84.

Rong, Y., Durden, D. L., Van Meir, E. G., and Brat, D. J. (2006). 'Pseudopalisading' necrosis in glioblastoma: a familiar morphologic feature that links vascular pathology, hypoxia, and angiogenesis. *Journal of neuropathology and experimental neurology*, 65(6):529–39.

Rosén, E., Mangukiya, H. B., Elfineh, L., Stockgard, R., Krona, C., Gerlee, P., and Nelander, S. (2023). Inference of glioblastoma migration and proliferation rates using single time-point images. *Communications Biology*, 6(1):402.

Rosenthal, M. A., Drummond, K. J., Dally, M., Murphy, M., Cher, L., Ashley, D., Thursfield, V., and Giles, G. G. (2006). Management of glioma in Victoria (1998-2000): retrospective cohort study. *The Medical journal of Australia*, 184(6):270–3.

Rossi, M. and Abdelmohsen, K. (2021). The Emergence of Senescent Surface Biomarkers as Senotherapeutic Targets. *Cells*, 10(7):1740.

Ruprecht, V., Wieser, S., Callan-Jones, A., Smutny, M., Morita, H., Sako, K., Barone, V., Ritsch-Marte, M., Sixt, M., Voituriez, R., and Heisenberg, C.-P. (2015). Cortical Contractility Triggers a Stochastic Switch to Fast Amoeboid Cell Motility. *Cell*, 160(4):673–685.

Russell, W. M. S. (1995). The development of the three Rs concept. *Alternatives to laboratory animals : ATLA*, 23(3):298–304.

Ryan, P. L., Foty, R. A., Kohn, J., and Steinberg, M. S. (2001). Tissue spreading on implantable substrates is a competitive outcome of cell–cell vs. cell–substratum adhesivity. *Proceedings of the National Academy of Sciences*, 98(8):4323–4327.

Sack, I., Beierbach, B., Wuerfel, J., Klatt, D., Hamhaber, U., Papazoglou, S., Martus, P., and Braun, J. (2009). The impact of aging and gender on brain viscoelasticity. *NeuroImage*, 46(3):652–657.

Sack, I., Jöhrens, K., Würfel, J., and Braun, J. (2013). Structure-sensitive elastography: on the viscoelastic powerlaw behavior of in vivo human tissue in health and disease. *Soft Matter*, 9(24):5672.

Sack, I., Streitberger, K.-J., Krefting, D., Paul, F., and Braun, J. (2011). The Influence of Physiological Aging and Atrophy on Brain Viscoelastic Properties in Humans. *PLoS ONE*, 6(9):e23451.

Salam, R., Saliou, A., Bielle, F., Bertrand, M., Antoniewski, C., Carpentier, C., Alentorn, A., Capelle, L., Sanson, M., Huillard, E., Bellenger, L., Guégan, J., and Le Roux, I. (2023). Cellular senescence in malignant cells promotes tumor progression in mouse and patient Glioblastoma. *Nature Communications*, 14(1):441.

Saraswathibhatla, A., Indana, D., and Chaudhuri, O. (2023). Cell–extracellular matrix mechanotransduction in 3D. *Nature Reviews Molecular Cell Biology*, 24(7):495–516.

Sarker, F. A., Prior, V. G., Bax, S., and O'Neill, G. M. (2020). Forcing a growth factor response – tissue-stiffness modulation of integrin signaling and crosstalk with growth factor receptors. *Journal of Cell Science*, 133(23).

Scherer, H. J. (1938). Structural Development in Gliomas. *The American Journal of Cancer*, 34(3):333–351.

Scherer, H. J. (1940). The Forms Of Growth In Gliomas Ans Their Practical Signifigance. *Brain*, 63(1):1–35.

Schindelin, J., Arganda-Carreras, I., Frise, E., Kaynig, V., Longair, M., Pietzsch, T., Preibisch, S., Rueden, C., Saalfeld, S., Schmid, B., Tinevez, J.-Y., White, D. J., Hartenstein, V., Eliceiri, K., Tomancak, P., and Cardona, A. (2012). Fiji: an open-source platform for biological-image analysis. *Nature Methods*, 9(7):676–682.

Schregel, K., Nowicki, M. O., Palotai, M., Nazari, N., Zane, R., Sinkus, R., Lawler, S. E., and Patz, S. (2020). Magnetic Resonance Elastography reveals effects of anti-angiogenic glioblastoma treatment on tumor stiffness and captures progression in an orthotopic mouse model. *Cancer Imaging*, 20(1):35.

Schueth, A., Hildebrand, S., Samarska, I., Sengupta, S., Kiessling, A., Herrler, A., zur Hausen, A., Capalbo, M., and Roebroeck, A. (2023). Efficient 3D light-sheet imaging of very large-scale optically cleared human brain and prostate tissue samples. *Communications Biology*, 6(1):170.

Seker-Polat, F., Pinarbasi Degirmenci, N., Solaroglu, I., and Bagci-Onder, T. (2022). Tumor Cell Infiltration into the Brain in Glioblastoma: From Mechanisms to Clinical Perspectives. *Cancers*, 14(2):443.

Semenkow, S., Li, S., Kahlert, U. D., Raabe, E. H., Xu, J., Arnold, A., Janowski, M., Oh, B. C., Brandacher, G., Bulte, J. W., Eberhart, C. G., and Walczak, P. (2017). An immunocompetent mouse model of human glioblastoma. *Oncotarget*, 8(37):61072–61082.

Shergalis, A., Bankhead, A., Luesakul, U., Muangsin, N., and Neamati, N. (2018). Current Challenges and Opportunities in Treating Glioblastoma. *Pharmacological reviews*, 70(3):412–445.

Shiina, T., Hosomichi, K., Inoko, H., and Kulski, J. K. (2009). The HLA genomic loci map: expression, interaction, diversity and disease. *Journal of Human Genetics*, 54(1):15–39.

Shinojima, N., Tada, K., Shiraishi, S., Kamiryo, T., Kochi, M., Nakamura, H., Makino, K., Saya, H., Hirano, H., Kuratsu, J.-I., Oka, K., Ishimaru, Y., and Ushio, Y. (2003). Prognostic value of epidermal growth factor receptor in patients with glioblastoma multiforme. *Cancer research*, 63(20):6962–70.

Sieg, D. J., Hauck, C. R., Ilic, D., Klingbeil, C. K., Schaefer, E., Damsky, C. H., and Schlaepfer, D. D. (2000). FAK integrates growth-factor and integrin signals to promote cell migration. *Nature Cell Biology*, 2(5):249–256.

Silva, C. G., Peyre, E., and Nguyen, L. (2019). Cell migration promotes dynamic cellular interactions to control cerebral cortex morphogenesis. *Nature Reviews Neuroscience*, 20(6):318–329.

Silva, R. V., Morr, A. S., Mueller, S., Koch, S. P., Boehm-Sturm, P., Rodriguez-Sillke, Y., Kunkel, D., Tzschätzsch, H., Kühl, A. A., Schnorr, J., Taupitz, M., Sack, I., and Infante-Duarte, C. (2021a). Contribution of Tissue Inflammation and Blood-Brain Barrier Disruption to Brain Softening in a Mouse Model of Multiple Sclerosis. *Frontiers in Neuroscience*, 15.

Silva, R. V., Morr, A. S., Mueller, S., Koch, S. P., Boehm-Sturm, P., Rodriguez-Sillke, Y., Kunkel, D., Tzschätzsch, H., Kühl, A. A., Schnorr, J., Taupitz, M., Sack, I., and Infante-Duarte, C. (2021b). Contribution of Tissue Inflammation and Blood-Brain Barrier Disruption to Brain Softening in a Mouse Model of Multiple Sclerosis. *Frontiers in Neuroscience*, 15.

Silvestri, L., Costantini, I., Sacconi, L., and Pavone, F. S. (2016). Clearing of fixed

tissue: a review from a microscopist's perspective. *Journal of Biomedical Optics*, 21(8):081205.

Simeonova, I. and Huillard, E. (2014). In vivo models of brain tumors: roles of genetically engineered mouse models in understanding tumor biology and use in preclinical studies. *Cellular and Molecular Life Sciences*, 71(20):4007–4026.

Simian, M. and Bissell, M. J. (2017). Organoids: A historical perspective of thinking in three dimensions. *The Journal of cell biology*, 216(1):31–40.

Singh, S. K., Clarke, I. D., Terasaki, M., Bonn, V. E., Hawkins, C., Squire, J., and Dirks, P. B. (2003). Identification of a cancer stem cell in human brain tumors. *Cancer research*, 63(18):5821–8.

Sjöstedt, E., Zhong, W., Fagerberg, L., Karlsson, M., Mitsios, N., Adori, C., Oksvold, P., Edfors, F., Limiszewska, A., Hikmet, F., Huang, J., Du, Y., Lin, L., Dong, Z., Yang, L., Liu, X., Jiang, H., Xu, X., Wang, J., Yang, H., Bolund, L., Mardinoglu, A., Zhang, C., von Feilitzen, K., Lindskog, C., Pontén, F., Luo, Y., Hökfelt, T., Uhlén, M., and Mulder, J. (2020). An atlas of the protein-coding genes in the human, pig, and mouse brain. *Science*, 367(6482).

Smart, A., Tisca, C., Huszar, I. N., Kor, D., Ansorge, O., Tachrount, M., Smart, S., Lerch, J. P., Miller, K. L., and Martins-Bach, A. B. (2023). Protocol for tissue processing and paraffin embedding of mouse brains following ex vivo MRI. *STAR Protocols*, 4(4):102681.

Smoll, N. R., Schaller, K., and Gautschi, O. P. (2013). Long-term survival of patients with glioblastoma multiforme (GBM). *Journal of Clinical Neuroscience*, 20(5):670–5.

Sohrabi, A., Lefebvre, A. E., Harrison, M. J., Condro, M. C., Sanazzaro, T. M., Safarians, G., Solomon, I., Bastola, S., Kordbacheh, S., Toh, N., Kornblum, H. I., Digman, M. A., and Seidlits, S. K. (2023). Microenvironmental stiffness induces metabolic reprogramming in glioblastoma. *Cell Reports*, 42(10):113175.

Sottoriva, A., Spiteri, I., Piccirillo, S. G. M., Touloumis, A., Collins, V. P., Marioni, J. C., Curtis, C., Watts, C., and Tavaré, S. (2013). Intratumor heterogeneity in human glioblastoma reflects cancer evolutionary dynamics. *Proceedings of the National Academy of Sciences*, 110(10):4009–4014.

Stewart, L. A. (2002). Chemotherapy in adult high-grade glioma: a systematic review and meta-analysis of individual patient data from 12 randomised trials. *Lancet (London, England)*, 359(9311):1011–8.

Streitberger, K.-J., Lilaj, L., Schrank, F., Braun, J., Hoffmann, K.-T., Reiss-Zimmermann, M., Käs, J. A., and Sack, I. (2020). How tissue fluidity influences brain tumor progression. *Proceedings of the National Academy of Sciences*, 117(1):128–134.

Streitberger, K.-J., Reiss-Zimmermann, M., Freimann, F. B., Bayerl, S., Guo, J., Arlt, F., Wuerfel, J., Braun, J., Hoffmann, K.-T., and Sack, I. (2014). High-Resolution Mechanical Imaging of Glioblastoma by Multifrequency Magnetic Resonance Elastography. *PLoS ONE*, 9(10):e110588.

Streitberger, K.-J., Sack, I., Krefting, D., Pfüller, C., Braun, J., Paul, F., and Wuerfel,

J. (2012). Brain Viscoelasticity Alteration in Chronic-Progressive Multiple Sclerosis. *PLoS ONE*, 7(1):e29888.

Stringer, B. W., Day, B. W., D'Souza, R. C. J., Jamieson, P. R., Ensbey, K. S., Bruce, Z. C., Lim, Y. C., Goasdoué, K., Offenhäuser, C., Akgül, S., Allan, S., Robertson, T., Lucas, P., Tollesson, G., Campbell, S., Winter, C., Do, H., Dobrovic, A., Inglis, P.-L., Jeffree, R. L., Johns, T. G., and Boyd, A. W. (2019). A reference collection of patient-derived cell line and xenograft models of proneural, classical and mesenchymal glioblastoma. *Scientific Reports*, 9(1):4902.

Stupp, R., Mason, W. P., van den Bent, M. J., Weller, M., Fisher, B., Taphoorn, M. J. B., Belanger, K., Brandes, A. A., Marosi, C., Bogdahn, U., Curschmann, J., Janzer, R. C., Ludwin, S. K., Gorlia, T., Allgeier, A., Lacombe, D., Cairncross, J. G., Eisenhauer, E., Mirimanoff, R. O., European Organisation for Research and Treatment of Cancer Brain Tumor and Radiotherapy Groups, and National Cancer Institute of Canada Clinical Trials Group (2005). Radiotherapy plus concomitant and adjuvant temozolomide for glioblastoma. *The New England journal of medicine*, 352(10):987–96.

Subramanian, A., Harris, A., Piggott, K., Shieff, C., and Bradford, R. (2002). Metastasis to and from the central nervous system–the 'relatively protected site'. *The Lancet. Oncology*, 3(8):498–507.

Subramanian, A., Tamayo, P., Mootha, V. K., Mukherjee, S., Ebert, B. L., Gillette, M. A., Paulovich, A., Pomeroy, S. L., Golub, T. R., Lander, E. S., and Mesirov, J. P. (2005).

Gene set enrichment analysis: a knowledge-based approach for interpreting genome-wide expression profiles. *Proceedings of the National Academy of Sciences of the United States of America*, 102(43):15545–50.

Suchorska, B., Weller, M., Tabatabai, G., Senft, C., Hau, P., Sabel, M. C., Herrlinger, U., Ketter, R., Schlegel, U., Marosi, C., Reifenberger, G., Wick, W., Tonn, J. C., and Wirsching, H.-G. (2016). Complete resection of contrast-enhancing tumor volume is associated with improved survival in recurrent glioblastoma-results from the DIRECTOR trial. *Neuro-oncology*, 18(4):549–56.

Sullivan, B., Light, T., Vu, V., Kapustka, A., Hristova, K., and Leckband, D. (2022). Mechanical disruption of E-cadherin complexes with epidermal growth factor receptor actuates growth factor–dependent signaling. *Proceedings of the National Academy of Sciences*, 119(4).

Swaminathan, V., Mythreye, K., O'Brien, E. T., Berchuck, A., Blobe, G. C., and Superfine, R. (2011). Mechanical Stiffness Grades Metastatic Potential in Patient Tumor Cells and in Cancer Cell Lines. *Cancer Research*, 71(15):5075–5080.

Taddei, M. L., Giannoni, E., Comito, G., and Chiarugi, P. (2013). Microenvironment and tumor cell plasticity: An easy way out. *Cancer Letters*, 341(1):80–96.

Takamura, T., Motosugi, U., Sasaki, Y., Kakegawa, T., Sato, K., Glaser, K. J., Ehman, R. L., and Onishi, H. (2020). Influence of Age on Global and Regional Brain Stiffness in Young and Middle-Aged Adults. *Journal of Magnetic Resonance Imaging*, 51(3):727–733.

Takebe, T., Imai, R., and Ono, S. (2018). The Current Status of Drug Discovery and Development as Originated in ¡scp¿United States¡/scp¿ Academia: The Influence of Industrial and Academic Collaboration on Drug Discovery and Development. *Clinical and Translational Science*, 11(6):597–606.

Talkenberger, K., Cavalcanti-Adam, E. A., Voss-Böhme, A., and Deutsch, A. (2017). Amoeboid-mesenchymal migration plasticity promotes invasion only in complex heterogeneous microenvironments. *Scientific Reports*, 7(1):9237.

Tang, M., Gao, G., Rueda, C. B., Yu, H., Thibodeaux, D. N., Awano, T., Engelstad, K. M., Sanchez-Quintero, M.-J., Yang, H., Li, F., Li, H., Su, Q., Shetler, K. E., Jones, L., Seo, R., McConathy, J., Hillman, E. M., Noebels, J. L., De Vivo, D. C., and Monani, U. R. (2017). Brain microvasculature defects and Glut1 deficiency syndrome averted by early repletion of the glucose transporter-1 protein. *Nature Communications*, 8(1):14152.

Taqi, S. A., Sami, S. A., Sami, L. B., and Zaki, S. A. (2018). A review of artifacts in histopathology. *Journal of oral and maxillofacial pathology : JOMFP*, 22(2):279.

Taube, J. M., Akturk, G., Angelo, M., Engle, E. L., Gnjatic, S., Greenbaum, S., Greenwald, N. F., Hedvat, C. V., Hollmann, T. J., Juco, J., Parra, E. R., Rebelatto, M. C., Rimm, D. L., Rodriguez-Canales, J., Schalper, K. A., Stack, E. C., Ferreira, C. S., Korski, K., Lako, A., Rodig, S. J., Schenck, E., Steele, K. E., Surace, M. J., Tetzlaff, M. T., von Loga, K., Wistuba, I. I., and Bifulco, C. B. (2020). The Society for Immunotherapy of Cancer statement on best practices for multiplex immunohistochemistry (IHC) and immunofluorescence (IF) staining and validation. *Journal for ImmunoTherapy of Cancer*, 8(1):e000155.

Taylor, Z. and Miller, K. (2004). Reassessment of brain elasticity for analysis of biomechanisms of hydrocephalus. *Journal of biomechanics*, 37(8):1263–9.

Thakkar, J. P., Dolecek, T. A., Horbinski, C., Ostrom, Q. T., Lightner, D. D., Barnholtz-Sloan, J. S., and Villano, J. L. (2014). Epidemiologic and molecular prognostic review of glioblastoma. *Cancer epidemiology, biomarkers & prevention : a publication of the American Association for Cancer Research, cosponsored by the American Society of Preventive Oncology*, 23(10):1985–96.

The Gene Ontology Consortium (2019). The Gene Ontology Resource: 20 years and still GOing strong. *Nucleic acids research*, 47(D1):D330–D338.

Thompson, A. J., Pillai, E. K., Dimov, I. B., Foster, S. K., Holt, C. E., and Franze, K. (2019). Rapid changes in tissue mechanics regulate cell behaviour in the developing embryonic brain. *eLife*, 8.

Thorne, R. G. and Nicholson, C. (2006). In vivo diffusion analysis with quantum dots and dextrans predicts the width of brain extracellular space. *Proceedings of the National Academy of Sciences of the United States of America*, 103(14):5567–72.

Thul, P. J., Åkesson, L., Wiking, M., Mahdessian, D., Geladaki, A., Ait Blal, H., Alm, T., Asplund, A., Björk, L., Breckels, L. M., Bäckström, A., Danielsson, F., Fagerberg, L., Fall, J., Gatto, L., Gnann, C., Hober, S., Hjelmare, M., Johansson, F., Lee, S., Lindskog, C., Mulder, J., Mulvey, C. M., Nilsson, P., Oksvold, P., Rockberg, J., Schutten, R., Schwenk, J. M., Sivertsson, , Sjöstedt, E., Skogs, M., Stadler, C., Sullivan, D. P., Tegel, H., Winsnes, C., Zhang, C., Zwahlen, M., Mardinoglu, A., Pontén, F., von Feilitzen,

K., Lilley, K. S., Uhlén, M., and Lundberg, E. (2017). A subcellular map of the human proteome. *Science*, 356(6340).

Uhlén, M., Fagerberg, L., Hallström, B. M., Lindskog, C., Oksvold, P., Mardinoglu, A., Sivertsson, , Kampf, C., Sjöstedt, E., Asplund, A., Olsson, I., Edlund, K., Lundberg, E., Navani, S., Szigyarto, C. A.-K., Odeberg, J., Djureinovic, D., Takanen, J. O., Hober, S., Alm, T., Edqvist, P.-H., Berling, H., Tegel, H., Mulder, J., Rockberg, J., Nilsson, P., Schwenk, J. M., Hamsten, M., von Feilitzen, K., Forsberg, M., Persson, L., Johansson, F., Zwahlen, M., von Heijne, G., Nielsen, J., and Pontén, F. (2015). Tissue-based map of the human proteome. *Science*, 347(6220).

Uhlen, M., Zhang, C., Lee, S., Sjöstedt, E., Fagerberg, L., Bidkhori, G., Benfeitas, R., Arif, M., Liu, Z., Edfors, F., Sanli, K., von Feilitzen, K., Oksvold, P., Lundberg, E., Hober, S., Nilsson, P., Mattsson, J., Schwenk, J. M., Brunnström, H., Glimelius, B., Sjöblom, T., Edqvist, P.-H., Djureinovic, D., Micke, P., Lindskog, C., Mardinoglu, A., and Ponten, F. (2017). A pathology atlas of the human cancer transcriptome. *Science*, 357(6352).

Ulrich, T. A., de Juan Pardo, E. M., and Kumar, S. (2009). The mechanical rigidity of the extracellular matrix regulates the structure, motility, and proliferation of glioma cells. *Cancer research*, 69(10):4167–74.

Umesh, V., Rape, A. D., Ulrich, T. A., and Kumar, S. (2014). Microenvironmental Stiffness Enhances Glioma Cell Proliferation by Stimulating Epidermal Growth Factor Receptor Signaling. *PLoS ONE*, 9(7):e101771.

Uyar, R. (2022). Glioblastoma microenvironment: The stromal interactions. *Pathology - Research and Practice*, 232:153813.

Velling, T., Nilsson, S., Stefansson, A., and Johansson, S. (2004). β1-Integrins induce phosphorylation of Akt on serine 473 independently of focal adhesion kinase and Src family kinases. *EMBO reports*, 5(9):901–905.

Venkataramani, V., Yang, Y., Schubert, M. C., Reyhan, E., Tetzlaff, S. K., Wißmann, N., Botz, M., Soyka, S. J., Beretta, C. A., Pramatarov, R. L., Fankhauser, L., Garofano, L., Freudenberg, A., Wagner, J., Tanev, D. I., Ratliff, M., Xie, R., Kessler, T., Hoffmann, D. C., Hai, L., Dörflinger, Y., Hoppe, S., Yabo, Y. A., Golebiewska, A., Niclou, S. P., Sahm, F., Lasorella, A., Slowik, M., Döring, L., Iavarone, A., Wick, W., Kuner, T., and Winkler, F. (2022). Glioblastoma hijacks neuronal mechanisms for brain invasion. *Cell*, 185(16):2899–2917.

Verhaak, R. G. W., Hoadley, K. A., Purdom, E., Wang, V., Qi, Y., Wilkerson, M. D., Miller, C. R., Ding, L., Golub, T., Mesirov, J. P., Alexe, G., Lawrence, M., O'Kelly, M., Tamayo, P., Weir, B. A., Gabriel, S., Winckler, W., Gupta, S., Jakkula, L., Feiler, H. S., Hodgson, J. G., James, C. D., Sarkaria, J. N., Brennan, C., Kahn, A., Spellman, P. T., Wilson, R. K., Speed, T. P., Gray, J. W., Meyerson, M., Getz, G., Perou, C. M., Hayes, D. N., and Cancer Genome Atlas Research Network (2010). Integrated genomic analysis identifies clinically relevant subtypes of glioblastoma characterized by abnormalities in PDGFRA, IDH1, EGFR, and NF1. *Cancer cell*, 17(1):98–110.

Vollmann-Zwerenz, A., Leidgens, V., Feliciello, G., Klein, C. A., and Hau, P. (2020).

Tumor Cell Invasion in Glioblastoma. *International journal of molecular sciences*, 21(6).

Volovetz, J., Berezovsky, A. D., Alban, T., Chen, Y., Lauko, A., Aranjuez, G. F., Burtscher, A., Shibuya, K., Silver, D. J., Peterson, J., Manor, D., McDonald, J. A., and Lathia, J. D. (2020). Identifying conserved molecular targets required for cell migration of glioblastoma cancer stem cells. *Cell Death & Disease*, 11(2):152.

von Hippel, P. T. (2015). The heterogeneity statistic I2 can be biased in small meta-analyses. *BMC Medical Research Methodology*, 15(1):35.

Walker, M. D., Strike, T. A., and Sheline, G. E. (1979). An analysis of dose-effect relationship in the radiotherapy of malignant gliomas. *International journal of radiation oncology, biology, physics*, 5(10):1725–31.

Wan, X., Wang, W., Liu, J., and Tong, T. (2014). Estimating the sample mean and standard deviation from the sample size, median, range and/or interquartile range. *BMC Medical Research Methodology*, 14(1):135.

Wang, C., Sinha, S., Jiang, X., Murphy, L., Fitch, S., Wilson, C., Grant, G., and Yang, F. (2021). Matrix Stiffness Modulates Patient-Derived Glioblastoma Cell Fates in Three-Dimensional Hydrogels. *Tissue Engineering Part A*, 27(5-6):390–401.

Wang, J., Cazzato, E., Ladewig, E., Frattini, V., Rosenbloom, D. I. S., Zairis, S., Abate, F., Liu, Z., Elliott, O., Shin, Y.-J., Lee, J.-K., Lee, I.-H., Park, W.-Y., Eoli, M., Blumberg, A. J., Lasorella, A., Nam, D.-H., Finocchiaro, G., Iavarone, A., and Rabadan, R.

(2016a). Clonal evolution of glioblastoma under therapy. *Nature Genetics*, 48(7):768–776.

Wang, K., Kievit, F. M., Erickson, A. E., Silber, J. R., Ellenbogen, R. G., and Zhang, M. (2016b). Culture on 3D Chitosan-Hyaluronic Acid Scaffolds Enhances Stem Cell Marker Expression and Drug Resistance in Human Glioblastoma Cancer Stem Cells. *Advanced Healthcare Materials*, 5(24):3173–3181.

Wang, Q., Chen, W., Wan, Z., and Liu, W. (2022). Clonal Outbreak of Trichophyton tonsurans Causing Tinea Capitis Among a Wrestling Team in Beijing, China. *Mycopathologia*, pages –.

Wang, Q., Hu, B., Hu, X., Kim, H., Squatrito, M., Scarpace, L., deCarvalho, A. C., Lyu, S., Li, P., Li, Y., Barthel, F., Cho, H. J., Lin, Y.-H., Satani, N., Martinez-Ledesma, E., Zheng, S., Chang, E., Sauvé, C.-E. G., Olar, A., Lan, Z. D., Finocchiaro, G., Phillips, J. J., Berger, M. S., Gabrusiewicz, K. R., Wang, G., Eskilsson, E., Hu, J., Mikkelsen, T., DePinho, R. A., Muller, F., Heimberger, A. B., Sulman, E. P., Nam, D.-H., and Verhaak, R. G. W. (2017). Tumor Evolution of Glioma-Intrinsic Gene Expression Subtypes Associates with Immunological Changes in the Microenvironment. *Cancer cell*, 32(1):42–56.

Watanabe, K., Tachibana, O., Sata, K., Yonekawa, Y., Kleihues, P., and Ohgaki, H. (1996). Overexpression of the EGF receptor and p53 mutations are mutually exclusive in the evolution of primary and secondary glioblastomas. *Brain pathology (Zurich, Switzerland)*, 6(3):217–23.

Watts, G. S., Pieper, R. O., Costello, J. F., Peng, Y. M., Dalton, W. S., and Futscher, B. W. (1997). Methylation of discrete regions of the O6-methylguanine DNA methyltransferase (MGMT) CpG island is associated with heterochromatinization of the MGMT transcription start site and silencing of the gene. *Molecular and cellular biology*, 17(9):5612–9.

Wehrle-Haller, B. and Imhof, B. A. (2003). Actin, microtubules and focal adhesion dynamics during cell migration. *The International Journal of Biochemistry & Cell Biology*, 35(1):39–50.

Weickenmeier, J., de Rooij, R., Budday, S., Steinmann, P., Ovaert, T., and Kuhl, E. (2016). Brain stiffness increases with myelin content. *Acta Biomaterialia*, 42:265–272.

Weickenmeier, J., Kurt, M., Ozkaya, E., Wintermark, M., Pauly, K. B., and Kuhl, E. (2018). Magnetic resonance elastography of the brain: A comparison between pigs and humans. *Journal of the Mechanical Behavior of Biomedical Materials*, 77:702–710.

Welch, M. (2015). Cell Migration, Freshly Squeezed. *Cell*, 160(4):581–582.

Weller, M., van den Bent, M., Hopkins, K., Tonn, J. C., Stupp, R., Falini, A., Cohen-Jonathan-Moyal, E., Frappaz, D., Henriksson, R., Balana, C., Chinot, O., Ram, Z., Reifenberger, G., Soffietti, R., Wick, W., and European Association for Neuro-Oncology (EANO) Task Force on Malignant Glioma (2014). EANO guideline for the diagnosis and treatment of anaplastic gliomas and glioblastoma. *The Lancet. Oncology*, 15(9):395–403.

Weller, M., Wick, W., Aldape, K., Brada, M., Berger, M., Pfister, S. M., Nishikawa, R.,

Rosenthal, M., Wen, P. Y., Stupp, R., and Reifenberger, G. (2015). Glioma. *Nature reviews. Disease primers*, 1(1):15017.

Willemsen, M., Krebbers, G., Bekkenk, M. W., Teunissen, M. B., and Luiten, R. M. (2021). Improvement of Opal Multiplex Immunofluorescence Workflow for Human Tissue Sections. *Journal of Histochemistry & Cytochemistry*, 69(5):339–346.

Winkler, F., Kienast, Y., Fuhrmann, M., Von Baumgarten, L., Burgold, S., Mitteregger, G., Kretzschmar, H., and Herms, J. (2009). Imaging glioma cell invasion in vivo reveals mechanisms of dissemination and peritumoral angiogenesis. *Glia*, 57(12):1306–1315.

Winkler, J., Abisoye-Ogunniyan, A., Metcalf, K. J., and Werb, Z. (2020). Concepts of extracellular matrix remodelling in tumour progression and metastasis. *Nature Communications*, 11(1):5120.

Wirsching, H.-G., Galanis, E., and Weller, M. (2016). Glioblastoma. *Handbook of clinical neurology*, 134:381–97.

Wolf, K., Wu, Y. I., Liu, Y., Geiger, J., Tam, E., Overall, C., Stack, M. S., and Friedl, P. (2007). Multi-step pericellular proteolysis controls the transition from individual to collective cancer cell invasion. *Nature Cell Biology*, 9(8):893–904.

Wolfram, L., Gimpel, C., Schwämmle, M., Clark, S. J., Böhringer, D., and Schlunck, G. (2024). The impact of substrate stiffness on morphological, transcriptional and functional aspects in RPE. *Scientific Reports*, 14(1):7488.

Wozniak, M. A., Modzelewska, K., Kwong, L., and Keely, P. J. (2004). Focal adhesion

regulation of cell behavior. *Biochimica et Biophysica Acta (BBA) - Molecular Cell Research*, 1692(2-3):103–119.

Wu, J.-s., Jiang, J., Chen, B.-j., Wang, K., Tang, Y.-l., and Liang, X.-h. (2021). Plasticity of cancer cell invasion: Patterns and mechanisms. *Translational Oncology*, 14(1):100899.

Wuerfel, J., Paul, F., Beierbach, B., Hamhaber, U., Klatt, D., Papazoglou, S., Zipp, F., Martus, P., Braun, J., and Sack, I. (2010). MR-elastography reveals degradation of tissue integrity in multiple sclerosis. *NeuroImage*, 49(3):2520–2525.

Xie, Q., Mittal, S., and Berens, M. E. (2014). Targeting adaptive glioblastoma: an overview of proliferation and invasion. *Neuro-oncology*, 16(12):1575–84.

Xie, Y., Bergström, T., Jiang, Y., Johansson, P., Marinescu, V. D., Lindberg, N., Segerman, A., Wicher, G., Niklasson, M., Baskaran, S., Sreedharan, S., Everlien, I., Kastemar, M., Hermansson, A., Elfineh, L., Libard, S., Holland, E. C., Hesselager, G., Alafuzoff, I., Westermark, B., Nelander, S., Forsberg-Nilsson, K., and Uhrbom, L. (2015). The Human Glioblastoma Cell Culture Resource: Validated Cell Models Representing All Molecular Subtypes. *EBioMedicine*, 2(10):1351–63.

Xie, Z., Bailey, A., Kuleshov, M. V., Clarke, D. J. B., Evangelista, J. E., Jenkins, S. L., Lachmann, A., Wojciechowicz, M. L., Kropiwnicki, E., Jagodnik, K. M., Jeon, M., and Ma'ayan, A. (2021). Gene Set Knowledge Discovery with Enrichr. *Current protocols*, 1(3):e90.

Xin, Y., Li, K., Huang, M., Liang, C., Siemann, D., Wu, L., Tan, Y., and Tang, X. (2023).

Biophysics in tumor growth and progression: from single mechano-sensitive molecules to mechanomedicine. *Oncogene*, 42(47):3457–3490.

Yamaguchi, Y. (2000). Lecticans: organizers of the brain extracellular matrix. *Cellular and Molecular Life Sciences*, 57(2):276–289.

Yan, H., Parsons, D. W., Jin, G., McLendon, R., Rasheed, B. A., Yuan, W., Kos, I., Batinic-Haberle, I., Jones, S., Riggins, G. J., Friedman, H., Friedman, A., Reardon, D., Herndon, J., Kinzler, K. W., Velculescu, V. E., Vogelstein, B., and Bigner, D. D. (2009). IDH1 and IDH2 mutations in gliomas. *The New England journal of medicine*, 360(8):765–73.

Yang, K., Wu, Z., Zhang, H., Zhang, N., Wu, W., Wang, Z., Dai, Z., Zhang, X., Zhang, L., Peng, Y., Ye, W., Zeng, W., Liu, Z., and Cheng, Q. (2022). Glioma targeted therapy: insight into future of molecular approaches. *Molecular Cancer*, 21(1):39.

Yang, Y.-l., Motte, S., and Kaufman, L. J. (2010). Pore size variable type I collagen gels and their interaction with glioma cells. *Biomaterials*, 31(21):5678–5688.

Yeoman, B., Shatkin, G., Beri, P., Banisadr, A., Katira, P., and Engler, A. J. (2021). Adhesion strength and contractility enable metastatic cells to become adurotactic. *Cell Reports*, 34(10):108816.

Yin, Z., Romano, A. J., Manduca, A., Ehman, R. L., and Huston, J. (2018). Stiffness and Beyond. *Topics in Magnetic Resonance Imaging*, 27(5):305–318.

Zada, G., Yashar, P., Robison, A., Winer, J., Khalessi, A., Mack, W. J., and Giannotta,

S. L. (2013). A proposed grading system for standardizing tumor consistency of intracranial meningiomas. *Neurosurgical Focus*, 35(6):E1.

Zhang, P., Xia, Q., Liu, L., Li, S., and Dong, L. (2020). Current Opinion on Molecular Characterization for GBM Classification in Guiding Clinical Diagnosis, Prognosis, and Therapy. *Frontiers in Molecular Biosciences*, 7.

Zhong, J., Paul, A., Kellie, S. J., and O'Neill, G. M. (2010). Mesenchymal migration as a therapeutic target in glioblastoma. *Journal of oncology*, 2010:430142.

Zhou, D. W., Fernández-Yagüe, M. A., Holland, E. N., García, A. F., Castro, N. S., O'Neill, E. B., Eyckmans, J., Chen, C. S., Fu, J., Schlaepfer, D. D., and García, A. J. (2021). Force-FAK signaling coupling at individual focal adhesions coordinates mechanosensing and microtissue repair. *Nature Communications*, 12(1):2359.

Zou, P., Xu, H., Chen, P., Yan, Q., Zhao, L., Zhao, P., and Gu, A. (2013). IDH1/IDH2 mutations define the prognosis and molecular profiles of patients with gliomas: a meta-analysis. *PloS one*, 8(7):e68782.